1967

Flow Losses in Flexible Hose.

Kenneth Lloyd Riley
Louisiana State University and Agricultural & Mechanical College

FLOW LOSSES IN FLEXIBLE HOSE

A Dissertation

Submitted to the Graduate Faculty of the
Louisiana State University and
Agricultural and Mechanical College
in partial fulfillment of the
requirements for the degree of
Doctor of Philosophy

in

The Department of Chemical Engineering

by
Kenneth Lloyd Riley
B.S., Louisiana State University, 1963
M.S., Louisiana State University, 1965
May, 1967

ACKNOWLEDGEMENT

This research was conducted under the guidance of Dr. Bernard S. Pressburg, Professor of Chemical Engineering. I want to express my appreciation to him for the consideration and encouragement shown throughout this study. I also want to thank Dr. Charles A. Whitehurst, Associate Professor of Research in the Division of Engineering Research. His assistance had a great deal to do with the successful completion of this project.

The contributions of W. T. Durbin and J. R. Langley to this work are greatly appreciated.

The financial assistance of the Esso Research Laboratories and the National Aeronautics and Space Administration is gratefully acknowledged. This study was supported by funds provided by the National Aeronautics and Space Administration through contract NAS 9-4630. I also want to thank the Dr. Charles E. Coates Memorial Fund of the L.S.U. Foundation, donated by George H. Coates, for financial assistance in the preparation of this manuscript.

Special acknowledgement is given to my wife, Delphine. Her patience and help was a very important contribution in everything that was done.

TABLE OF CONTENTS

APPENDIX

LIST OF TABLES

LIST OF FIGURES

LIST OF ILLUSTRATIONS

NOMENCLATURE

A	Characteristic area, ft^2
A (E^+)	Friction similarity function defined by equation (II-51)
B	Constant defined in equation (II-40)
C_D	Drag coefficient, dimensionless
C_o	Proportionality constant in equation (II-47)
C_p	Specific heat at constant pressure, BTU/(lb) (°F)
C_v	Specific heat at constant volume, BTU/(lb) (°F)
D	Minimum inside diameter, ft; D_o, maximum inside diameter (see Illustration III-1)
D_{ave}	Arithmetic mean diameter $(D + D_o)/2$, ft
E	Energy, ft-lb_f; $\dot{E}$, energy per unit time, ft-lb_f/sec
E^+	Re $(\varepsilon/D_o)\sqrt{f/2}$
F	Force, lb_f; F_s, force exerted by stationery fluid; F_k, force associated with moving fluid; $F_{k,d}$, force associated with moving fluid due to drag friction
G_{max}	The mass velocity through the minimum free area of flow perpindicular to the flow stream for a bank of tubes, lb/(sec)(ft^2)
H_f	Friction, ft-lb_f/lb; $H_{f,s}$, skin friction; $H_{f,d}$, drag friction
K	Characteristic kinetic energy per unit volume, (ft)(lb_f)/ft^3
L	Length of conduit, ft; L', effective flow length $N_T S_L$, ft
M	Mach number; M_1 inlet Mach number
N	Number of convolutions per foot; N_r, number of transverse rows in a tube bundle

Nomenclature (cont'd)

P	Absolute pressure, lb_f/ft^2
R	Inside radius of circular conduit, ft
$\overline{R}$	Universal gas law constant, 10.73 (psia) $(ft^3)/(°R)$(lb mole)
S_L	Spacing of longitudinal rows of a tube bundle, ft.
T	Absolute temperature, °R
W	Mass flow rate, lb/hr
X	Defined by equation (II-49)
Y	Defined by equation (II-49)
c	Velocity of sound for an ideal gas $\sqrt{\frac{g_c \gamma RT}{MW}}$, ft/sec
d'	Modified volumetric equivalent diameter, ft 4 (minimum area of flow)$(N_T S_L)$/heat-transfer area in exchanger
f	Fanning friction factor for straight conduit; f_B, friction factor for curved conduit; f_{KL}, defined by equation (V-1)
g(Re)	Indicates some function of Re
g_c	Newton's law conversion factor, 32.174 (ft)(lb)/$(lb_f)(sec^2)$
h	Loss of head due to friction, $(ft)(lb_f)/lb$
j_h	Colburn factor, defined by equation (II-26)
k	Thermal conductivity, BTU/(hr)(ft)(°F)
m	Mass, lb.
n	Exponent in equation (II-28), exponent in equation (II-47)
p	Wetted perimeter, ft

Nomenclature (cont'd)

r	Radial length from the axis of a circular conduit, ft; r_B, bend radius (see Illustration III-4)
t	Time, seconds
v	Net local velocity, ft/sec; $\bar{v}$, average velocity; v_{max}, maximum local net velocity in a closed conduit; v_o, velocity near the crest of the convolution; v_r, the tangential velocity of an element in the groove vortex
v^+	v/v^*
v^*	Friction velocity $\sqrt{(g_c)(\tau_o)/\rho}$, ft/sec
x	Distance in axial direction, ft
y	Distance in radial direction, ft
y^+	$(y)(v^*)/\nu$
z	Distance in a vertical direction, ft
α	Geometric constant defined by equation (II-52)
β	Geometric constant defined by equation (II-52)
γ	Ratio of specific heats, C_p/C_v (equation II-13)
ΔP	Pressure drop, lb_f/ft^2; ΔP_s, pressure drop due to skin friction; ΔP_d, pressure drop due to drag friction
ϵ	Effective height of a roughness element, ft (see Illustration III-1)
ϵ^+	$Re(\epsilon/D)\sqrt{f/2}$
θ	Bend angle, degrees
λ	Longitudinal spacing of roughness elements, ft
μ	Viscosity of fluid, lb/(ft)(sec)

Nomenclature (cont'd)

ν	Kinematic viscosity μ/ρ, ft^2/sec
ρ	Density of fluid, lb/ft^3
σ	Width of convolution, ft (see Illustration III-1)
τ	Shear force, $(lb_f)/(ft^2)$; τ_o, shear force at the wall of a conduit
ϕ	Defined by equation (IV-8) and (IV-18)
χ	Defined by equation (IV-7) and (IV-17)
$\psi(Re^*)$	Indicates a function of Re*
ω	Angular velocity of vortex, radians/sec
§	Defined by equation (IV-10)
De	Dean number, $(1/2)(Re)\sqrt{R/r_B}$
Re	Reynolds number; $D\rho\bar{v}/\mu$; Re', defined by equation (V-2); Re*, roughness Reynolds number, $Re\sqrt{f}/(D/\lambda)$

ABSTRACT

The objective of this study was to develop an empirical method for predicting flow losses in flexible metal hose. Hoses with annular and helical convolutions were used; their diameters ranged from 1/2 to 3 inches. To obtain a wide range of flow rates two test fluids were used: air and water.

The correlations developed in this study, for both straight and curved hose, relate the Fanning friction factor with Reynolds number and hose geometry. For straight hose the correlation has the form:

$$\frac{1}{\sqrt{f}} - 4 \log \left(\frac{D}{\lambda}\right) = \psi (Re^*)$$

where $\psi(Re^*)$ is a function of Re^*. Results indicate that two correlations are necessary: one for annular-type hose and another for helical-type hose. These correlations are presented both graphically and mathematically. A statistical analysis shows that the correlations may be used to predict friction factors with an accuracy of about $\pm$ 20% for Reynolds numbers from 10,000 to 340,000. Data obtained from the literature indicate that the correlations can be extended to include Reynolds numbers from 2100 to 2,000,000. Data from this study also indicate that correlations given by Daniels and Cleveland, Morris, and workers at Mississippi State University may be used to accurately predict values of the friction factor for flow in flexible metal hose.

For a given hose the flow behavior can be described by considering the friction factor as a function of Reynolds number. For Reynolds numbers in the lower end of the turbulent flow regime (10,000 to about 70,000), the friction factor is independent of Reynolds number and has a value of about 0.020. As the flow rate increases above this range the friction factor begins to increase with an increase in Reynolds number. At very high Reynolds numbers the friction factor again becomes independent of the Reynolds number. The friction factor at very high Reynolds numbers has been found to be as much as three times the value in the low range. A flow model is proposed which accounts for this behavior.

The correlation for curved hose has been found to be applicable for both annular and helical hoses. The relationship for the ratio of the friction factor for a curved hose to that for a straight hose is:

$$\frac{f_B}{f} = 1.0 + 59.0 \left(\frac{D}{r_B}\right) (Re)^{-0.17}$$

where D is the inside diameter and r_B is the bend radius. Curved sections of hose were studied with the bend angle varying from 0° (straight hose) to 180°; tests were run at 30° intervals within this range. This correlation may be used to predict friction factors with an accuracy of about $\pm$ 20%.

CHAPTER I

INTRODUCTION

Approximately twenty percent of the total investment in a typical chemical plant is for equipment associated with the transportation of fluids. An engineer must have accurate design correlations if he is to minimize this invested capital and make the most effective use of it. This study is part of a continuing effort to provide these correlations.

Problem Definition:

In the process industries, fluids are usually carried in closed conduits--sometimes square or rectangular in cross-section but more often circular. In a chemical plant the conduits in which fluids are transported - ducts, pipe, and tubing - are usually circular. This shape gives the lowest wetted surface area to volume ratio of any cross-sectional geometry; as a consequence flow through a circular conduit consumes less energy than would flow through a conduit of the same flow area but of different shape.

The characteristics designed into any conduit are dictated by the service for which it is intended. The material of construction depends upon the properties of the fluid being transported; to obtain resistance to attack by corrosive fluids, the conduit may have to be a special metal alloy. The strength of a conduit must be such as to withstand the pressure of the fluid; wall thickness must be increased as fluid pressure is increased.

To obtain a practical, operable system, additional factors must be considered. Conduits are usually exposed to a range of temperatures, which in some high temperature lines, may be very large. Temperature changes cause the conduit to expand and contract. If the conduit is rigidly fixed to its supports it may bend, be torn loose, or even rupture. In the process industries almost all metal pipes are used at temperatures other than that at which they are installed. For this reason, provision must be made for taking up the expansion or contraction, thus avoiding any tendency to subject the pipe to excessive strain. This is done by bends or loops in the pipe, by packed expansion joints, by bellows or "packless" joints, and increasingly by flexible metal hose.

Figure I-1 shows a sectional view of a typical flexible metal hose. This hose has a corrugated (or "convoluted") inner tube of brass, monel, Inconel, or stainless steel sheathed with a woven metal cover to give it strength. The flexible metal hose has three major advantages over conventional pipe: (1) it compensates for thermal expansion, (2) it can allow for misalignment, and (3) it permits relative motion between two rigid hydraulic lines. Short lengths are often used in piping systems to eliminate strain; longer pieces are useful in connecting process lines to vibrating or moving machinery and in places like drum-filling equipment where the line must be moved frequently. Flexible metal hoses are also used in space-oriented applications. Flow lines in the primary and secondary propulsion systems of NASA spacecraft are made of flexible metal hose.

Perhaps the most significant design criterion for any conduit system is the energy degradation due to fluid friction. From the designers'

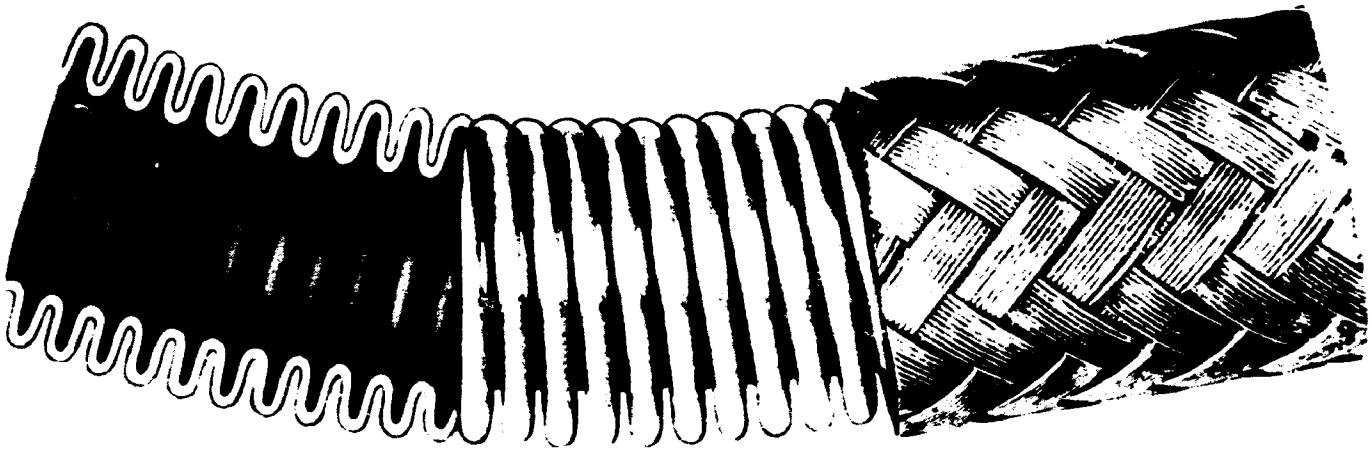

FIGURE I-1

FLEXIBLE METAL HOSE

viewpoint this is a serious limitation on the use of flexible metal hoses. The flow loss through a given size flexible hose may be as high as 7 to 15 times greater than that of a comparable size standard pipe. This increased flow loss is due to the convoluted nature of the tube wall which increases the surface to volume ratio and also creates significant turbulence over and above that occurring in an ordinary pipe.

Despite the increasingly widespread use of flexible metal hose in the process industries and space-oriented work, their selection and use is essentially an art. Information on the performance of one hose is of little or no value in predicting the performance of another hose of different size or of different geometric design.

Design methods for flexible metal hoses may be described as being in a "rule of thumb" stage. One such design procedure is: "In a straight line installation, corrugated hose will produce three times the pressure loss normally expected in pipe and interlocked hose double the pressure loss of pipe." Since experimental observations have shown that a flexible hose can give as much as 15 times the pressure loss as that expected in pipe, it is obvious that this rule is not a very safe design correlation.

As both a prerequisite for and a consequence of the increasing use of flexible metal hose, design methods must advance from the "rule of thumb" stage. Flow losses must be related in a more fundamental way to the resistance of flow through the conduit. The conventional way of doing this for circular pipes is to correlate a friction factor as a function of flow conditions, e.g., Reynolds number, and conduit geometry.

Hopefully, this type of relationship can be developed for flexible hoses and some work has already been done along these lines using the results for smooth pipes as a guide.

The purpose of this study is to extend and interpret this approach for flexible metal hoses. It is hoped that the end product is an accurate design correlation for the engineer engaged in designing flexible hose systems.

CHAPTER II

LITERATURE SURVEY

This section deals with previous studies which form the basis for the development of the relationship between flow losses and flow rate in flexible metal hose. Published data on flow in flexible metal hoses are meager. Furthermore, empirical correlations developed from the data are often conflicting.

This section begins by considering the definition of the friction factor. The relationship between the Reynolds number and the friction factor is then discussed for various cases. The first case considered is for flow in a smooth conduit of circular cross section. The discussion then turns to circular conduits with rough surfaces. Surface roughness is considered in two parts: regular roughness elements and irregular roughness elements.

Definition of Friction Factor:

Consider the steady flow of a fluid in a conduit of uniform cross section. The fluid will exert a force F on the solid surface of the conduit. This force may be split into two parts: F_s, that force which would be exerted by the fluid even if it were stationery, and F_k, that additional force associated with the kinetic behavior of the fluid.

The magnitude of the force F_k may be arbitrarily expressed as the product of a characteristic area A, a characteristic kinetic energy per unit volume K, and a dimensionless quantity f, known as the friction factor:

$$F_k = Akf \qquad \text{(II-1)}$$

Note that f is not defined until A and K are specified. With this definition f can usually be given as a relatively simple function of the Reynolds number and the system shape.

In this study A is taken to be πDL, where D is the minimum inside diameter of the flexible hose, and K is taken to be the quantity $1/2\ \rho v^2$. Specifically, f is defined as

$$F_k = (\pi DL)\left(\frac{1}{2g_c}\rho\bar{v}^2\right)f \qquad \text{(II-2)}$$

The quantity f defined in this manner is sometimes called the Fanning friction factor.

Momentum Balance:

According to Newton's second law, the rate of change of momentum equals the net applied force:

$$\frac{d(mv)}{dt} = g_c\ (\Sigma F) \qquad \text{(II-3)}$$

The surface forces acting on an element of fluid in a pipe are due to the upstream pressure, the downstream pressure, and the peripheral shear. The momentum equation for a differential element of fluid is then

$$P\frac{\pi D^2}{4} - (P + dP)\frac{\pi D^2}{4} - \tau_o \pi D dx = \frac{\pi D^2}{4}\left(\frac{\rho}{g_c}\right)\bar{v}d\bar{v} \qquad \text{(II-4)}$$

The peripheral shear stress can be expressed in terms of the friction factor f. From the definition of the friction factor

$$\frac{F_k}{A} = \tau_o = Kf = \frac{\rho v^2}{2g_c}f \qquad \text{(II-5)}$$

Inserting this relationship into equation (II-4) and simplifying gives:

$$\frac{dP}{\rho} + \frac{\bar{v}d\bar{v}}{g_c} + \frac{4f\bar{v}^2 dx}{D2g_c} = 0 \qquad \text{(II-6)}$$

This equation can then be integrated to give the working equation for the evaluation of the friction factor.

Friction Factor for the Water System:

For the flow of an incompressible fluid in a horizontal pipe of uniform cross-section the integration of the momentum equation is straightforward.

$d\bar{v} = 0$ $\qquad\qquad$ ρ = constant

therefore

$$\frac{-\Delta P}{\rho} = 4f \frac{L}{D} \frac{\bar{v}^2}{2g_c} \qquad \text{(II-7)}$$

From this equation it follows that

$$f = \frac{1}{4} \frac{D}{L} \frac{-\Delta P g_c}{\frac{1}{2}\rho\bar{v}^2} \qquad \text{(II-8)}$$

This equation shows explicitly how f can be calculated from experimental data.

Friction Factor for the Air System:

In order to integrate the momentum equation for a compressible fluid the variable density and velocity have to be expressed in terms of the variable pressure. It will be assumed that the system is operating under approximately isothermal conditions.

If all conditions are known at some upstream section, those at any arbitrary section downstream can be expressed in terms of known values at the upstream section. From the ideal gas equation of state,

$$\frac{p}{\rho} = \frac{p_1}{\rho} = \frac{\overline{RT}}{MW} = \text{constant} \qquad \text{(II- 9)}$$

From the equation of continuity,

$$\bar{v}\rho = \bar{v}_1\rho_1 = \text{constant} \qquad \text{(II-10)}$$

therefore

$$\frac{d\bar{v}}{\bar{v}} = \frac{-dP}{P} \qquad \text{(II-11)}$$

Inserting these relationships into the momentum equation and integrating gives:

$$\rho_1^2 - \rho_2^2 = \frac{\rho_1 \bar{v}^2 \rho_1}{g_c}\left(4f\frac{L}{D} - 2\ln\left(\frac{P_2}{P_1}\right)\right) \qquad \text{(II-12)}$$

Introducing the Mach number $M = v/c$, the final working equation becomes

$$4f\frac{L}{D} = \frac{1}{\gamma M_1^2}\left[1 - \left(\frac{P_2}{P_1}\right)^2\right] - 2\ln\left(\frac{P_1}{P_2}\right) \qquad \text{(II-13)}$$

Laminar Flow in a Smooth Pipe:

For fully developed isothermal laminar flow of an incompressible fluid in a horizontal pipe, the momentum balance and the definition of viscosity can be used to show that (34):

$$f = \frac{16}{Re} \qquad \text{(II-14)}$$

This result can be arrived at from purely theoretical reasoning. The data of Stanton and Pannell (1) and Senecal and Rothfus (2) show excellent agreement with equation (II-14) up to a Reynolds number of about 2000.

Equation (II-14) is valid only for flow in straight pipes. If the pipe is not straight, the velocity distribution over the cross-section is altered. This leads to a secondary flow in the pipe and hence the frictional losses are greater than those in a straight pipe. Dean (3) and Adler (4) have made theoretical calculations for the case of laminar flow. It was found that the characteristic dimensionless variable, which determines the influence of curvature for laminar flow, is the Dean number:

$$De = \frac{1}{2} (Re) \sqrt{\frac{R}{r_B}} \qquad \text{(II-15)}$$

The experimental results of Adler (4) showed a large increase in the resistance to flow caused by the curvature for $\left(Re \sqrt{\frac{R}{r_B}} \right) > 3.16$. According to his calculations the following relationship held:

$$\frac{f_B}{f} = 0.1064 \left[Re \sqrt{\frac{R}{r_B}} \right]^{1/2} \qquad \text{(II-16)}$$

where f_B denotes the friction factor for a curved pipe. Additional experimental data indicated, however, that this relationship was invalid for values of the parameter $Re \sqrt{\frac{R}{r_B}}$ less than 630. Prandtl developed the following empirical relationship which closely approximates experimental data:

$$\frac{f_B}{f} = 0.37\ (De)^{0.36} \qquad \text{(II-17)}$$

This equation gives good agreement in the range

$$40 < Re\sqrt{\frac{R}{r_B}} < 1000$$

McAdams (6) presents a convenient graphical correlation which shows the effect of curvature on f for laminar flow in circular pipes. This plot also shows the effect of curvature on the transition Reynolds number.

The curvature of a pipe has a marked effect upon the transition Reynolds number causing transition to be delayed to higher Reynolds numbers. This effect is also caused by the distortion of the velocity profile. Transition Reynolds numbers as high as 8000 have been reported for pipes with high curvature.

For laminar flow in a straight pipe the particles of fluid move in a direction parallel to the solid boundaries, and there is no velocity component normal to the axis of the conduit. For fully developed laminar flow in a circular pipe of constant cross-section the velocity profile is parabolic and the following relationships hold:

$$\bar{v} = \frac{v_{max}}{2} \qquad \text{(II-18)}$$

$$v = v_{max}\left[1 - \left(\frac{r}{R}\right)^2\right] \qquad \text{(II-19)}$$

Experimental investigations have substantiated the accuracy of these equations.

Turbulent Flow in a Smooth Pipe:

At a Reynolds number of about 2100 the behavior of the friction factor changes drastically from that predicted by equation (II-14). Below a Reynolds number of 2100 the friction factor steadily decreases with increasing Reynolds number. When the friction factor reaches a value of 0.0075 - corresponding to a Reynolds number of about 2100 - it then begins to increase with further increases in the Reynolds number. This increase continues until a value of about 0.011 is reached - corresponding to a Reynolds number of about 3300. From this point on, the friction factor decreases steadily with increasing Reynolds number.

The reason the friction factor changes its behavior in such an abrupt manner is that there is a change in the flow mechanism. In the Reynolds number range 2100 - 3300 the flow is changing from a laminar type, characterized by fluid particles moving in a straight path, to a turbulent type, characterized by fluid particles where motions vary chaotically with time in magnitude and direction.

The turbulent flow regime normally occurs above a Reynolds number of about 3300. For the case of a smooth pipe of constant circular cross-section, this regime is characterized by a constantly decreasing friction factor out to a Reynolds number past 10^7.

In 1913 Blasius (7) made a critical survey of all available data and arranged them in dimensionless form in accordance with Reynolds' law of similarity. He was able to establish the following empirical equation:

$$f' = \frac{0.079}{Re^{0.25}} \qquad \text{(II-20)}$$

This relationship is valid for smooth pipes of circular cross-section and is known as the Blasius formula. It is accurate up to a Reynolds number of 100,000. At the time when Blasius made his study, data were not available at higher values.

In 1914 Stanton and Pannell (1) conducted experiments on the flow of air, water, and oil, covering a range of Reynolds numbers from 10 to 500,000. Later, Nikuradse (8) investigated the flow of water in smooth pipes for Reynolds numbers ranging from 4,000 to 3,240,000. The data obtained by these workers clearly showed that the Blasius equation could not be used to predict values of friction factors for Reynolds numbers above 100,000. It was shown that the Blasius equation predicted a friction factor which was lower than that actually measured.

Using his own data and that of Stanton and Pannell, Nikuradse obtained the following relationship between f and Re:

$$\frac{1}{\sqrt{f}} = 4.0 \log (Re \sqrt{f}) - 0.40 \qquad \text{(II-21)}$$

This equation is applicable over a Reynolds number range of 4000 to 3,240,000. The theoretical work of von Karman (9) and Prandtl (10) led to the derivation of an equation with the same form as equation (II-21) but differing in the values of the constants. The relationship which was derived is:

$$\frac{1}{\sqrt{f}} = 4.06 \log (Re \sqrt{f}) - 0.60 \qquad \text{(II-22)}$$

The difference between the values predicted by these two equations is very small.

The flow of gases through smooth pipes at very high velocities was investigated by Froessel (11). By taking into account the fact that the density of the fluid was not constant along the length of the pipe and that the velocity changed between the inlet and outlet of the test section, he concluded that the friction factors are not markedly different from those in incompressible flow. Data obtained by Keenan and Neumann (12) also indicates that the friction factor is the same function of Reynolds number for compressible flow as for incompressible flow.

Neither equation (II-21) nor (II-22) can be used to solve directly for a friction factor given a value of the Reynolds number; hence an iterative technique must be used since the friction factor appears in the logarithmic term. Because of this, a simpler relationship between the Reynolds number and the friction factor is desirable. Drew et al (13) developed an empirical relationship based on 1,310 experiments covering a Reynolds number range from 3,000 to 3,000,000. This relationship has the following form:

$$f = 0.00140 + 0.125\ (Re)^{-0.32} \qquad \text{(II-23)}$$

The friction factor plot based on this equation has been used extensively in reference texts (14,15). From equation (II-23) it is apparent that as the Reynolds number increases, the friction factor approaches a minimum value of 0.0014. This implies that at large values of Reynolds number the friction factor becomes independent of viscosity--

i.e., the contribution of viscous shear is negligible in comparison with kinetic effects.

There is another relationship (58) which is often found in the chemical engineering literature. It is used in heat tranfer calculations which make use of the analogy between the transfer of momentum and the transfer of heat.

$$f = \frac{0.046}{Re^{0.20}} \qquad \text{(II-24)}$$

Note that this relationship is similar to the Blasius formula.

Turbulent flow in circular tubes has been studied extensively since it occurs most frequently in practice. Numerous velocity profiles for flow in smooth tubes have been determined experimentally and a universal relationship which expresses the velocity distribution in a tube has been determined. The studies of Stanton et al (16), Nikuradse (8), Reichardt (17), Deissler (18), and Rothfus and Monrad (19) have provided data for this development.

The velocity profile in turbulent flow is quite different from that in laminar flow. For fully developed turbulent flow in a smooth circular pipe of constant cross-section the following relationships hold:

$$\bar{v} = \frac{v_{max}}{1.25} \qquad \text{(II-25)}$$

$$v = v_{max}\left[1 - \frac{r}{R}\right]^{\frac{1}{7}}$$

Note that these relationships are based on empirical correlations and are only approximations.

The work of Nikuradse (8) is especially interesting. His experimental investigations led to the relationship:

$$v = v_{max} \left[1 - \frac{r}{R}\right]^{\frac{1}{n}} \qquad \text{(II-27)}$$

where the exponent n varies with the Reynolds number. The value of the exponent for the lowest Reynolds number studied (Re = 4000) is n = 6; it increases to n = 7 at Re = 110,000 and to n = 10 at the highest Reynolds number attained (Re = 3,240,000). Nikuradse's work can be used to express the relationship between the mean and the maximum velocity:

$$\bar{v} = \left[\frac{2n^2}{(n + 1)(2n + 1)}\right] v_{max} \qquad \text{(II-28)}$$

For a value of n = 6, v/v max = 0.791: for n = 10, v/v max = 0.865.

Another concept which has been shown to be quite useful is that of the "universal velocity distribution". This concept begins by considering the fluid in a pipe as being divided into three separate zones: a central zone, in which only turbulent effects are important, a buffer zone, in which both laminar and turbulent effects are important, and a laminar sublayer in which only laminar effects are important. The velocity distribution for each one of the zones is then determined using expressions for the shear stresses. An excellent treatment of this topic is given in Bird, Stewart, and Lightfoot (20) and Knudsen and Katz (21). Analytically, the universal velocity distribution is given by the equations:

1. Laminar sublayer:

$$v^+ = y^+ \qquad 0 < y^+ < 5 \qquad \text{(II-29)}$$

2. Buffer zone:

$$v^+ = 5.0 \ln y^+ - 3.05 \qquad 5 < y^+ < 30 \qquad \text{(II-30)}$$

3. Central (turbulent) zone:

$$v^+ = 2.5 \ln y^+ + 5.5 \qquad 30 < y^+ \qquad \text{(II-31)}$$

It was from the concept of the universal velocity distribution that equation (II-22) was developed.

The previous results for turbulent flow in a smooth pipe apply only to straight pipes. In curved pipes, the friction factor is always greater. White (22) has found that the friction factor for turbulent flow in a curved pipe can be represented by the equation:

$$\frac{f_B}{f} = 1.0 + 0.075\ Re^{1/4} \left(\frac{R}{r_B}\right)^{1/2} \qquad \text{(II-32)}$$

In turbulent flow Ito (23) found that the relationship could be expressed as:

$$\frac{f_B}{f} = Re \left(\frac{R}{r_B}\right)^2 \quad 0.05 \qquad \text{(II-33)}$$

for $Re\ (R/r_B)^2 > 6$

Ito also developed a complementary relationship:

$$f_B \left(\frac{r_B}{R}\right)^{1/2} = 0.00725 + 0.076 \left[Re \left(\frac{R}{r_B}\right)^2\right]^{-0.25} \qquad \text{(II-34)}$$

for $300 > Re\ (R/r_B)^2 > 0.34$

Hawthorne (24) gives an analytical study of the phenomenon of secondary flow in curved pipes. Extensive measurements and theoretical calculations on flow losses in turbulent flow have also been carried out by Detra (25) who included curved pipes of noncircular cross-section in his studies. It should also be noted that the curvature of a pipe has a large effect upon the transition Reynolds number causing transition to be delayed to higher Reynolds numbers.

Turbulent Flow in Rough Pipes - Irregular Roughness:

The discussion thus far has been limited to smooth pipes, without really defining smoothness. It has long been known that, for turbulent flow, a rough pipe leads to a larger friction factor for a given Reynolds number than does a smooth pipe. If the roughness in a pipe is reduced, the friction factor will be reduced. Continued polishing can get a pipe so smooth that additional polishing has no further effect on the reduction in the friction factor for a given Reynolds number. The pipe is then said to be hydraulically smooth. The previous relationships for turbulent flow are valid for this case only.

In order to discuss in a quantitative way the effect of roughness, some parameter which describes the roughness must be defined. The most exact procedure is to describe the height, the spacing, and the orientation of the projections into a pipe. In some cases, this complete description will not be required - in others, we must be precise as to the geometric nature of the projections.

As stated previously, the resistance to flow offered by a rough wall is greater than that of a smooth wall. This is indicated by the larger value of the friction factor for the rough wall at a given

Reynolds number. Since the value of the friction factor plays a significant part in the design of most piping systems, a critical question involves the matter of evaluating the degree of roughness and the extent to which this increases the friction factor over that of smooth pipe.

In 1933, Nikuradse (26) made a very intensive study of this problem. In this study he used circular pipes covered on the inside as tightly as possible with sand of a definite grain size glued to the wall. By choosing pipes of varying diameters and changing the size of the grain, he was able to vary the relative roughness ε/R from about 1/500 to 1/15.

In the region of laminar flow Nikuradse found that all rough pipes had the same friction factor as a smooth pipe. The critical Reynolds number was also found to be independent of roughness. The change in the behavior of the friction factor was also observed above a Reynolds number of about 2100. Again, as in the case of a smooth pipe, the friction factor increased with an increase in Reynolds number until a Reynolds number of about 3000 was reached. In the turbulent region he found that there is a range of Reynolds numbers over which pipes of a given relative roughness behave in the same way as smooth pipes, that is, they follow the relationship

$$\frac{1}{\sqrt{f}} = 4.0 \log (Re\sqrt{f}) - 0.40 \qquad \text{(II-21)}$$

The rough pipe can, therefore, be said to be hydraulically smooth in this range and the friction factor depends on Reynolds number only. Beginning with a definite Reynolds number, the magnitude of which increases as ε/R decreases, the friction factor deviates from the smooth pipe relationship. At first, the friction factor continues to decrease, but then it

passes through a minimum and then increases to its final asymptotic value. Nikuradse concluded that three regimes must be considered:

1. Hydraulically smooth regime:

$$0 < \frac{\varepsilon v^*}{\nu} < 5 \ , \ f = g(Re)$$

The size of the roughness is so small that all protrusions are contained within the laminar sublayer.

2. Transition regime:

$$5 < \frac{\varepsilon v^*}{\nu} < 70 \ , \ f = g(\varepsilon/R, \ Re)$$

Protrusions extend partly outside the laminar sublayer and the additional resistance, compared with a smooth pipe, is due mainly to the form drag caused by the protrusions in the boundary layer.

3. Completely rough regime:

$$\frac{\varepsilon v^*}{\nu} > 70 \ , \ f = g(\varepsilon/R)$$

All protrusions reach outside the laminar sublayer and the resistance to flow is due to the form drag on them.

In the hydraulically smooth regime Nikuradse showed that equation (II-21) could be used to correlate his results. In the completely rough regime he found that the following equation could be used:

$$\frac{1}{\sqrt{f}} = 4.0 \log \left(\frac{D}{\varepsilon}\right) + 2.28 \qquad \text{(II-35)}$$

Note that this relationship is independent of the Reynolds number and is accurate for values of $\frac{R/\varepsilon}{Re\sqrt{f}} > 0.005$.

An equation which correlates the entire region from hydraulically smooth to completely rough flow was established by Colebrook and White (27).

$$\frac{1}{\sqrt{f}} = 4.0 \log \frac{D}{\varepsilon} + 2.28 - 4.0 \log \left(1 - 4.67 \frac{D/\varepsilon}{Re\sqrt{f}} \right) \qquad \text{(II-36)}$$

For $\varepsilon \to 0$ this equation transforms into equation (II-21) valid for hydraulically smooth pipes. For $Re \to \infty$, it transforms into equation (II-36) for the completely rough regime. In the transition region this equation can be used as a good approximation to the data. Note that in the transition region the friction factor is a function of both the relative roughness and the Reynolds number.

Nedderman and Shearer (28) present an improved correlation for the transition region. They reason that the flow in the turbulent core is only affected by that part of the roughness element which projects beyond the sublayer. Thus one would expect the friction factor to correlate better with $\varepsilon - 5y^+$ than with ε. The relationship which they developed is as follows:

$$\frac{1}{\sqrt{f}} = 3.48 - 4.0 \log \left[\frac{\varepsilon}{R} - \frac{14.14}{Re\sqrt{f}} \right] \qquad \text{(II-37)}$$

This equation is valid for values of $\varepsilon^+ > 12$.

Dukler (29) gives a single equation which he claims will accommodate the full range of Reynolds numbers and relative roughness which are of commercial interest. He expresses the effect of wall roughness as a shift in the velocity distribution curve, when this curve is expressed in the usual dimensionless coordinates. The expression he develops for the friction factor at any roughness condition and Reynolds number is:

$$\frac{1}{\sqrt{f/2}} = 1.03 + 5.76 \log \left\{ \frac{Re}{2} \sqrt{\frac{f}{2}} \right\} - 1.75\, \epsilon^{+} - 1.10\, (\log \epsilon^{+})^2 \qquad \text{(II-38)}$$

where $\epsilon^{+} = Re\ (\epsilon/D)\ \sqrt{f/2}$. This equation is valid for $\epsilon > 0.05$. Below this, equation (II-21) should be used.

Knudsen and Katz (21) present a friction factor chart for the determination of the Fanning friction factor in either smooth or rough pipes. The chart is derived from equation (II-14) for laminar flow, equation (II-21) for turbulent flow in smooth tubes, equation (II-35) for fully turbulent flow in rough pipes, and equation (II-36) for the transition region, where the friction factor is a function of both the roughness and the Reynolds number. Also presented is a chart giving the roughness of commercial pipe as a function of the diameter. Various materials of construction are considered.

It should be noted that the behavior of a sand-roughened pipe is different from that of a rough commercial pipe. Nedderman and Shearer (28) state that the fundamental difference between the two types of roughness can be illustrated by a comparison of the relationship between the friction factor and the Reynolds number. For turbulent flow in a commercial pipe the friction factor decreases smoothly as the Reynolds number is increased and reaches an asymptotic value at high Reynolds numbers. In a sand-roughened pipe the friction factor at first decreases, passes through a minimum and then increases to its final asymptotic value. They attribute this difference in behavior to the fact that the roughness in an artificially sand-roughened pipe is more or less regular in form whereas the roughness in a commercial pipe is doubtless of a random nature.

As might be expected, the velocity distribution in a rough pipe is different from that in a smooth pipe. Expressing the velocity distribution function by a power formula similar to equation (II-27), i.e.,

$$v = v_{max} \left(1 - \frac{r}{R}\right)^{1/n} \qquad \text{(II-27)}$$

gives a value of the exponent of from 1/4 to 1/5.

Tyul'panov (30) noted that as the relative roughness of a tube increased the velocity profile became more pointed. Evaluating his experiments in the form of a power law, Tyul'panov showed that the value of n, for flow in tubes with roughness $\varepsilon/R = 0.1$ and 0.2, changed along the tube radius and had values from 2 to 4 (for Re = 10,000) and from 2.5 to 4 (for Re = 135,000). This deviation from the power law indicated that to some degree of approximation the velocity profile could be described by a parabolic relationship.

Also, the logarithmic law for velocity distribution was found to be valid for rough pipes. This relationship can be represented by an equation of the form:

$$v^+ = 2.5 \ln \frac{y}{\varepsilon} + B \qquad \text{(II-39)}$$

where B assumes different values for the three ranges of roughness discussed previously. In the completely rough regime experiment indicates that B = 8.5, so that in this region equation (II-40) becomes:

$$v^+ = 2.5 \ln \frac{y}{\varepsilon} + 8.5 \qquad \text{(II-40)}$$

In general, B is found to be a function of the roughness Reynolds number $v^*\varepsilon/\nu$. For the hydraulically smooth region it can readily be shown that

$$B = 5.5 + 2.5 \ln \frac{v^*\varepsilon}{\nu} \qquad \text{(II-41)}$$

Nedderman and Shearer (28) also give a relationship for the velocity profile in a rough pipe:

$$v^+ = 2.5 \ln \left(\frac{y^+}{\varepsilon^+ - 5} \right) + 8.5 \qquad \text{(II-42)}$$

This equation is valid for values of $\varepsilon^+ > 12$.

Turbulent Flow in Rough Conduits - Regular Roughness.

Since the grains of sand were glued to the wall as closely to each other as possible, the roughness obtained by Nikuradse can be said to be of maximum density. In many common situations the roughness density of pipe walls is considerably smaller and such roughness can no longer be completely described by the height of a protrusion ε, or by the relative roughness ε/D only. When this is the case, Schlichting (31) recommends that such roughness be arranged on a scale of standard roughness and to adopt Nikuradse's sand roughness for correlation. This approach is most convenient when the flow is in the completely rough region and the friction factor is given by an equation similar to equation (I-22). The method involves correlating any given roughness with its equivalent sand roughness and to define it as that value which gives the actual friction factor when inserted into equation (II-35).

Schlichting (32) experimentally determined values of equivalent sand roughness for a large number of roughnesses arranged in a regular fashion. Similar measurements were made by Morbius (33) on pipes which had been made rough by cutting threads of various forms into them.

The difficulty in applying the above methods is that it is sometimes impossible to fit rough surfaces satisfactorily into the scale of sand roughness. Schlichting (31) relates how a peculiar type of roughness, giving very large values of the friction factor, was discovered in a water duct in the valley of the Ecker. This pipe had a diameter of 500 mm. and after a long period of usage it was noted that the mass flow had decreased by more than 50 percent. Upon examination it was found that the walls of the pipe were covered with a rib-like deposit only 0.5 mm high, the ribs being at right angles to the flow direction. The effective sand roughness indicated values of ε/R of 1/40 to 1/20, however, the actual geometric relative roughness had the value of 1/1000. It appears that rib-like corrugations lead to much higher values of friction factor than sand roughness of the same absolute dimension.

Kundsen and Katz (34) report the determination of friction factors for the turbulent flow of water in annuli containing transverse-fin tubes. For this system the friction factor is seen to be a function of two geometric dimensionless numbers. The relationship between the friction factor and the two dimensionless groups is presented in the form of a chart.

Konobeev and Zhavoronkov (35) of the Soviet Union report a detailed study on the hydraulic resistances in tubes with wavy roughness. They investigate pipes of both long and short wave roughness. Long-wave roughness is defined as that in which the ratio of the wavelength, λ, to the height, ε, is so large that the laminar sublayer is not destroyed at any point along the wall. The relationship for the friction factor in the case of long-wave roughness is:

$$f = \frac{0.079 + 8.2\ (\varepsilon/\lambda)^2}{Re^{0.25}} \qquad \text{(II-43)}$$

Note that as the value of ε/λ goes to zero ($\varepsilon \to 0$ or $\lambda \to \infty$) this equation reduces to the Blasius formula, equation (II-20).

Short-wave roughness is defined as being the condition in which the laminar sublayer is destroyed. Experimentally, it was found that the parameter $E = 2\varepsilon\ D_{ave}/\lambda^2$ could be used to differentiate between long-wave and short-wave roughness. Long-wave roughness corresponds to values of E less than 0.32, and short-wave roughness to values greater than 0.6. All values of E between 0.32 and 0.6 define an intermediate transitional region. For short-wave roughness the relationship for the friction factor was found to be:

$$f = \frac{0.03075}{\left[\log\ (D_{ave}/2\varepsilon)\right]^2} \qquad \text{(II-44)}$$

Note that this relationship is independent of the Reynolds number and the wavelength.

Nunner (36) reports some interesting results from his study on flow through artificially roughened tubes. He placed semicircular rings in in a tube so as to give a corrugated wall geometry. His results indicate a suddenly increasing friction factor near a Reynolds number of about 100,000. This increase occurs as a change from an otherwise constant value following the laminar to turbulent transition.

Koch (37) also performed work on an artificially roughened tube. The roughness pattern he studied was formed from orifice-shaped discs inside a smooth tube. Koch also reports a tendency for the friction factor to increase for a Reynolds number of about 100,000.

In 1953 Wieghardt (38) conducted experiments involving flow over rectangular ribs placed at right angles to the flow. He also conducted studies of flow over circular cavities. Both of these systems gave an increase in the drag coefficient of the plate to which the ribs were attached or in which the holes were drilled. Photographs in the article show vortex patterns observed in the holes.

Morris (39) proposed a concept of flow over rough pipe based upon the effect of the longitudinal spacing of surface roughness elements and their associated vorticity streams. He recognized three basic types of rough conduit flow: (a) isolated-roughness flow, (b) wake-interference flow, and (c) quasi-smooth or skimming flow. Morris states that wake-interference flow is characterized by friction factor-Reynolds number curves in which the friction factor increases with increasing Reynolds number or is independent of Reynolds number at high values of Reynolds number.

Flow in Flexible Metal Hoses:

Reliable published data on flow losses in flexible hose are limited in that the data presented primarily deals with straight hose. Bend angle effects and other topological considerations have been neglected to a great extent. Also, the data that are available produce wide variations in the correlations presented by different investigators.

Gibson (40) gave the results of experiments on a pipe of 2.0 in. maximum bore, 1.8 in. minimum bore, and 0.4 in. pitch of corrugations. He observed that the loss of head was proportional to the mean velocity raised to an index greater than two. By dimensional analysis he then argued that this would lead to the apparently paradoxical result than an increase of viscosity would cause a decrease in the loss of head at a given rate of discharge. Further tests which he performed using water at two different temperatures confirmed this conclusion.

Neill (41) investigated the losses in "standard" corrugated piping having a minimum diameter of 15 inches with corrugations 1/2 inch deep and a pitch of 2/3 inch. Using these results and the data obtained by other investigators he suggested the following relationship:

$$f = 0.16 \left(\frac{\varepsilon}{D}\right)^{1/2} \qquad \text{(II-45)}$$

Note that this expression is independent of Reynolds number and therefore the friction factor should be determined by pipe geometry alone.

Straub and Morris (42) also investigated flow in corrugated pipes. They state that the friction factor was found to increase with increases in the flow rate and water temperature. This result was found to occur throughout the range of Reynolds numbers from 76,000 to 1,263,000. In the words of the authors, "This unanticipated result was indicated quite definitely and systematically by the experiments."

This trend for the friction factor to increase can also be seen in the results of the roughest of pipes tested by Streeter (43). He concluded that the shape of the grooves was nearly as important as their depth in the determination of the friction factor. In addition, he noted

that, by comparison with the results of Nikuradse, the diameters of the equivalent grains of sand used in roughening the pipes always exceeded the depths of the grooves.

A comparison between Streeter's and Nikuradse's results is shown by Finniecome (44). This comparison clearly shows that the friction factor for a corrugated pipe does not tend to become constant until a higher Reynolds number has been reached than would be the case for a pipe roughened by grains of sand. However, the friction factor does eventually approach a constant value.

It seems that for pipes with the deepest corrugations, there is a tendency for the rising portion of the graph of f versus Reynolds number to be prolonged in comparison with the readings obtained from tests on smoother pipes. This effect was observed by Hoeck (57) from many experiments on pipes with varying degrees of roughness and having internal diameters ranging from 31.5 to 86.6 inches.

Allen (45) performed experiments on a corrugated pipe of 0.5 inch minimum diameter, 0.813 inch maximum diameter and 0.104 inch pitch. For the transition from laminar to turbulent flow he found a critical Reynolds number of 1700 - for flow in a smooth pipe the value is about 2100. Also, he found that the index of the mean velocity $\bar{v}$ in the equation

$$h = c_o \bar{v}^n \qquad \text{(II-46)}$$

(where h is the loss of head and c_o a proportionality constant) is approximately 2.31 over the upper portion of the velocity range. Alternatively, a value of 2.434 was derived from a statistical analysis using the method of least squares. Allen's results clearly indicate that the corrugations have the effect of increasing the value of the friction

factor compared to the results of tests on smooth pipes. However, his results also show that the influence of the corrugations may be decreased if their pitch is so small that each corrugation forms a pocket of dead-water which takes no real part inthe general flow pattern. Some investigators describe the fluid in the corrugations as forming a "pseudo wall" under such conditions. The conclusion that Allen draws is that the effect of increasing the depth of corrugations in a pipe is small after a certain depth has been reached, because the disturbances are confined to the region adjacent to the crest of the corrugations, i.e., where the diameter of the pipe is a minimum.

Daniels (46) used the Weisbach-Darcy equation for frictional pressure loss and calculated friction coefficients for annular and helical type hoses. He indicates that the loss through a given size flexible hose may be seven to fifteen times greater than that of a comparable size conventional pipe. Also, he indicates that the helical type hose has a lower pressure loss than the annular type. Because his data were taken at very high Reynolds numbers (above 500,000), Daniels found that the friction factor was constant and not a function of Reynolds number.

Daniels and Fenton (47) present extensive data for both corrugated hose and interlocked hose. They conclude from their data that the loss factor for flexible hose elbows is normally higher than the value accepted for smooth pipe elbows. A correlation for the friction factor is also presented in this paper:

$$\frac{f}{ND} = 0.10 \left(\frac{\varepsilon}{D}\right)^{1.6} \qquad \text{(II-47)}$$

Daniels and Cleveland (48), gathering data from several sources, have developed a generalized graphical method for predicting the pressure loss in both straight and bent flexible sections. Their plots show an abrupt increase in the friction factor at a Reynolds number of about 100,000. At higher Reynolds numbers the friction factor approaches a constant value. Again, the relative roughness, ϵ/D, is used as a parameter on the friction factor--Reynolds number plot.

Pepersack (49) also presents graphical correlations to predict the pressure losses in straight and curved sections of flexible metal hose. The pressure drops reported are from 4 to 19 times the loss through an equivalent smooth tube. Recommended multiplying factors for predicting the pressure loss in straight flexible hose are presented as a function of Reynolds number. The data were taken using metal hoses with diameters from 1/2 to 4 inches. Also, presented as function of Reynolds number is a pressure loss coefficient for 90^{o} bends for flexible metal hose with $r_B/D = 6$ to 36. Pressure loss correction factors for bends other than 90^{o} are also included.

Workers at Mississippi State University (50) developed a correlating equation from which the pressure losses for a gas flowing in flexible convoluted connectors may be predicted. The equation has the form:

$$\frac{1}{\sqrt{f}} = 3.48 - A_o \ln\left[\frac{(A_1)^{A_2}}{1 + \frac{A_3}{(Re)^4}} + \frac{A_4}{Re\sqrt{f}}\right] \qquad \text{(II-48)}$$

where A_o, A_1, A_2, A_3, and A_4 are constants which are of themselves functions of the geometry of the hose and the Reynolds number. The

results obtained from this study also showed a sudden increase in the friction factor at a Reynolds number of about 100,000.

Daniels and Cleveland (51) have developed analytical expressions which fit the available data on flexible hose quite well. One such correlation, listed below, showed an average deviation of 17% between predicted and observed friction factors.

$$f = \frac{0.01975}{D^{0.2}} + \frac{(0.595)\ Y}{\left[6 \log\left(\frac{D}{\epsilon}\right) - 1.5\right]^3} \qquad \text{(II-49)}$$

where

$$Y = \frac{2}{\left((2.713)^X + \frac{1}{(2.713)^X}\right)}, \text{ and } X = \frac{3.84 \times 10^6}{Re^{1.224}}$$

Another correlation, based on the relationship developed by Nikuradse for flow in rough pipes, was also given for flow in flexible hoses.

$$f = \frac{2}{\left[A(E^+) - 3.75 - 2.0 \ln \frac{2\epsilon}{D_o}\right]^2} \qquad \text{(II-50)}$$

where the friction similarity function $A(E^+)$, must be determined empirically from a plot of $A(E^+)$ versus the parameter $E^+ = Re \sqrt{\frac{f}{2}} \left(\frac{\epsilon}{D_o}\right)$. The plot presented by Daniels and Cleveland can be represented by the following relationships:

$$\text{for } E^+ < 1000 \quad , \quad A(E^+) = 11.0$$

$$1000 < E^+ < 10{,}000 \quad , \quad A(E^+) = 3 \log E^+ + 20$$

$$10000 < E^+ \quad , \quad A(E^+) = 8.0$$

Hawthorne and von Helms (52) developed an analytical method for calculating pressure losses in corrugated hose by assuming that the corrugations behave as a series of uniformly spaced orifices. It is stated that flow losses are not induced in the valleys of the corrugations and therefore the relative roughness ε/D is not a relevant variable. They assume that the pressure drop is caused by a succession of individual flow expansions. The following is the equation given by Hawthorne and von Helms for straight sections:

$$f = \frac{1}{4}\left(\frac{D}{\lambda}\right)\left[1 - \left(\frac{D}{D + 0.438\lambda}\right)^2\right]^2 \qquad \text{(II-51)}$$

This paper also presents a correlation for bends and elbows.

In the study by Hawthorne and von Helms they assume that there is stagnant fluid in the valleys of the corrugations. This assumption has been attacked on the basis of a study by Knudsen and Katz (34). They report the observation of eddy patterns in an area between fins on a transverse-finned tube. They report that under almost all conditions of turbulent flow there is at least one eddy observed in the region between the fins. Their results can be analyzed by considering the ratio of the fin spacing to the fin height. For values of this ratio between 1.15 and 0.73 the flow pattern is characterized by one circular eddy between the fins, which becomes slightly elongated as the ratio nears the lower limit of 0.73. When the ratio ranges from 0.51 to 0.45, two circular eddies

form between the fins, and they rotate in opposite directions. When the ratio reaches a value of 0.31 a circular eddy forms at the outer edge of the fin space, but in the space between this eddy and the tube wall no steady circular eddies are observed.

Riley, et al (53) developed an equation for predicting friction factor in flexible hose which took the form:

$$f = \alpha\ (Re)^{\beta} \qquad \text{(II-52)}$$

where α and β are functions of hose geometry. It was found that two correlations were needed to define α - one for annular-type hose and one for helical-type hose. The functional form of the relationship for annular hose was found to be:

$$\alpha = 0.01588 \left(\frac{\lambda - \sigma}{\varepsilon}\right) - 0.00215 \qquad \text{(II-53)}$$

The correlation for the helical-type hose is similar:

$$\alpha = 0.0292 \left(\frac{\lambda - \sigma}{\varepsilon}\right) - 0.00886 \qquad \text{(II-54)}$$

The quantity β is a function of the geometric parameter $(\sigma\varepsilon/\lambda^2)$. The correlation developed with this parameter is independent of the type of hose used - that is, it can be used for both helical and annular-type hose.

$$\beta = 0.299 \left(\frac{\sigma\varepsilon}{\lambda^2}\right) - 0.0313 \qquad \text{(II-55)}$$

The correlation for curved flexible hose sections was also found to be independent of the type of hose used.

$$\frac{f_B}{f} = 1.0 + 7.898 \left(\frac{D}{r_B}\right)^{0.0896} \qquad \text{(II-56)}$$

Volume II of a report (54) on a National Aeronautics and Space Administration project performed at Louisiana State University contains all of the data used in this study. Also, Volume III of this report contains the data reduction computer programs used for the data reported in this dissertation.

A review of the existing literature on flow in flexible hoses indicates that previous design correlations have been developed almost entirely on an empirical basis. It is hoped that by using a mechanistic approach this study will lead to an accurate design correlation based on sound theoretical reasoning and that this will lead to a better understanding of the flow system.

CHAPTER III

EXPERIMENTAL CONSIDERATIONS

The experimental approach was to measure the frictional losses produced by flow in flexible metal hoses. Both air and water were chosen as test fluids so that the results would not depend too heavily on just one fluid system. Both straight and curved sections of hose were studied. Furthermore, the equipment was designed and operated with the objective of producing accurate and precise data.

Flexible Metal Hose:

There are basically two types of flexible metal hose - corrugated hose and interlocked hose. Both of these types are available in a wide variety of constructions, sizes, metals, pressure ratings, and flexibility. The most common method of manufacturing corrugated type hose involves corrugating thin-walled tubing. This type of hose obtains its flexibility from bending of the metal corrugations. The interlocked hose is made by winding a pre-formed metal strip into a helically interlocked length of flexible tubing. The flexibility is obtained from sliding of metal components in the interlock.

In this study only corrugated flexible hoses were tested. Manufacturers classify these corrugated hoses as follows:

I. Annular-type hose

   A. Close Pitch
   B. Open Pitch

II. Helical-type hose

The results of this study indicate that the annular-type hose need not be subclassified into open or close pitch in so far as flow loss correlations are concerned. The annular correlation developed was found to be applicable to either type. The designations annular and helical refer to the nature of the convolutions of the flexible hose. The convolutions of the annular hose are accordion-like: those of the helical hose are spiraled.

In order that the correlation cover a wide range of practical applications the hose tested had to cover a wide range of geometric variations. The geometric variables for corrugated flexible hose can be seen in Illustration III-1. Table A-1of the appendix gives the dimensions of the hoses used in this study.

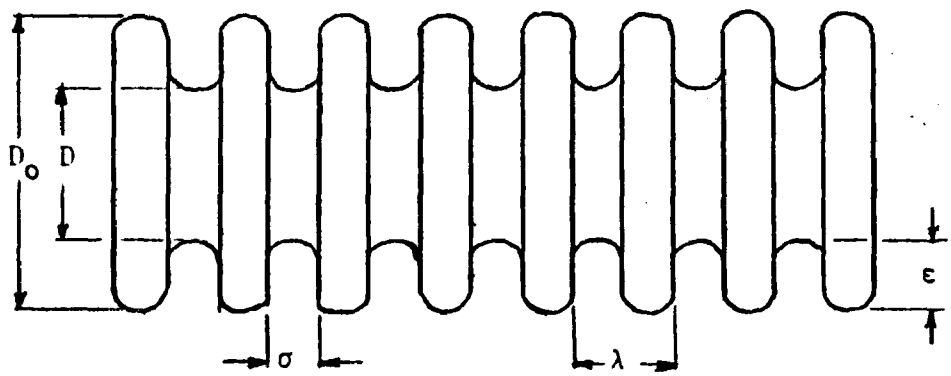

ILLUSTRATION III-1

Aside from the basic geometric linear variables there is also a shape factor which must be considered. This shape factor describes the nature of the convolutions. Illustration III-2 shows a "teardrop" shaped convolution.

ILLUSTRATION III-2

All flexible metal hoses studied in this work had a "finger" shaped convolution of the type shown in Illustration III-3.

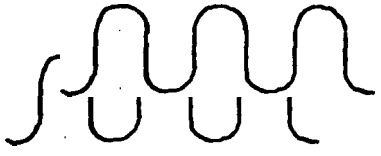

ILLUSTRATION III-3

One would expect that the "teardrop" shaped convolution would be more susceptible to having pockets of dead water between the corrugations. If so, the results reported in this work would be inapplicable to them.

In planning the experimental work it was decided that three types of corrugated hose would be used: closed pitch annular, open pitch annular, and helical. The sizes (nominal inside diameters) chosen were 1/2, 3/4, 1, 1 1/4, 1 1/2, 2, 2 1/2, and 3 inches. This gave a total of twenty-four flexible metal hoses. All test hoses were 10 feet in length with entrance and exit sections made of the same type flexible hose as was being tested.

Special note should be made of the flanges used to connect the test section with the entrance sections. Illustration III-4 is a schematic of a flange section.

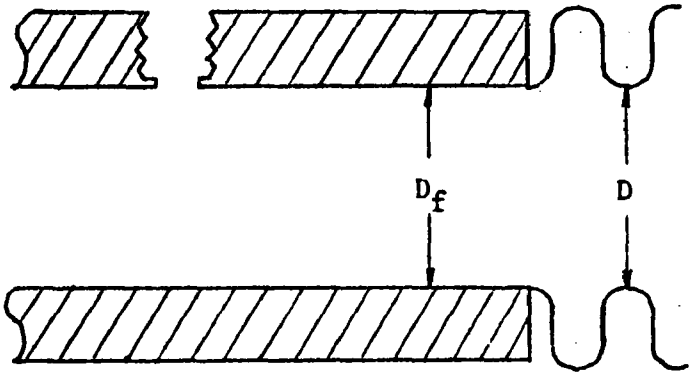

ILLUSTRATION III-4

There are two points which should be noted about this flange: (1) the pressure taps are included in the flange, and (2) D_F is equal to D--this is true for all hoses. Special care was also taken to see that the flange was connected to the flexible hose at the crest of a convolution.

As previously noted, the effect of bending the flexible hose was also to be investigated. Illustration III-5 shows the experimental set-up used to study this effect.

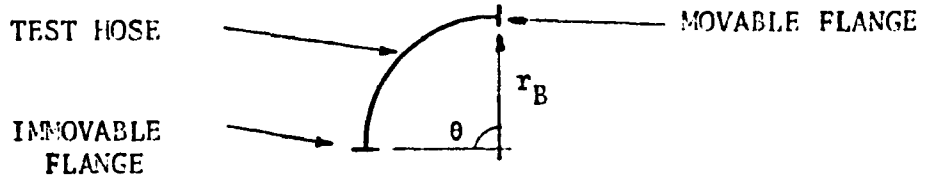

ILLUSTRATION III-5

Flow Systems:

The experimental equipment used in this study was designed and constructed to yield accurate data. Briefly, the equipment consisted of two units. The first was designed to measure the rate of flow of water through corrugated hose and the corresponding pressure loss; the second unit accomplishes the same objectives but with air as the flowing medium.

Water System:

Figure III-1 is a schematic diagram of the water system. Figures III-2 and III-3 are photographs of the test system showing the actual equipment. The following is a brief description of the individual pieces of equipment used.

1. Water was supplied by two centrifugal pumps connected in parallel. Each pump was powered by a U. S. Electrical, 3-phase, 220/440 volt, 7.5 h.p. electric motor and had the capacity to deliver 300 gpm with a 50 psig head. The water was stored in a rectangular tank and recirculated.

2. The flow rates were measured with two devices:

   a. A Builders Iron Foundry, Providence, R. I., 4.0 x 1.75 inch venturi meter for flow rates above 20 gpm; and

   b. A disc meter for flow rates below 20 gpm.

3. The flow rate was adjusted by manual setting of a 3" gate valve.

4. The pressure drop across the venturi meter was measured by a Builder-Providence, Inc., 22" single-arm, mercury manometer.

5. The pressure drop across the test section was measured by:

   a. Two "Bourdon" gauges for differentials above 15 psi

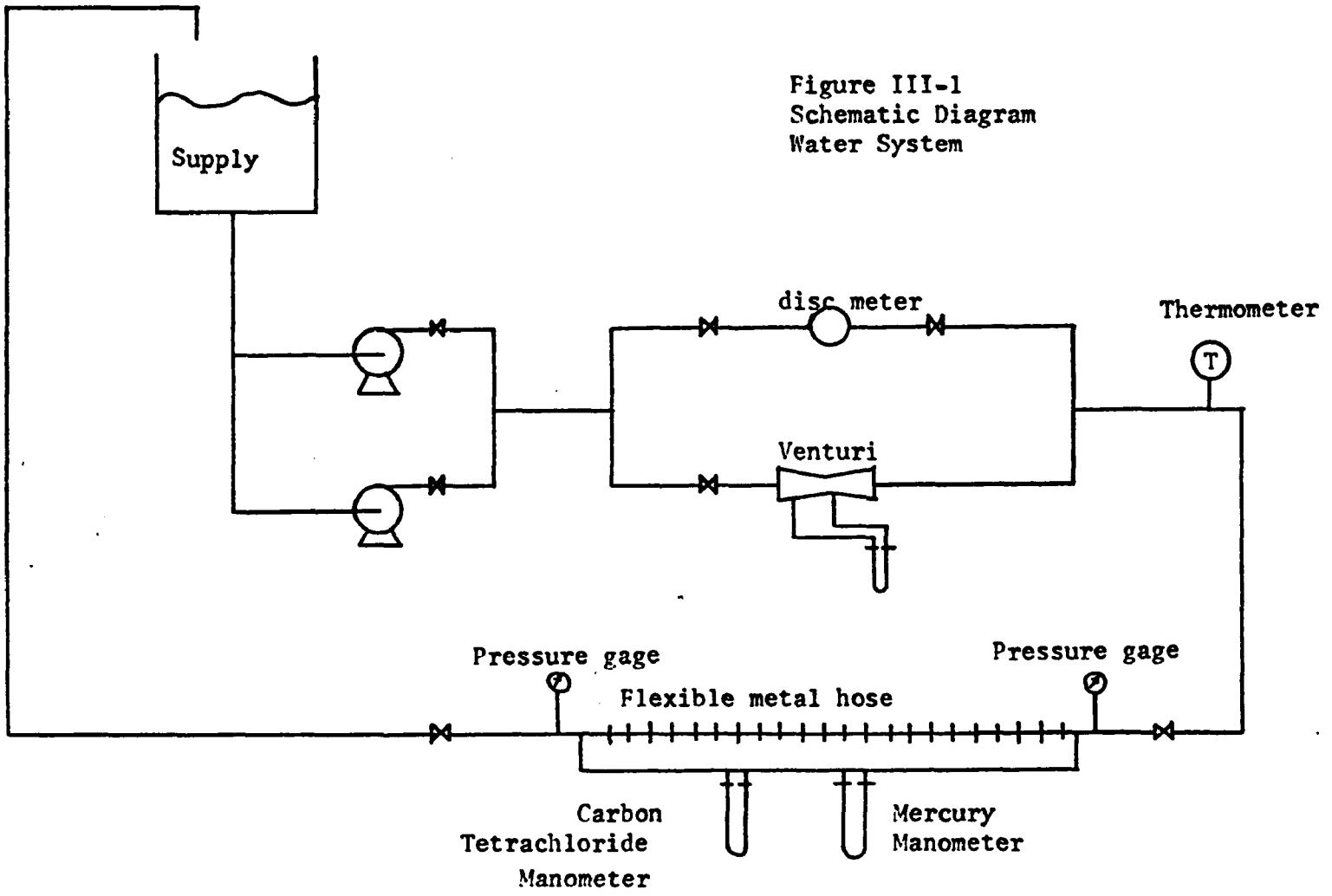

Figure III-1
Schematic Diagram
Water System

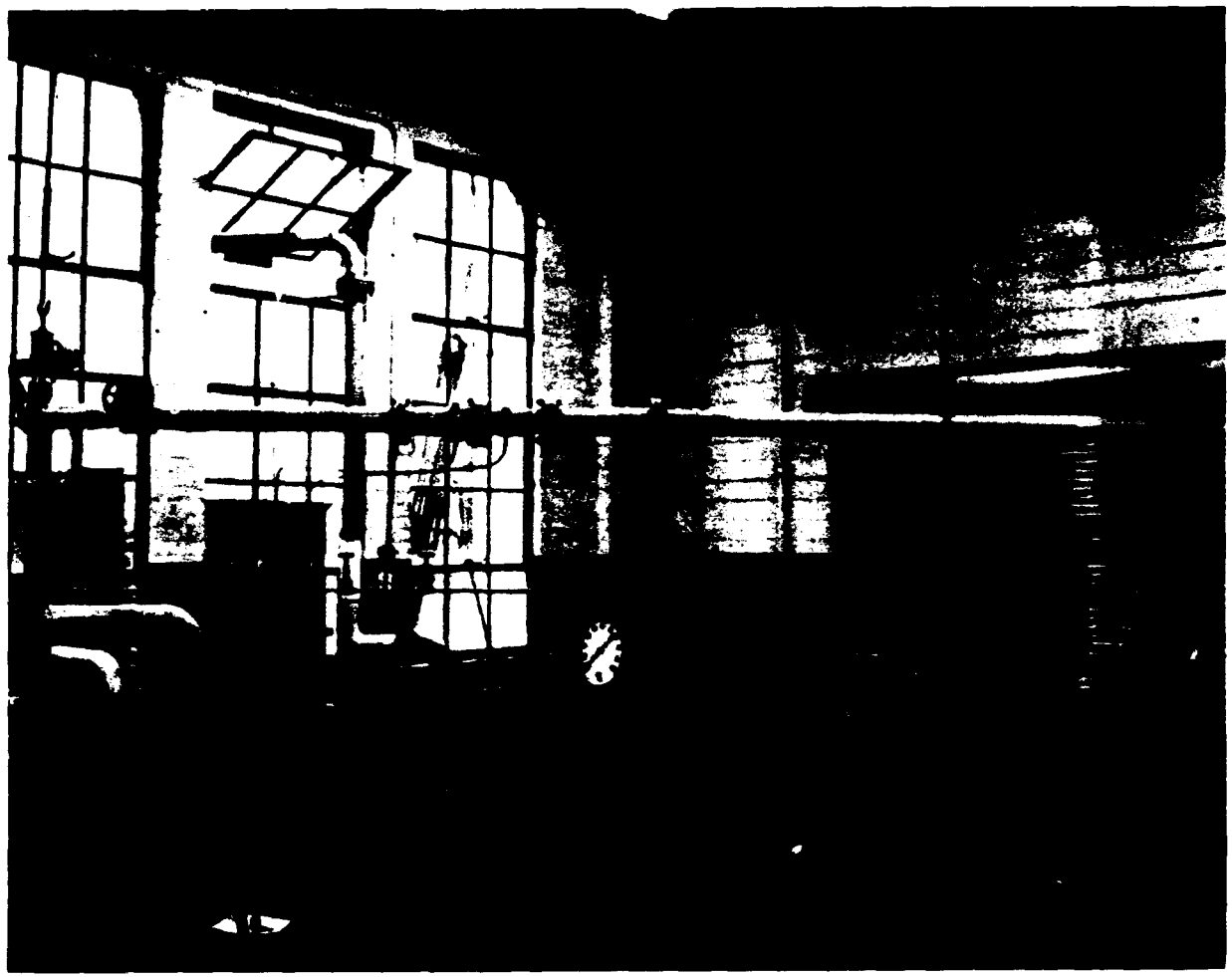

DATA PRODUCTION SYSTEM FOR WATER

FIGURE III-2

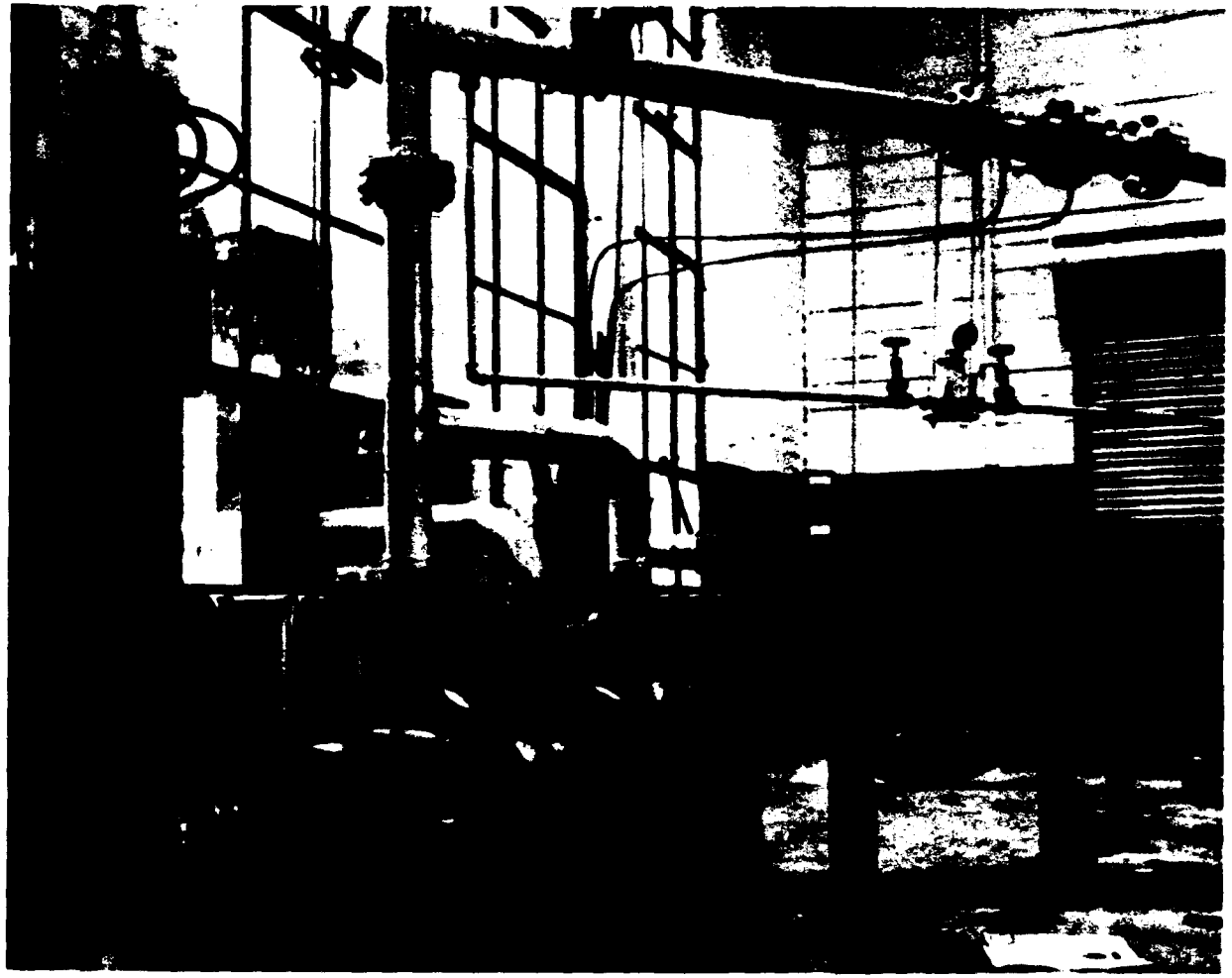

DATA PRODUCTION SYSTEM FOR WATER
SHOWING PUMPS AND CONTROLS

FIGURE III-3

b. A mercury u-tube manometer for differentials between 15 and 1 1/2 psi

c, A CCl4 u-tube manometer for differentials below 1 1/2 psi.

6. The temperature was measured by a 120°F mercury thermometer in a thermo-well.

Air System:

Figure III-4 is a schematic diagram of the air system. Figure III-5 is a photograph showing the control system used to control the flow rate of air through the flexible hose. The following is a brief description of the individual pieces of equipment used.

1. Air was supplied by

   a. One Davey Air Compressor rated at 210 CFM at 110 psi

   b. One Le Roi Air Compressor rated at 315 CFM at 125 psi

   c. A bank of electrically drive air compressors arranged in parallel to produce 250 CFM at 110 psi. The bank of compressors is located in the Mechanical Engineering Laboratories and were connected to this project in order to increase the overall capacity of the system.

2. The air-flow rate was measured with a standard orifice meter and mercury or carbon tetrachloride manometer.

3. The flow-rate was adjusted by use of a 3" Conoflow globe valve which was pneumatically actuated by a differential pressure ranging from 3 to 15 psi.

4. The inlet pressure to the hose was regulated and held constant by using a 2" Cash-Acme Pressure regulator, which had an operating pressure limit of 150 psi.

5. Pressure drops across the test sections were measured with standard type mercury or carbon tetrachloride differential manometers.

6. Pressure gauges and thermometers were installed in the system as indicated in Figure III-4.

7. Pressure taps were located in the connection flanges of the test section. Damping valves were used in the connectors to minimize fluctuations of the manometer fluid level.

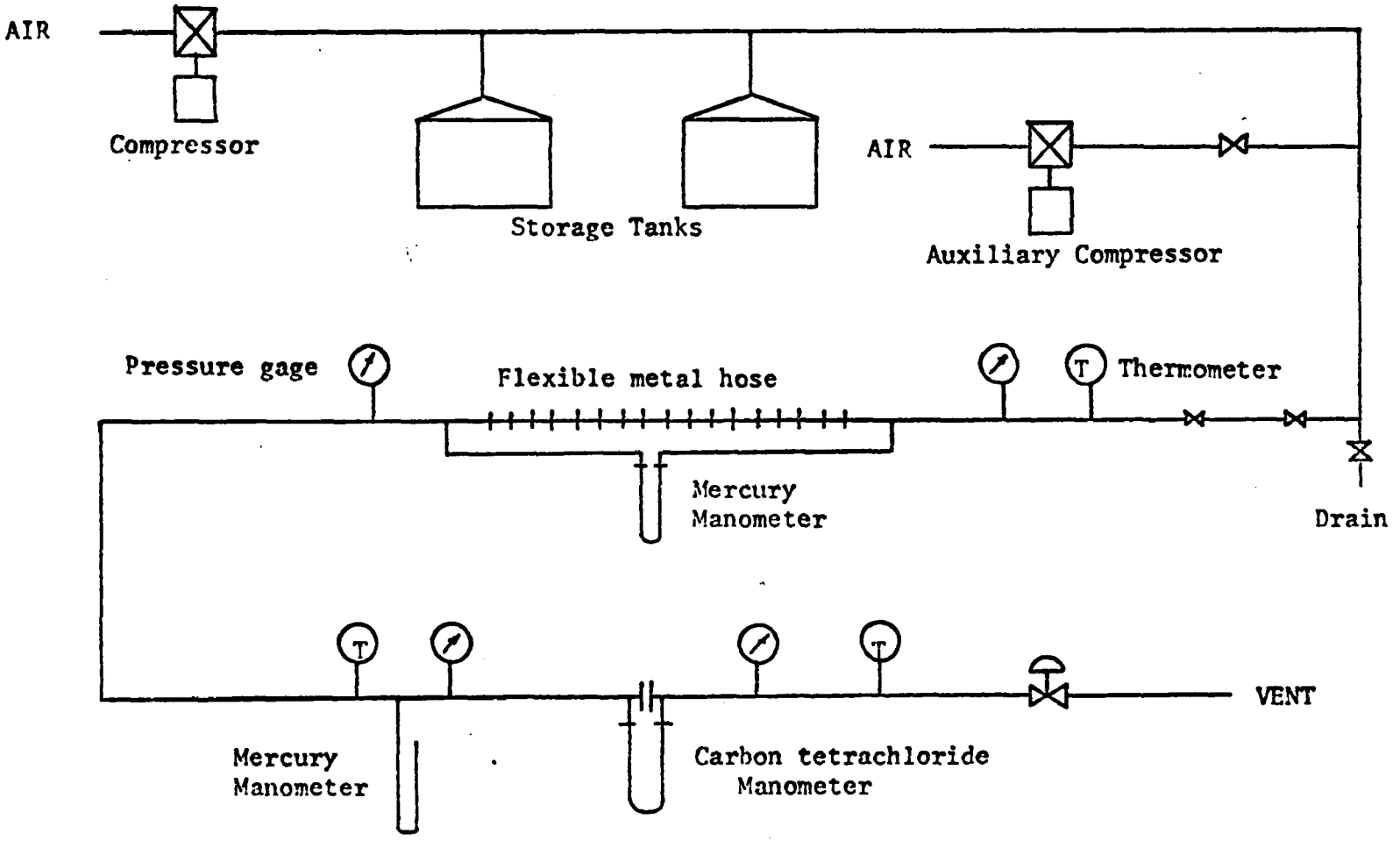

Figure III-4
Schematic Diagram
Air System

DATA PRODUCTION SYSTEM FOR AIR
SHOWING CONTROLS

FIGURE III-5

Experimental Procedure for Water System:

The basic experimental procedure employed for the water system is as follows:

1. Both pumps were started simultaneously and the system was allowed to stabilize.

2. The high rates were tested first so the control valve was opened until a maximum reading was obtained on the manometer connected to the venturi meter.

3. The pressure gauges on the test section were then observed to determine the range of pressure differential.

4. If the range was above 7 1/2 psi, the readings of the gauges were recorded along with the venturi manometer reading. If the range was below this value the appropriate manometer (u-tube) lead valves were opened, the lines bled, and the differential recorded instead of the gauge readings.

5. The flow rate was then decreased using the manometer across the venturi meter as a guide and the new flow meter and pressure differences were recorded.

6. The procedure in step 5 was followed until a flow rate of approximately twenty gallons per minute was observed. The flow was then directed through the disc meter and all subsequent flow rates were obtained by using a stop watch to determine the time for 5 to 10 gal. to pass through the disc meter.

Experimental Procedure for Air System:

The basic experimental procedure employed for the air system is as follows:

1. Depending on the size hose being tested, one, two or three of three available air compressors were started and the line pressure was allowed to reach 125 lbs. of pressure.

2. The first reading on any given hose was taken at a pressure of 40 psig (if achievable) on the inlet to the test section. The hose was initially at zero degree bend angle.

3. The flow rate was then varied until a predetermined pressure drop (across the test section) was approximated. The exact pressure drop was measured with a differential manometer.

4. This reading was then recorded along with the inlet temperature and pressure on the orifice section, and the pressure drop across the orifice.

   The pressure drops were measured with manometers and the other pressures with a gauge. Both temperatures were measured with Fahrenheit thermometers.

5. The flow rate was then increased, the inlet pressure being held constant, until the second predetermined pressure drop had been reached.

6. All readings were reached. This procedure was repeated for all other pressure drop settings.

7. Steps 1 through 6 were then repeated for all other bend angles being tested.

Range of Measurements:

Experimental measurements of flow rate, pressure drop, and temperature were carried out over a wide range of conditions.

For the water system:

Volumetric flow rate - 1 to 300 gpm

Average velocity - 1 to 25 ft./sec.

Reynolds number - 6000 to 380,000

Pressure drop across test section - 0.01 to 3.5 psi/ft.

Temperature - 40 to 80°F

For the air system:

Volumetric flow rate - 5 to 1100 SCFM

Reynolds number - 10,000 to 550,000

Pressure drop ratio ($-\Delta P/P_1$) - 0.001 to 0.5

Inlet pressure (P_1) - 20 to 50 psig

Temperature - 50 to 120°F

The temperatures for the water system varied with the season, whereas for the air system a combination of season and compressor effects caused the temperature to change.

Bend angles were varied from 0^{o} (straight hose) to 180^{o} - the tests being run at 30^{o} intervals. The radius of curvature varied from infinity (0^{o}) to 3.18 feet (180^{o}).

CHAPTER IV

RESULTS

The experimental equipment used in this study was described in Chapter III. As noted there, the flow of air was investigated in one system and the flow of water was investigated in a separate system. This chapter will describe the results obtained from these experimental systems and the correlations developed from these results.

Initially the results for the two systems will be described in separate sections, however, it will be shown in the latter parts of the chapter how the results from the two systems complement one another.

Experimental Results for Water System:

Figure IV-1 shows a plot of pressure drop versus Reynolds number for hose NASA 62. These data were taken on the water system with the hose in a straight configuration. The numbering system for the various hoses is described in Appendix A. A least squares analysis on these data indicates that a straight line relationship has a slope of 2.20. It appears that a characteristic of flow in flexible metal hose data plotted in this manner is that a slope with a value greater than 2.0 is obtained for a straight line relationship.

Figures IV-2 through IV-9 show pressure drop versus Reynolds number data for straight sections of all helical hoses tested. Note that except for hose NASH1 a least squares analysis shows that all of the slopes are greater than 2.0. Furthermore, statistical tests indicate that these

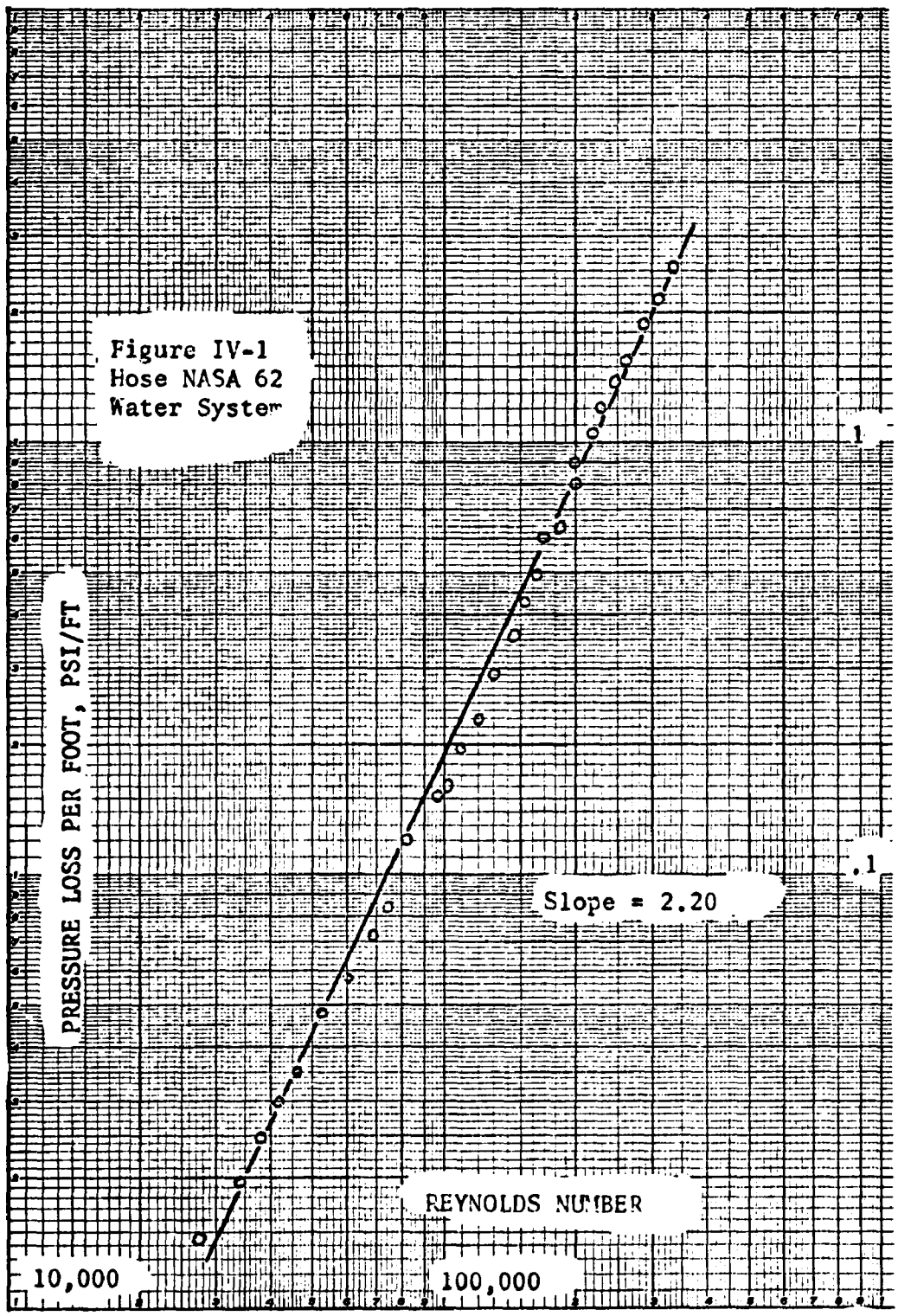
Figure IV-1
Hose NASA 62
Water Syste
PRESSURE LOSS PER FOOT, PSI/FT
1
.1
Slope = 2.20
REYNOLDS NUMBER
10,000
100,000

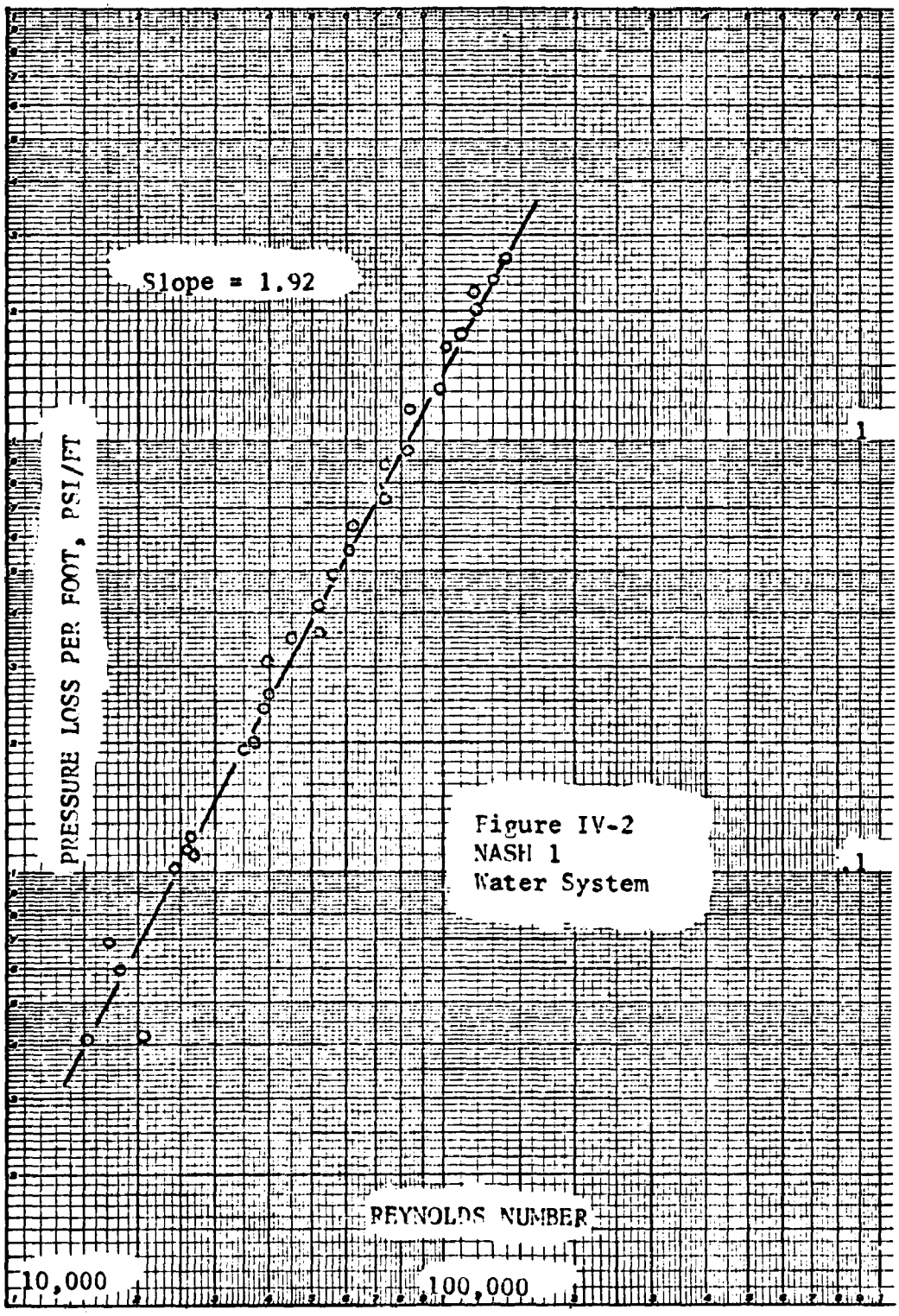

Figure IV-2
NASH 1
Water System

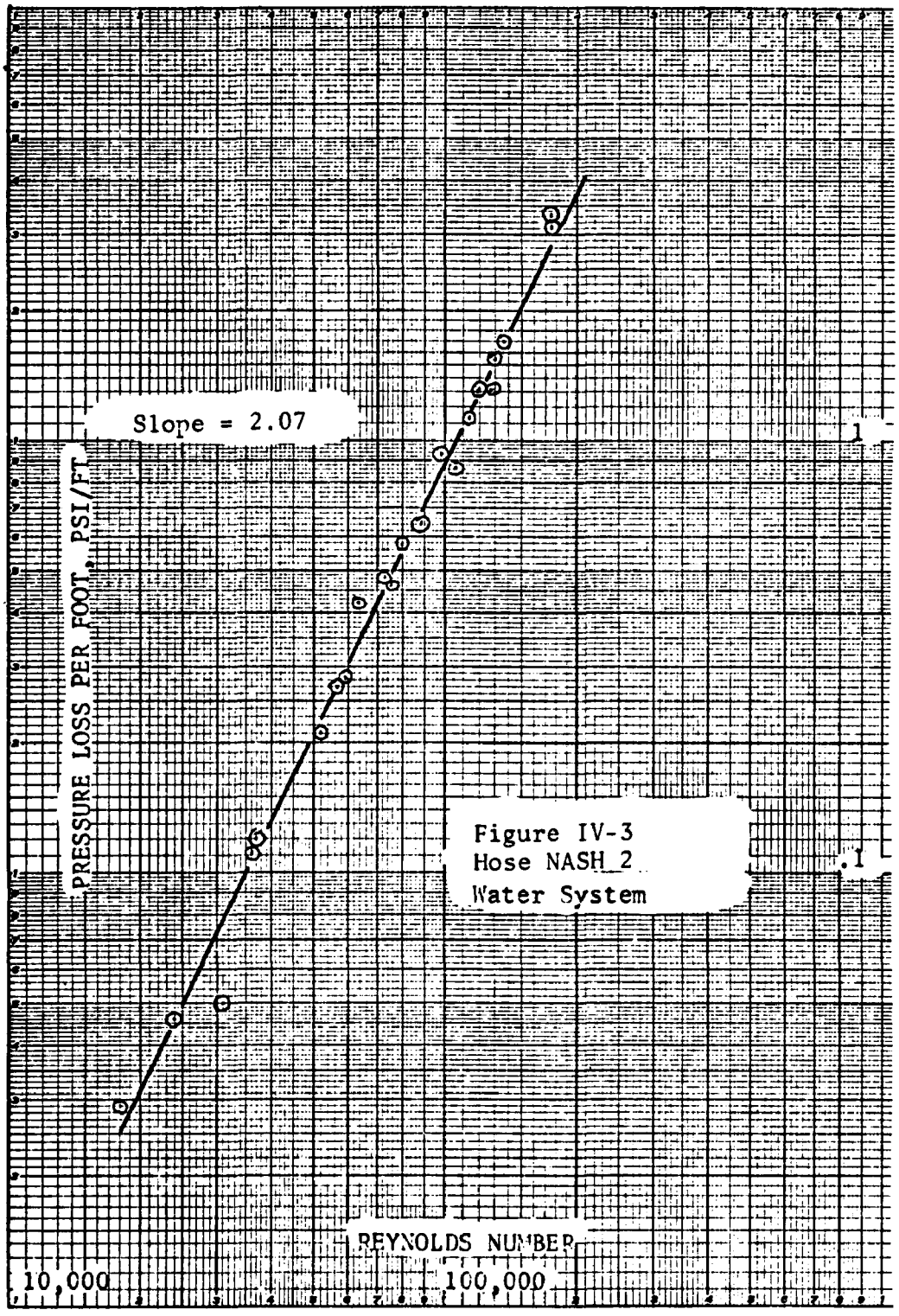

Figure IV-3
Hose NASH_2
Water System

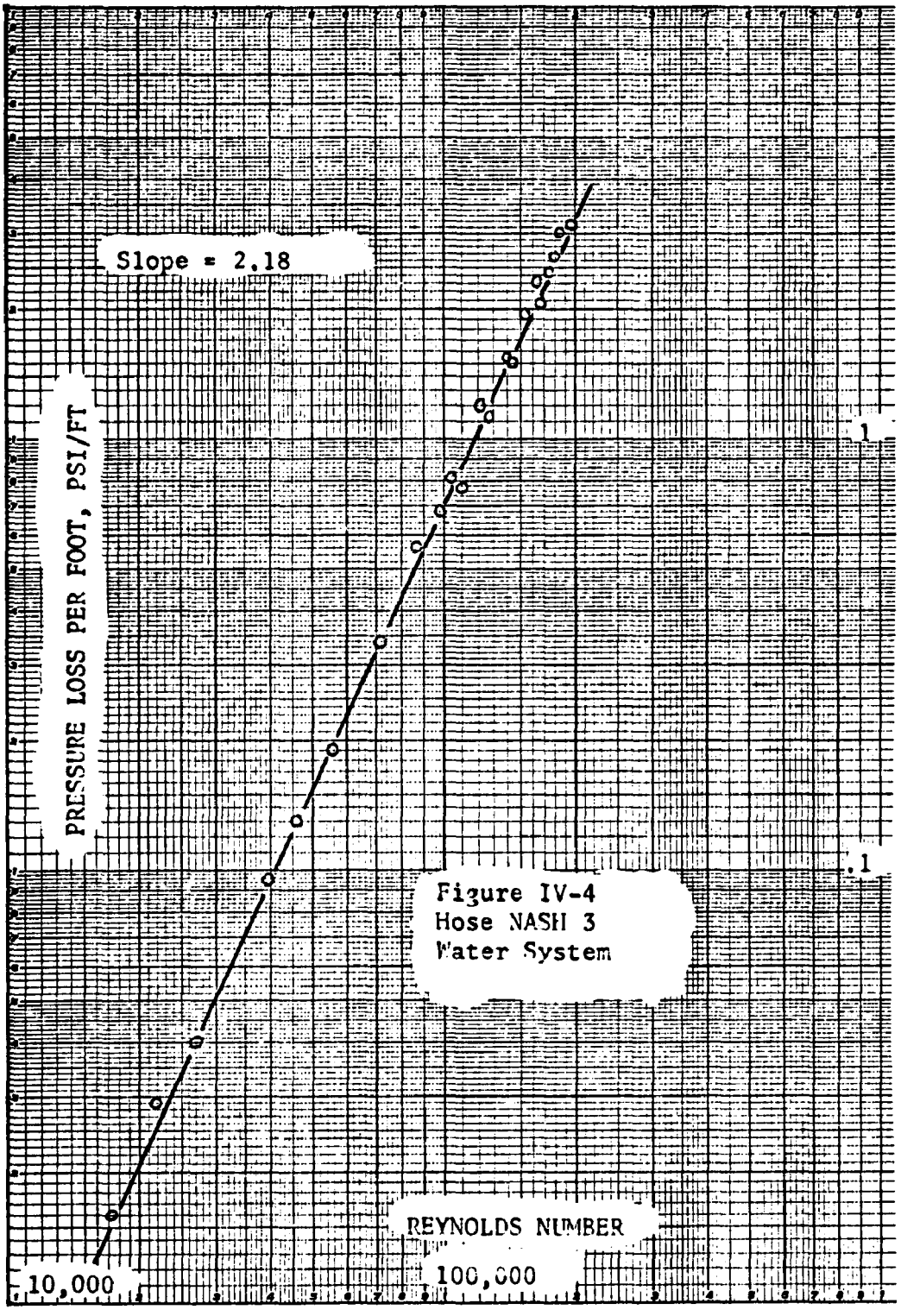

Figure IV-4
Hose NASH 3
Water System

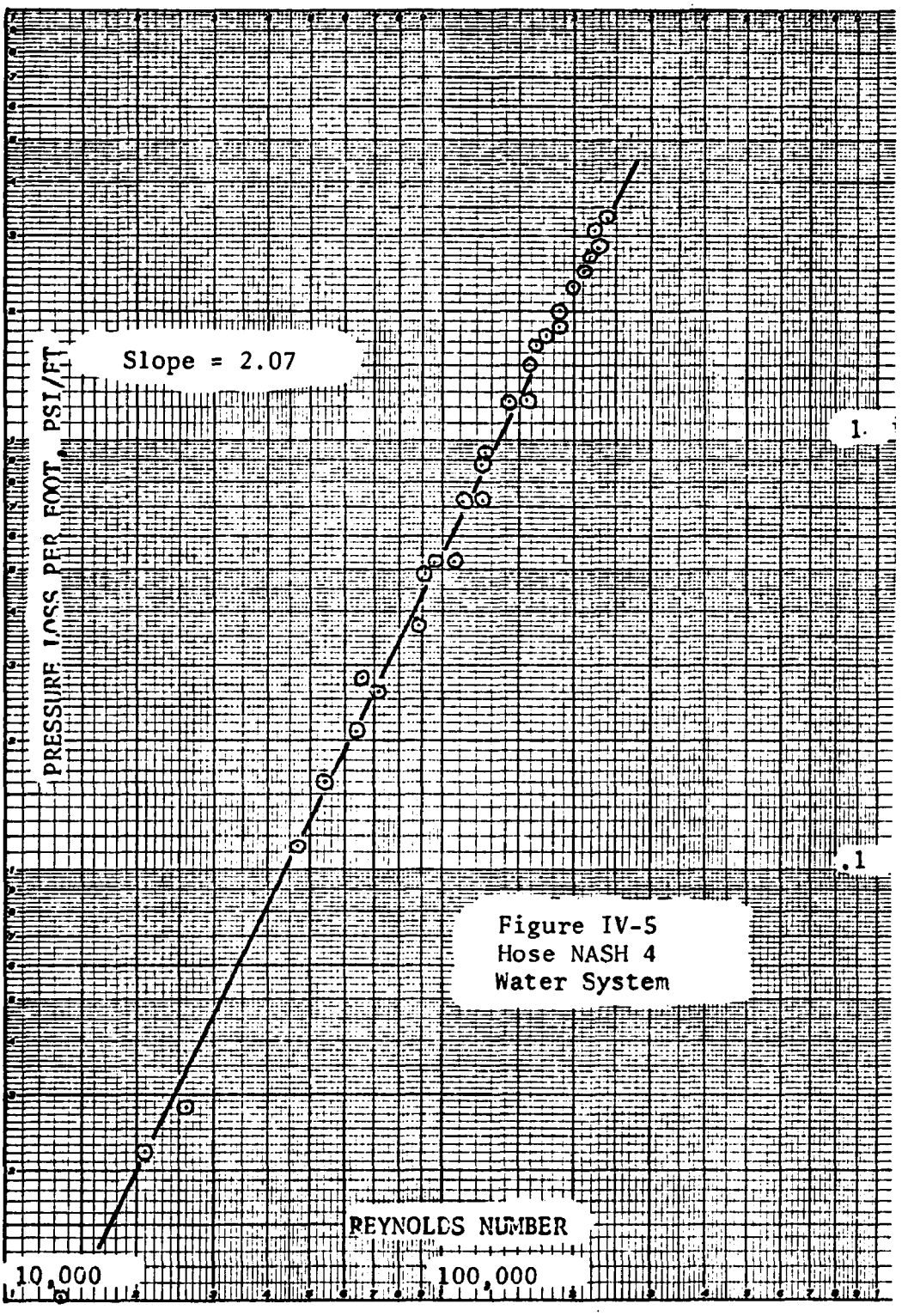

Figure IV-5
Hose NASH 4
Water System

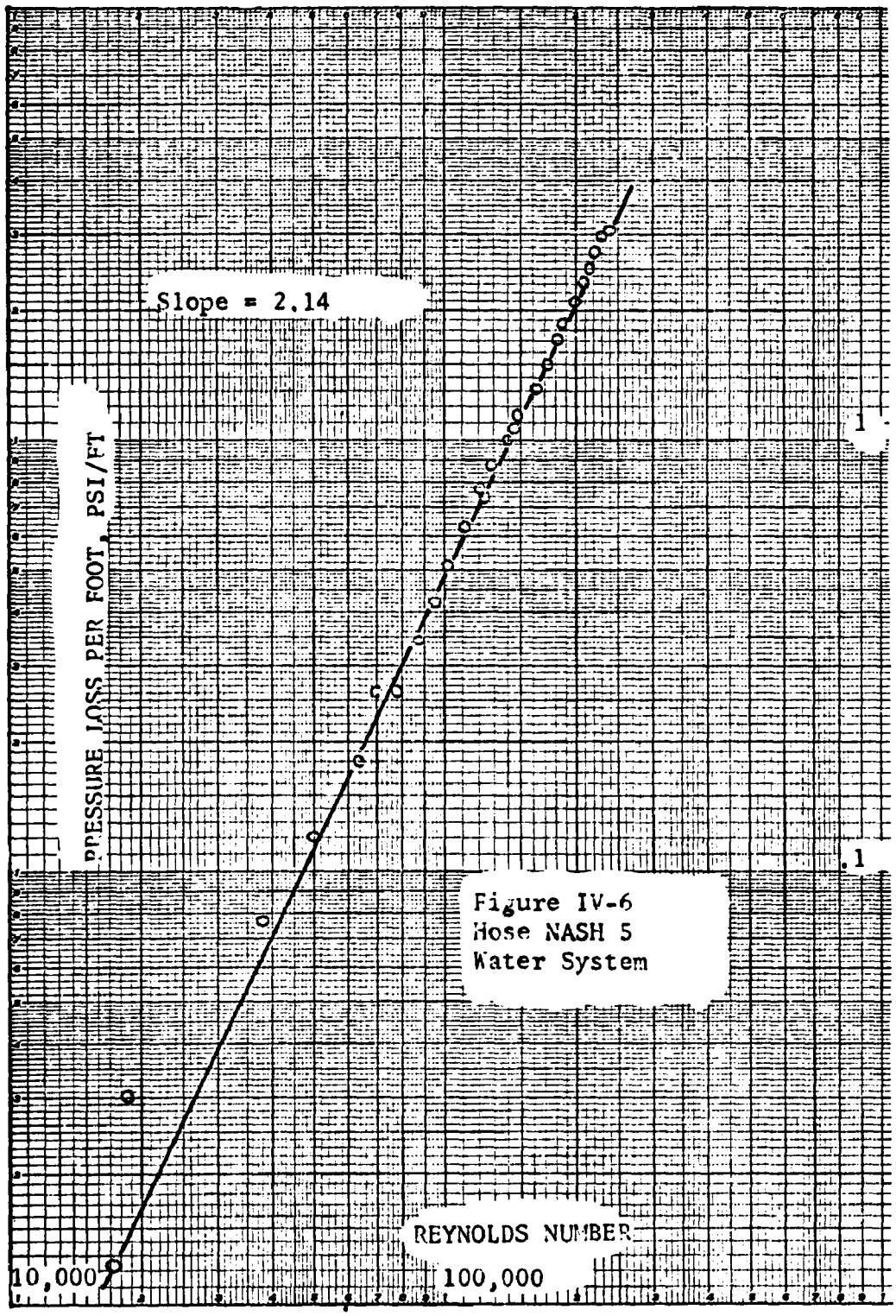

Figure IV-6
Hose NASH 5
Water System

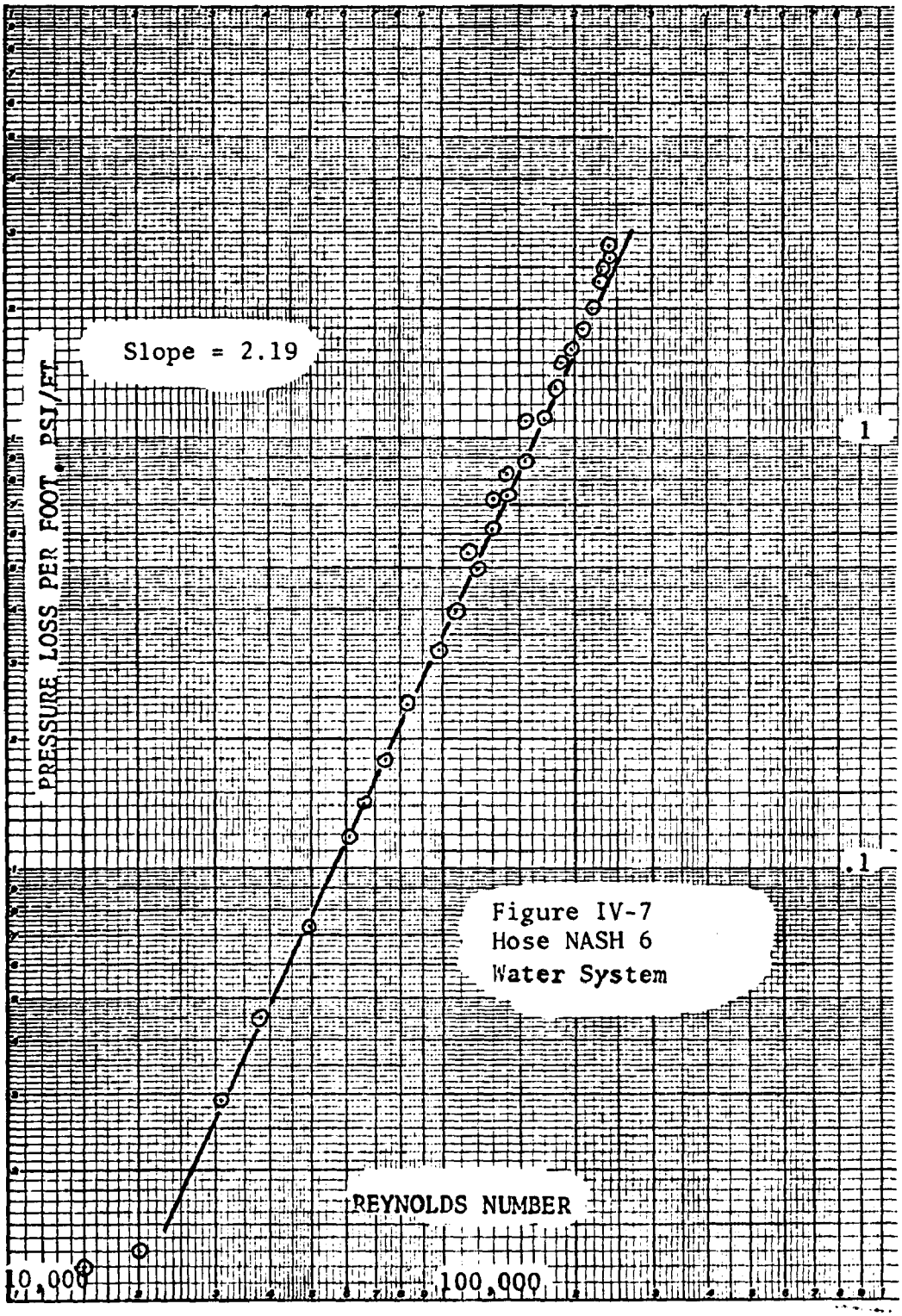

Figure IV-7
Hose NASH 6
Water System

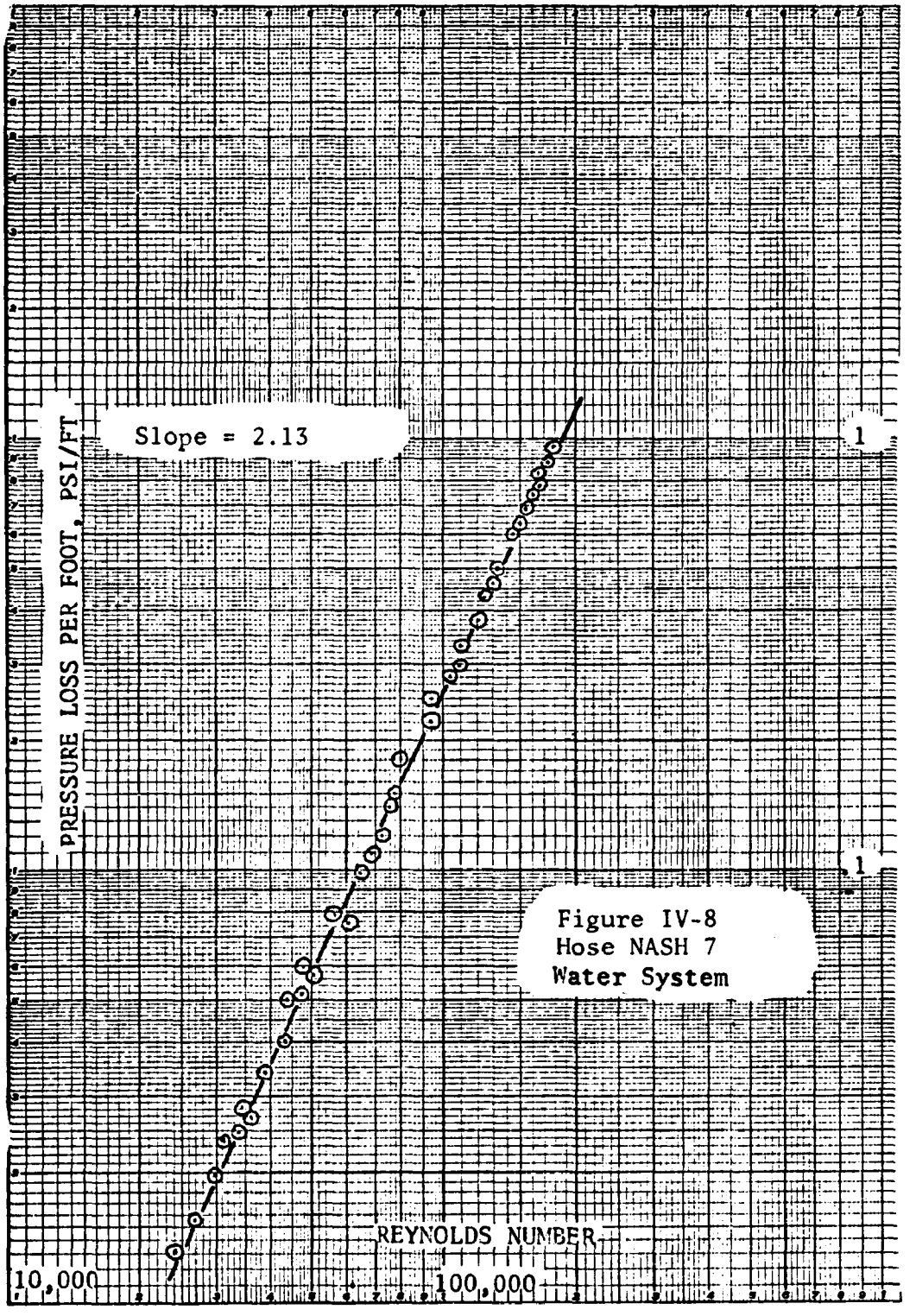

Figure IV-8
Hose NASH 7
Water System

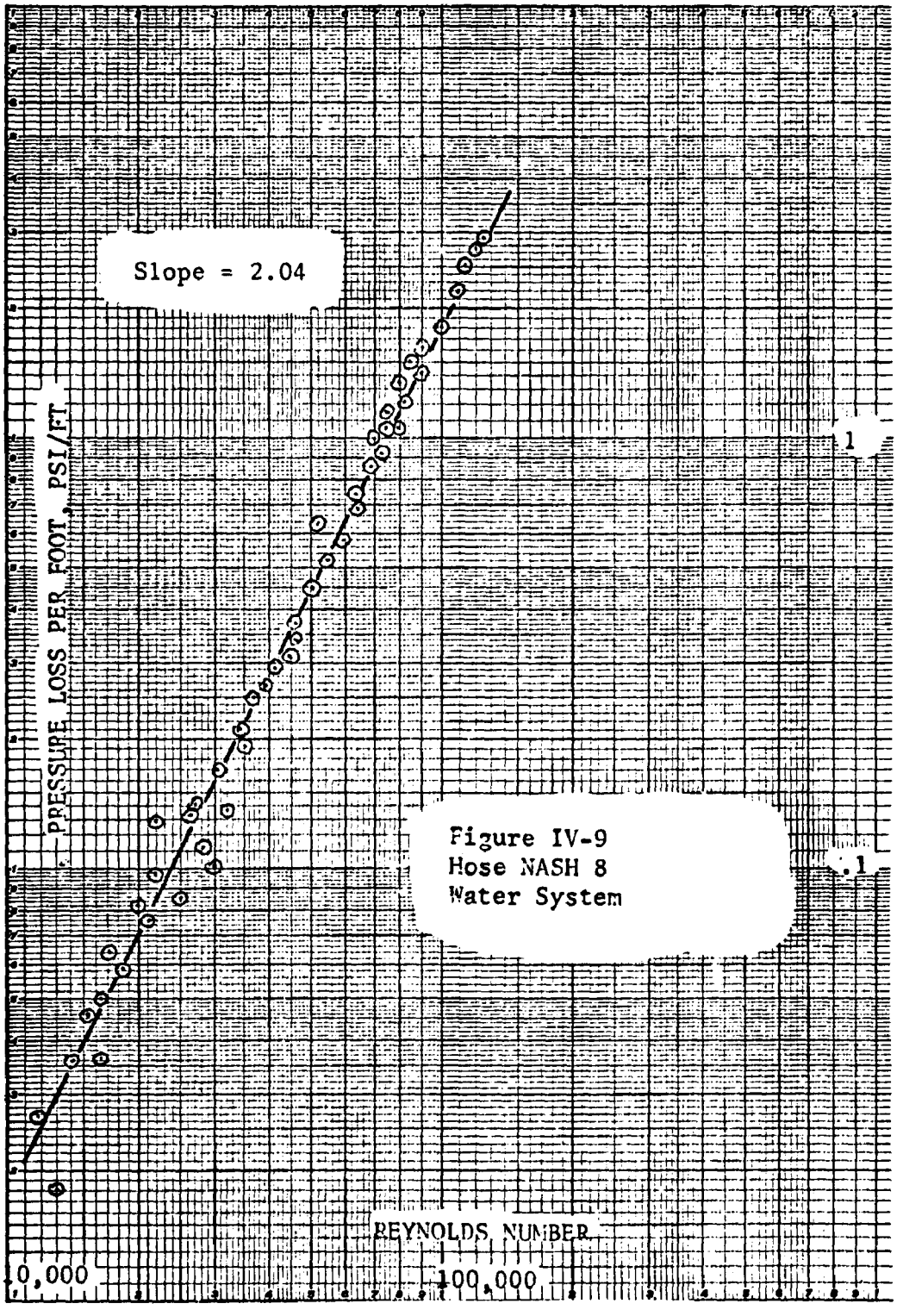

Figure IV-9
Hose NASH 8
Water System

slopes have different values - i.e., an average value would not adequately describe the data.

A value of 2.0 for the slope would indicate that the friction factor (defined in Chapter II) was independent of Reynolds number and hence was a constant value at all flow rates tested. Similarly, a value greater than 2.0 means that the friction factor would increase in value with an increase in Reynolds number. This can easily be seen from equation (II-7), noting that the Reynolds number is directly proportional to the mean velocity.

Figure IV-10 is a comparison plot of five of the helical hoses. Note that the abcissa is the mean velocity. Examination of these data shows that the experimental velocity range was from 1.0 ft./sec. to about 25.0 ft./sec.

Figure IV-11 is a plot of pressure drop versus Reynolds number for hose NASH7 at angles of curvature of 0°, 60°, 120° and 180°. These data clearly show that for a given value of Reynolds number an increase in bend angle increases the friction. Data for all other hoses follow the same trend as that shown in Figure IV-11.

Friction Factor versus Reynolds Number for Water System:

Figures IV-12 through IV-24 show the relationship between the Fanning friction factor and the Reynolds number for flow of water in a straight section of flexible hose. These data indicate that initially there is a region of low Reynolds numbers where the friction factor remains constant: i.e., it is a function of hose geometry only. However, at some value of Reynolds number the friction factor no longer remains constant but instead begins to increase with an increase in Reynolds

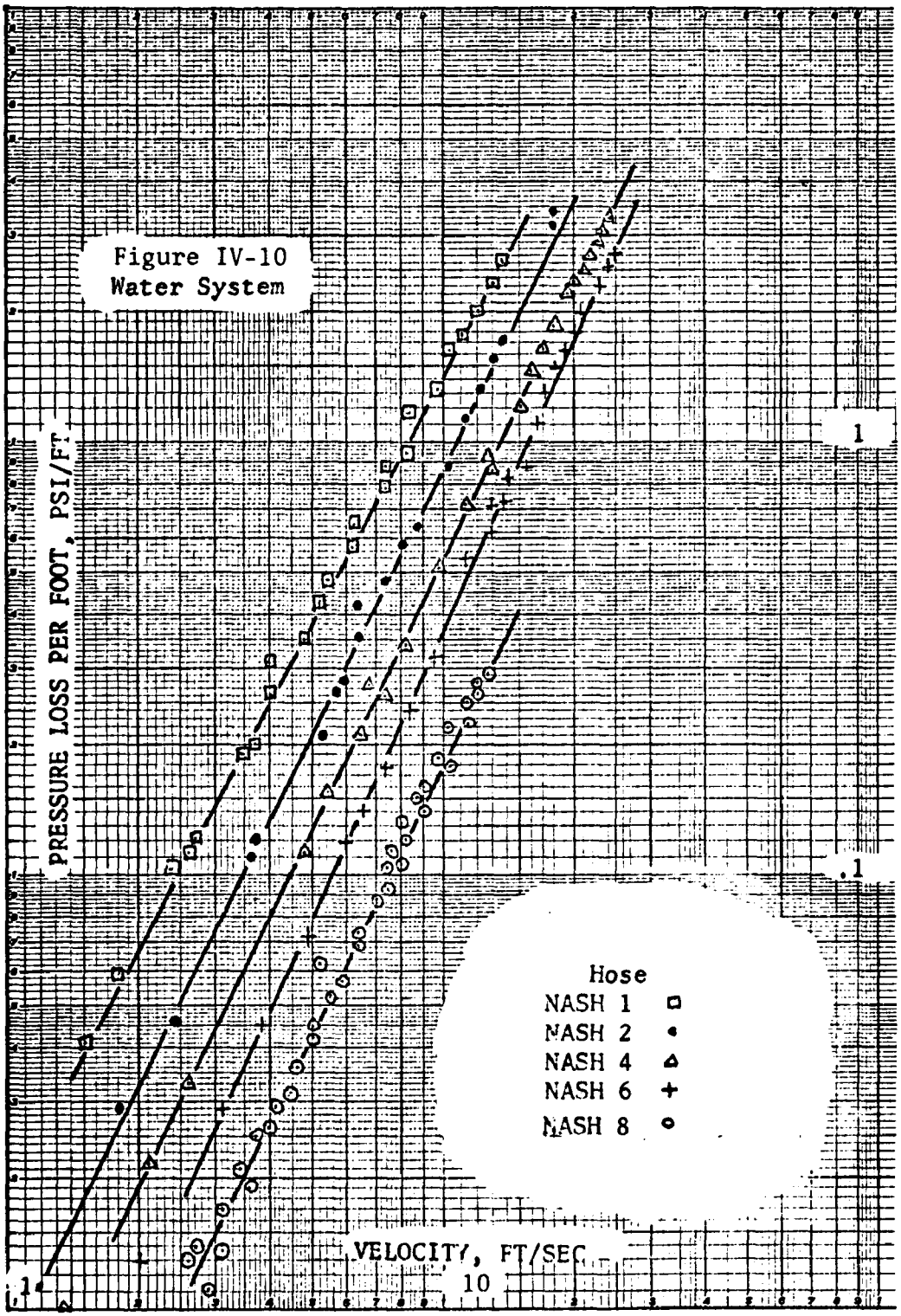
Figure IV-10
Water System
PRESSURE LOSS PER FOOT, PSI/FT
1
.1
Hose
NASH 1
NASH 2
NASH 4
NASH 6
NASH 8
VELOCITY, FT/SEC
1
10

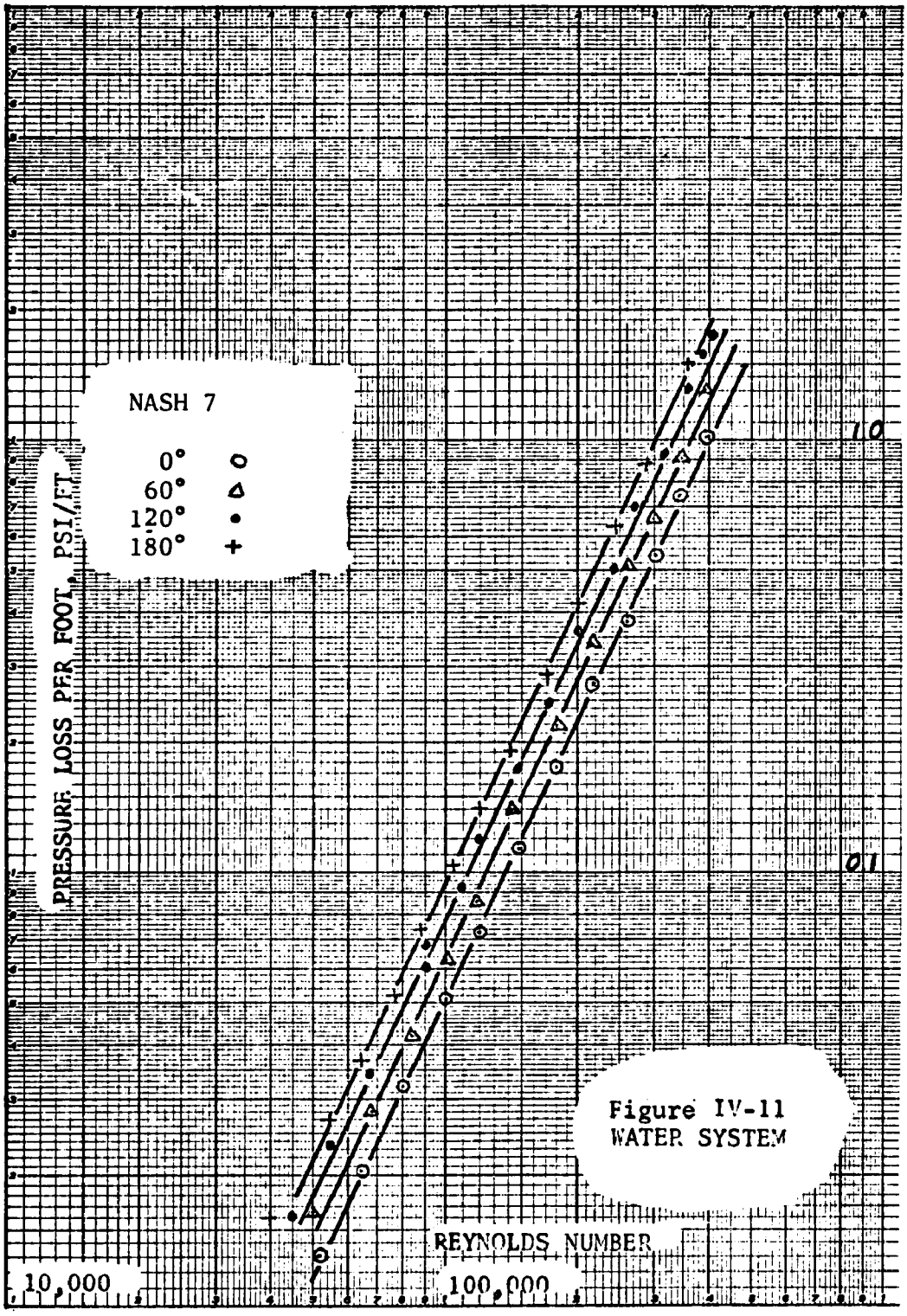

Figure IV-11
WATER SYSTEM

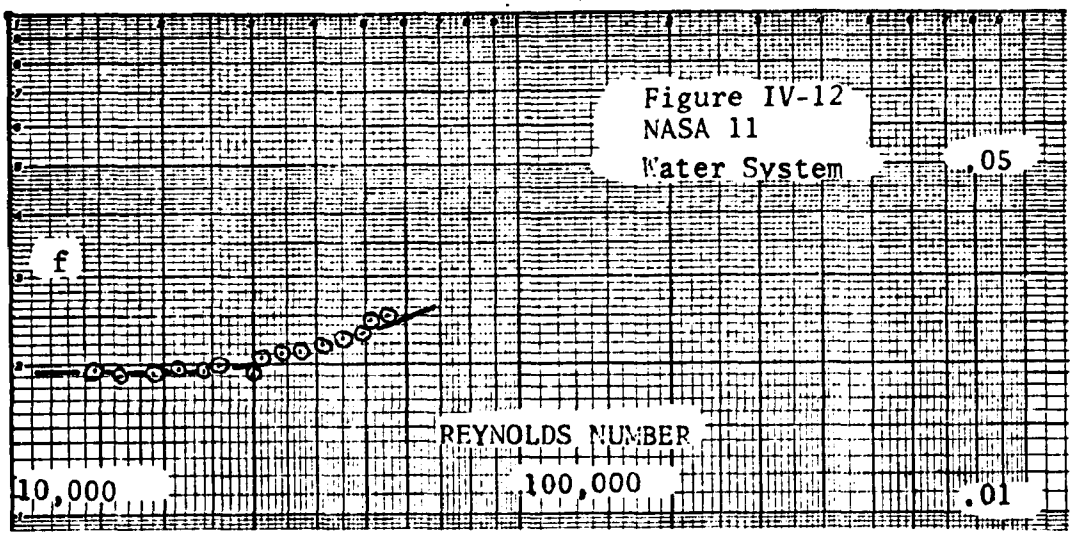
Figure IV-12
NASA 11
Water System
.05
f
REYNOLDS NUMBER
10,000
100,000
.01

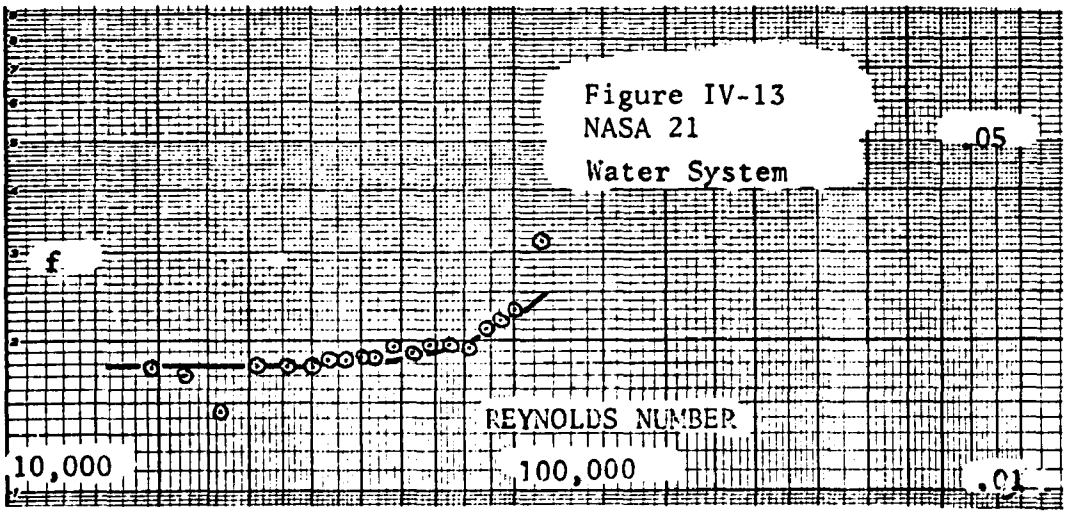
Figure IV-13
NASA 21
Water System
.05
f
REYNOLDS NUMBER
10,000
100,000
.01

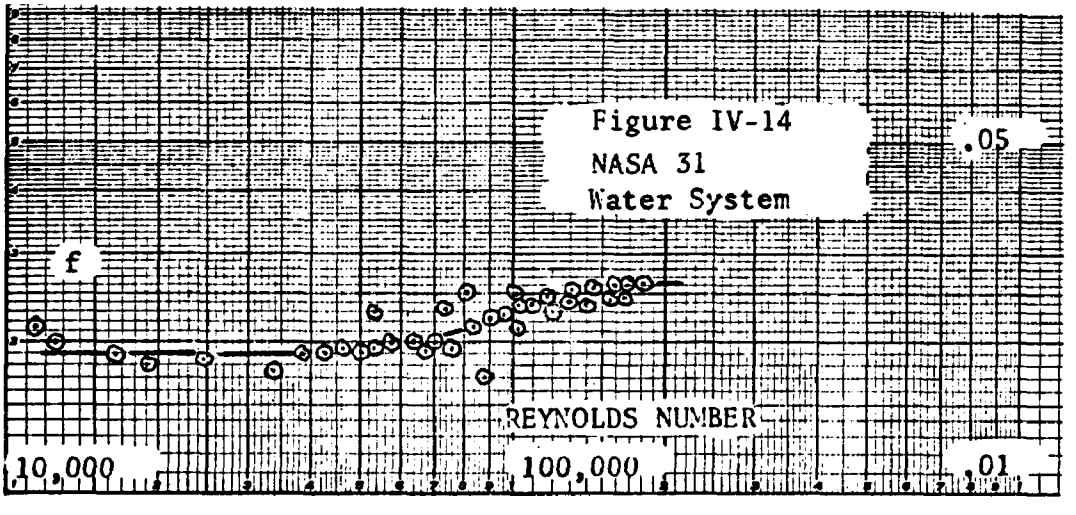
Figure IV-14
NASA 31
Water System
.05
f
REYNOLDS NUMBER
10,000
100,000
.01

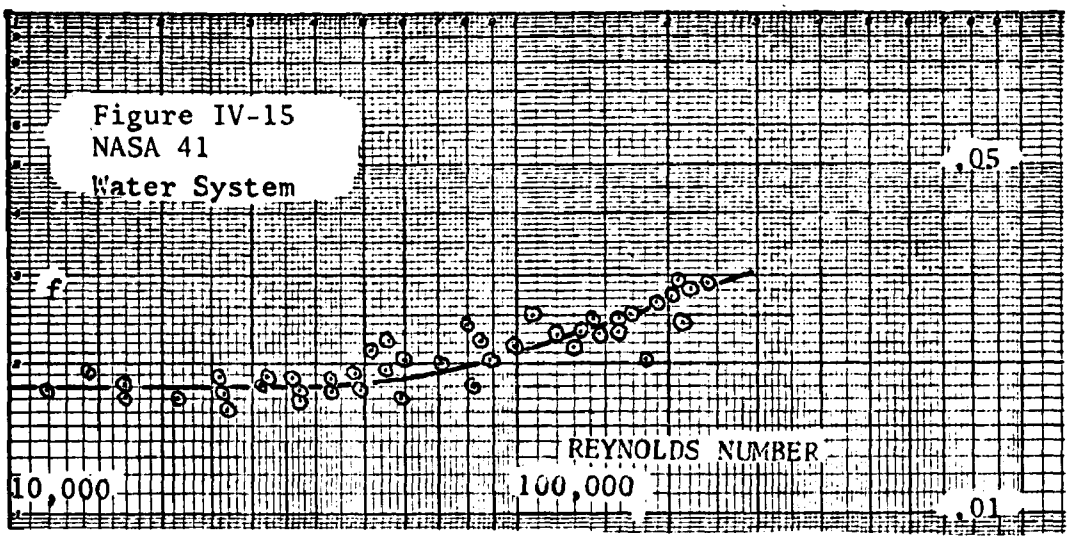
Figure IV-15
NASA 41
Water System
.05
f
REYNOLDS NUMBER
10,000
100,000
.01

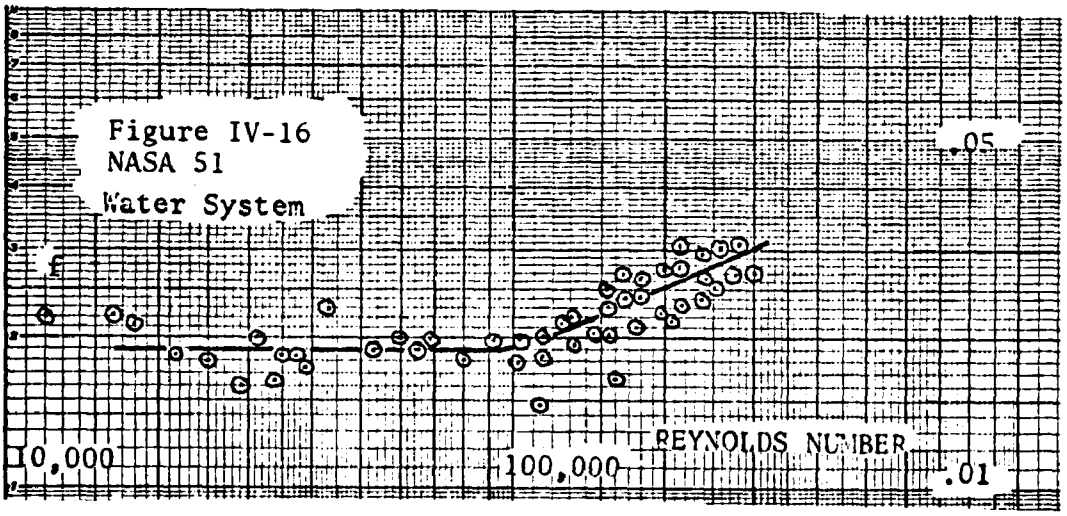
Figure IV-16
NASA 51
Water System
.05
f
REYNOLDS NUMBER
10,000
100,000
.01

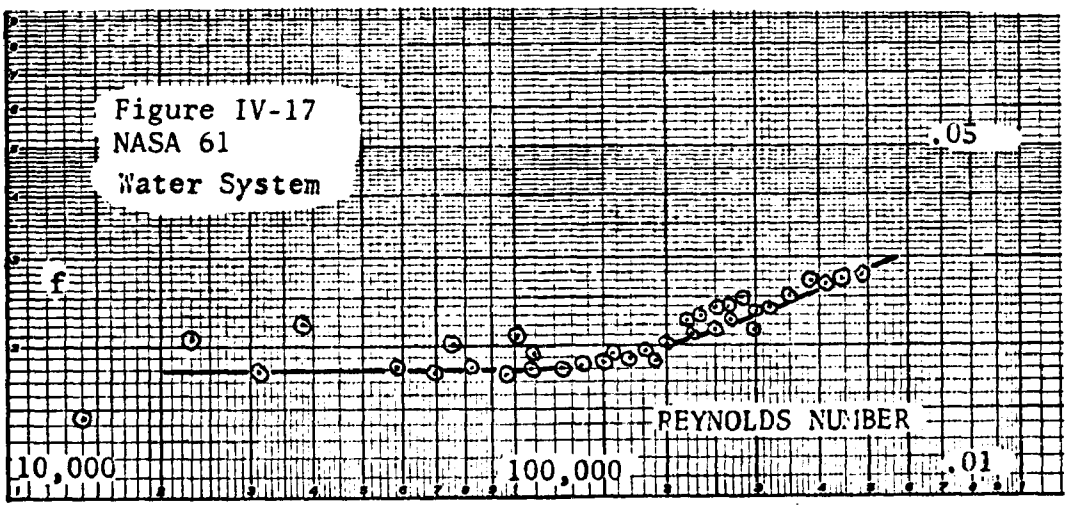
Figure IV-17
NASA 61
Water System
.05
f
REYNOLDS NUMBER
10,000
100,000
.01

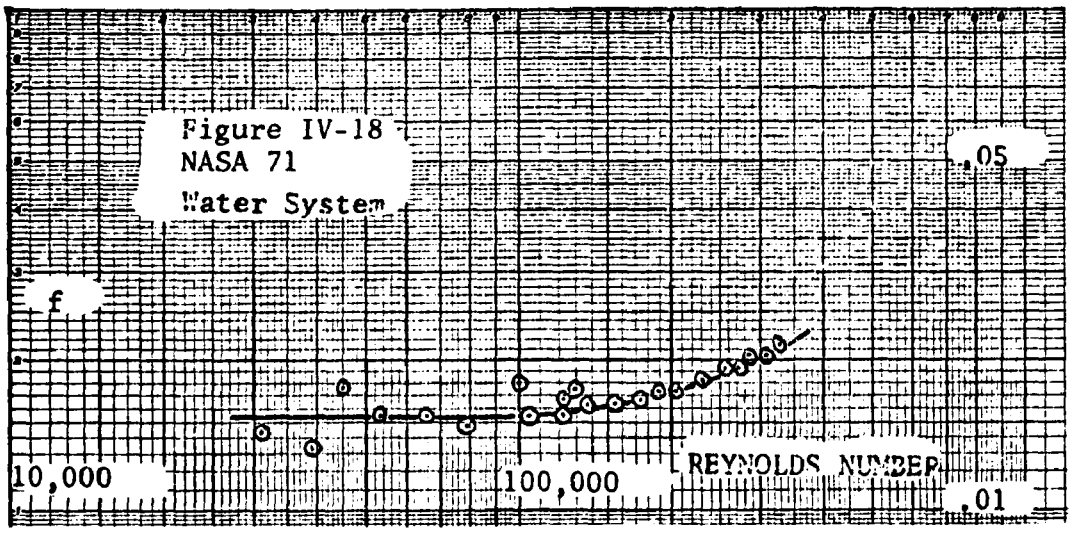
Figure IV-18
NASA 71
Water System
f
.05
.01
10,000
100,000
REYNOLDS NUMBER

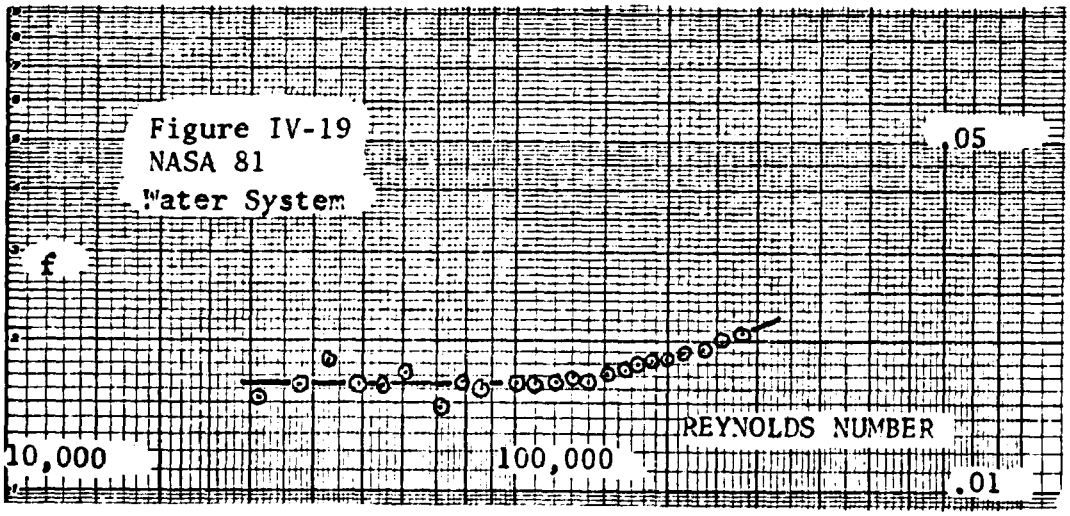
Figure IV-19
NASA 81
Water System
f
.05
.01
10,000
100,000
REYNOLDS NUMBER

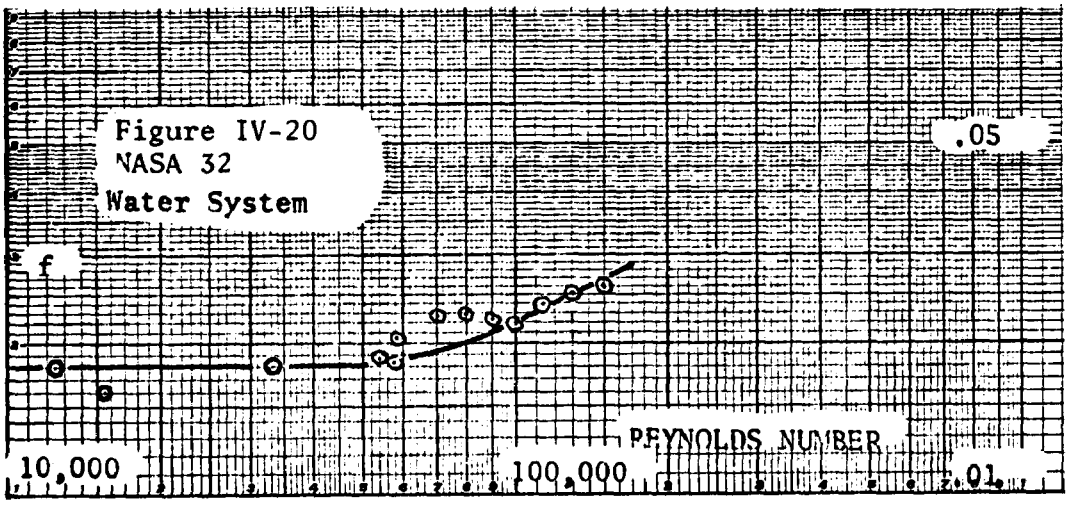
Figure IV-20
NASA 32
Water System
f
.05
.01
10,000
100,000
REYNOLDS NUMBER

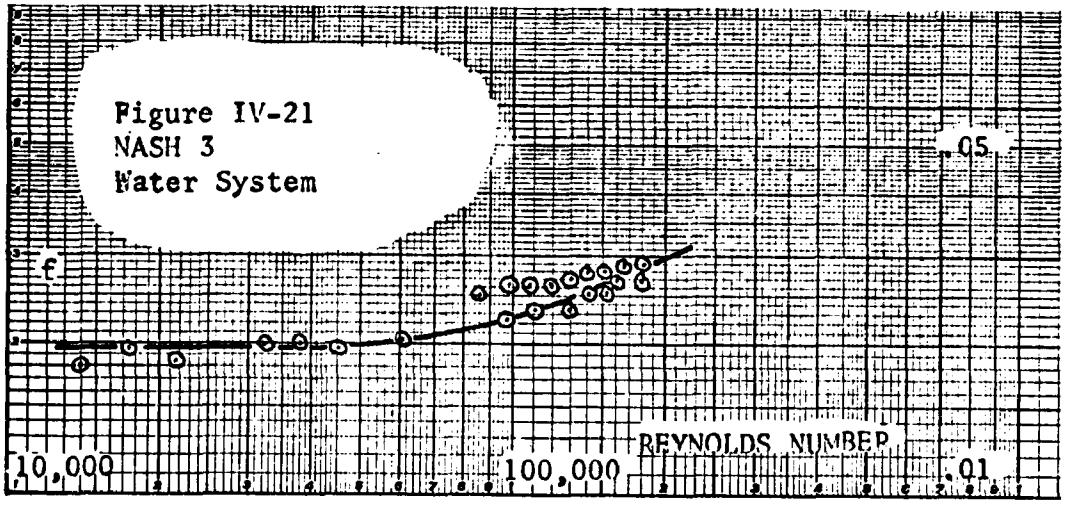

Figure IV-21
NASH 3
Water System

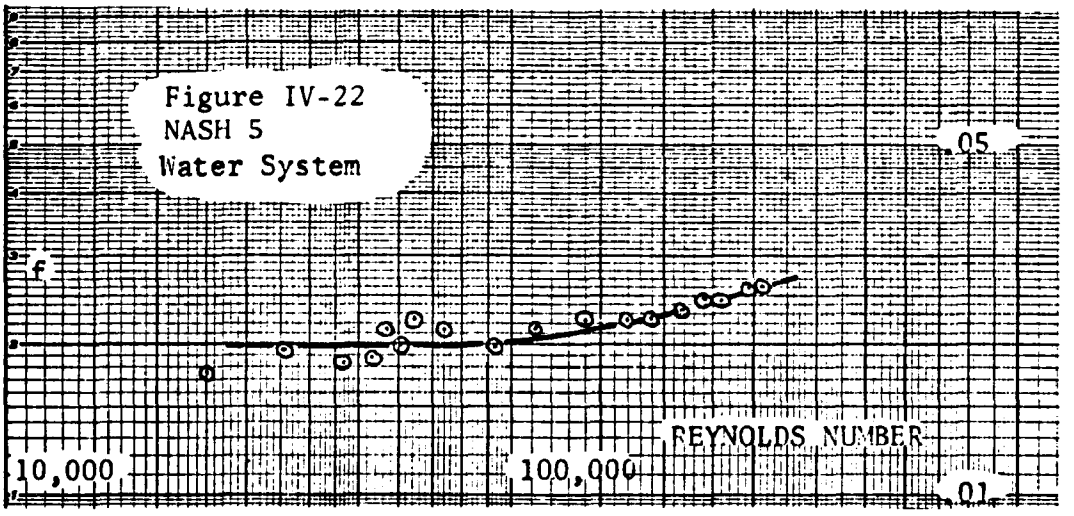

Figure IV-22
NASH 5
Water System

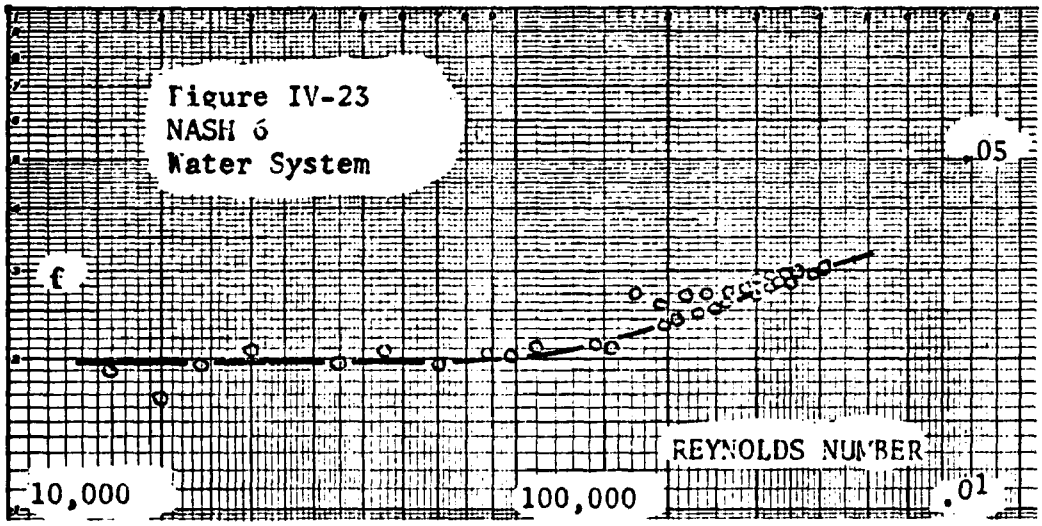
Figure IV-23
NASH 6
Water System
.05
f
REYNOLDS NUMBER
10,000
100,000
.01

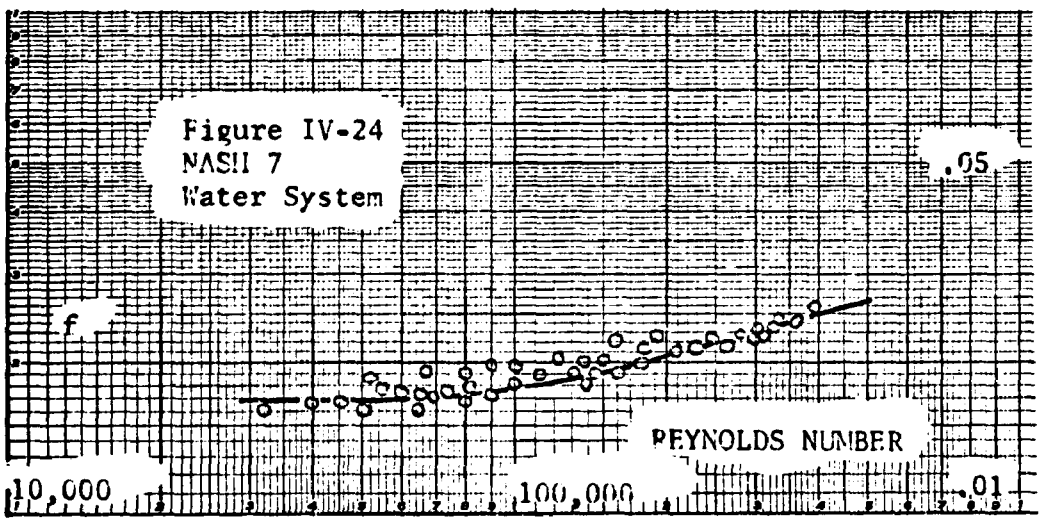
Figure IV-24
NASH 7
Water System
.05
f
REYNOLDS NUMBER
10,000
100,000
.01

number. The results from hoses NASA 31, NASA 61, and NASA 72 seem to indicate that the friction factor again approaches a constant value at some higher Reynolds number.

A plot of pressure loss versus Reynolds number must be consistent with a plot of friction factor versus Reynolds number. Figures IV-1 through IV-9 indicate a straight line relationship (on a logarithmic basis) for pressure loss and Reynolds number. However, Figures IV-12 through IV-24 indicate a straight line relationship is not adequate for friction factor and Reynolds number.

This phenomena can be explained by considering the magnitude of the slopes of these curves. A slope of 2.0 on the pressure loss versus Reynolds number curve corresponds to a slope of 0.0 on the friction factor versus Reynolds number curve, It is much easier to detect the difference in slopes between 0.0 and 0.2 than it is to detect the difference between 2.0 and 2.2. The reason the pressure loss versus Reynolds number curve appears straight is that the percentage change in the slope is very small.

Special note should also be made of the magnitude of these Fanning friction factors. In the low Reynolds number region (<75,000) the magnitude is about 0.020. For turbulent flow in a smooth pipe the Fanning friction factor at a Reynolds number of 60,000 is about 0.005. This indicates that mechanical energy is degradated into heat by friction at a rate four times greater for flow in flexible hose than for flow in a smooth pipe. Furthermore, since the friction factor increases for higher flow rates in flexible hose, the ratio of energy degradation becomes even greater.

Experimental Results for the Air System:

Figure IV-25 is a plot showing the relationship between pressure drop and volumetric flow rate (SCFM) for hose NASA 51 (30° bend angle): the parameter is the inlet pressure to the test section. To condense these data into a single curve $(-\Delta P)/P_1$ was plotted as a function of $W\sqrt{T}/P_1$. Figure IV-26 shows the results for hose NASA 51 plotted in this manner. Figure IV-27 is a plot of the data for hose NASA 32 and Figure IV-28 is a plot of the data for hose NASH 4. Below a value of $(-\Delta P)/P_1$ less than about 0.1 the relationship appears linear. Above this value, the linear relationship breaks down and the line begins to curve with increasing slope.

Figure IV-29 shows the results obtained for four bend angles on hose NASA 72. Because of the lack of compressor capacity it was impossible to investigate the nonlinear region for hoses with diameters larger than two inches.

Note that the pressure drop data can be correlated for a given hose by plotting $(-\Delta P)/P_1$ versus $W\sqrt{T}/P_1$ on log-log paper. This particular approach was suggested by the following equations:

$$(-\Delta P)/\rho_1 = C_1 v_1^2 \qquad \text{(IV-1)}$$

$$\rho_1 = C_2 P_1/T \qquad \text{(IV-2)}$$

$$W = C_3 \rho_1 v_1 \qquad \text{(IV-3)}$$

where C_1, C_2, and C_3 are proportionality constants and subscript 1 refers to inlet conditions.

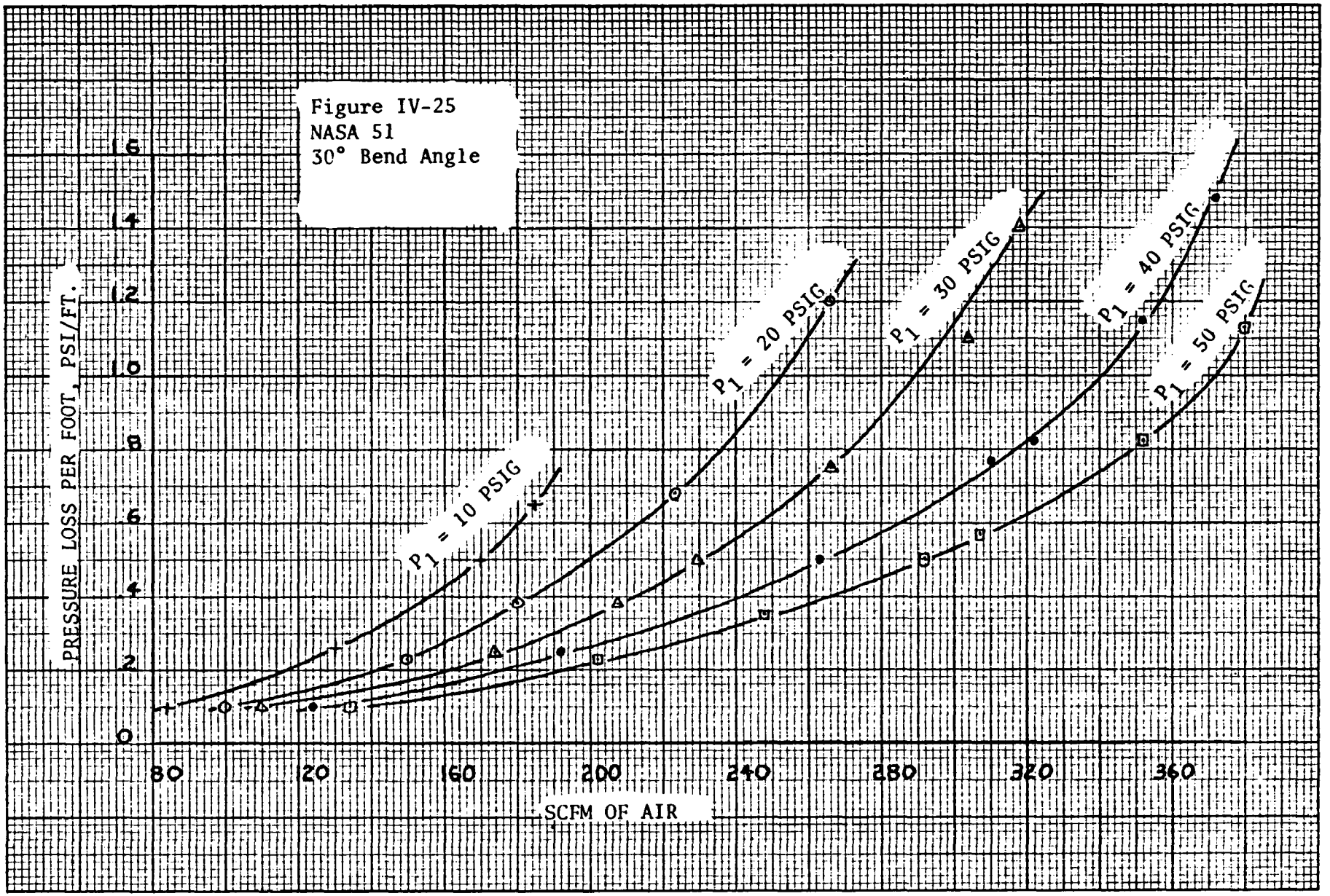
Figure IV-25
NASA 51
30° Bend Angle
PRESSURE LOSS PER FOOT, PSI/FT.
16
14
12
10
8
6
4
2
0
80
120
160
200
240
280
320
360
SCFM OF AIR
P1 = 10 PSIG
P1 = 20 PSIG
P1 = 30 PSIG
P1 = 40 PSIG
P1 = 50 PSIG

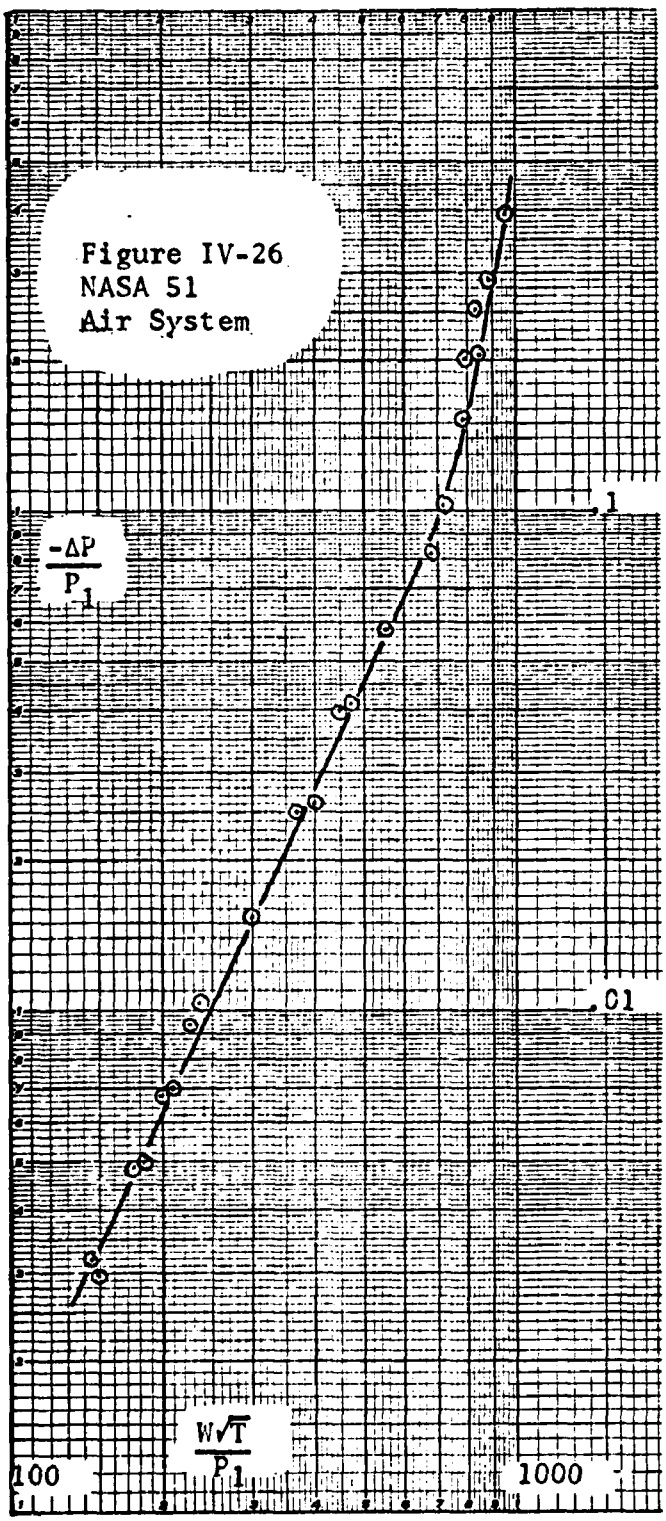

Figure IV-26
NASA 51
Air System

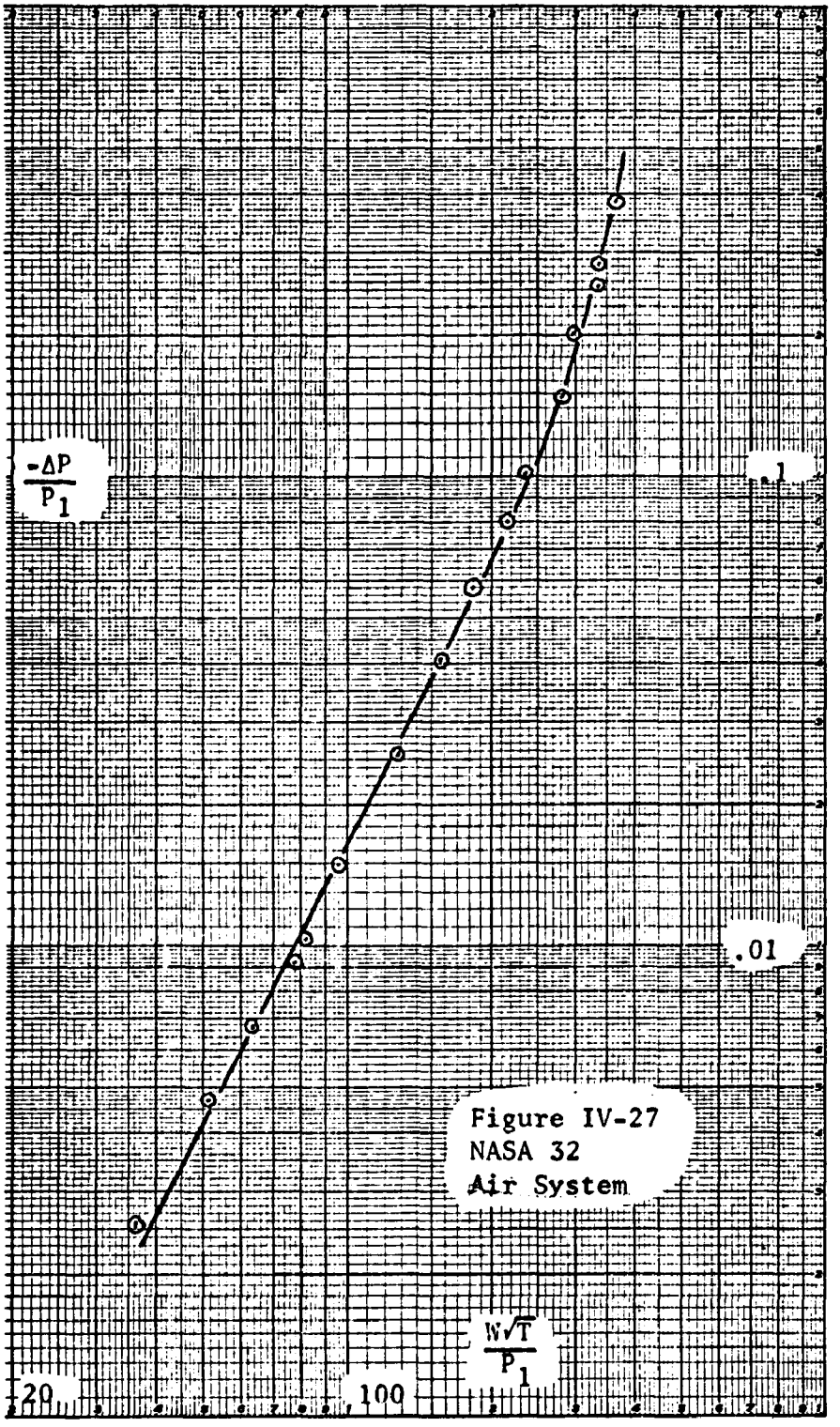

Figure IV-27
NASA 32
Air System

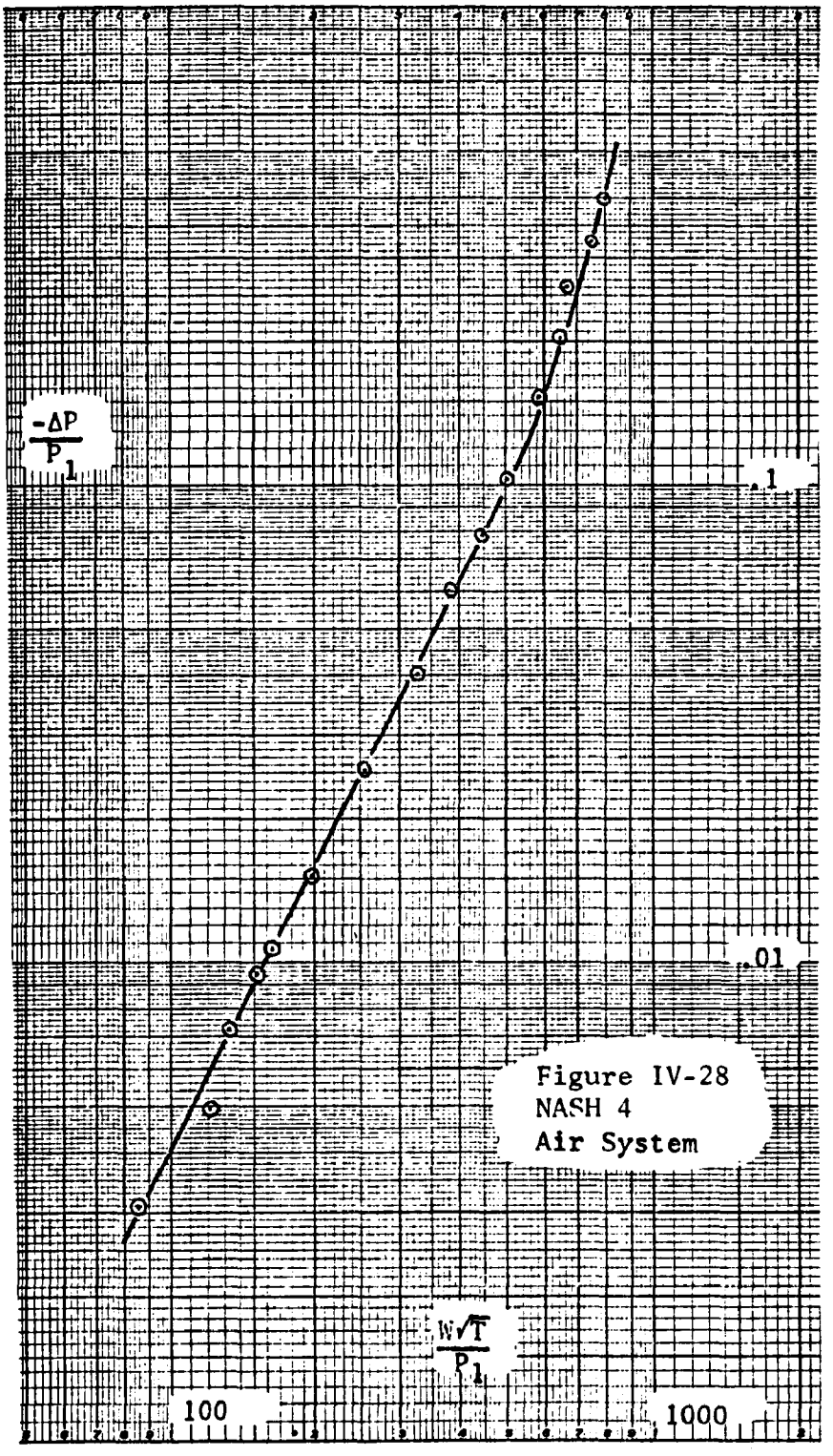

Figure IV-28
NASH 4
Air System

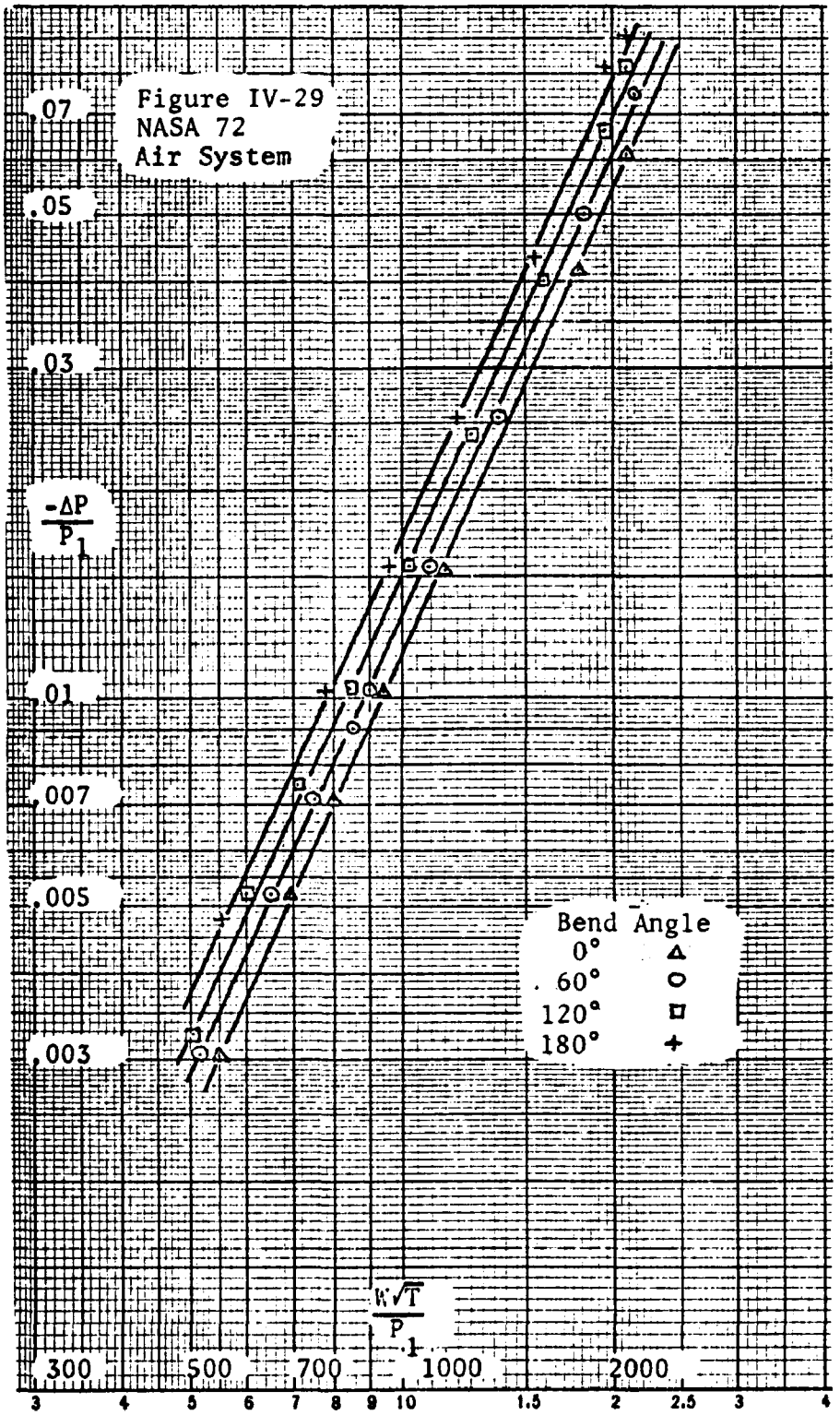
Figure IV-29
NASA 72
Air System
.07
.05
.03
$\frac{-\Delta P}{P_1}$
.01
.007
.005
.003
Bend Angle
0° △
60° ○
120° □
180° +
$\frac{W\sqrt{T}}{P_1}$
300
500
700
1000
2000
3
4
5
6
7
8
9
10
1.5
2
2.5
3
4

Friction Factor versus Reynolds Number for Air System:

Figures IV-30 through IV-36 show data obtained for the flow of air in straight sections of flexible metal hose. The increase in friction factor with an increase in Reynolds number is particularly striking. Note also that the data for hoses NASA21 and NASH2 indicate that the friction factor again approaches a region where it is independent of Reynolds number.

Combined Results for Air and Water Systems:

Figures IV-37 throught IV-42 show the results obtained by combining data from both the air and water systems. From these data a general pattern is noted for the behavior of the friction factor as a function of Reynolds number. Initially, the friction factor is independent of the Reynolds number and depends only on the hose geometry. However, at some point the friction factor begins to increase with an increase in Reynolds number. This range of increasing friction factor data leads to a sigmoid-type curve, i.e., the data take the form of an elongated S when plotted, the curve being characterized by a very small initial slope followed by a period of rapidly increasing slope which gives way to an interval of nearly constant slope succeeded by a period when the rapidly decreasing slope approaches zero. At larger Reynolds numbers the friction factor once again assumes a constant value which depends only on hose geometry. The overall increase in the friction factor can be as much as 200 per cent.

Friction Factor Correlations for Straight Sections of Hose:

In general, the friction factor for flow in a conduit is a function of both Reynolds number and conduit geometry. As has been discussed in previous sections of this chapter this is true for flow in flexible metal

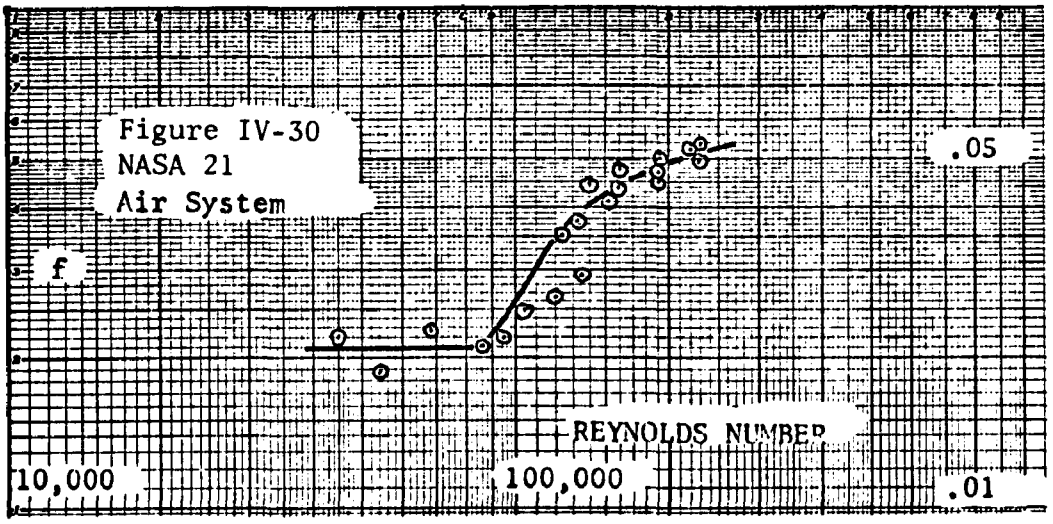
Figure IV-30
NASA 21
Air System
f
.05
REYNOLDS NUMBER
10,000
100,000
.01

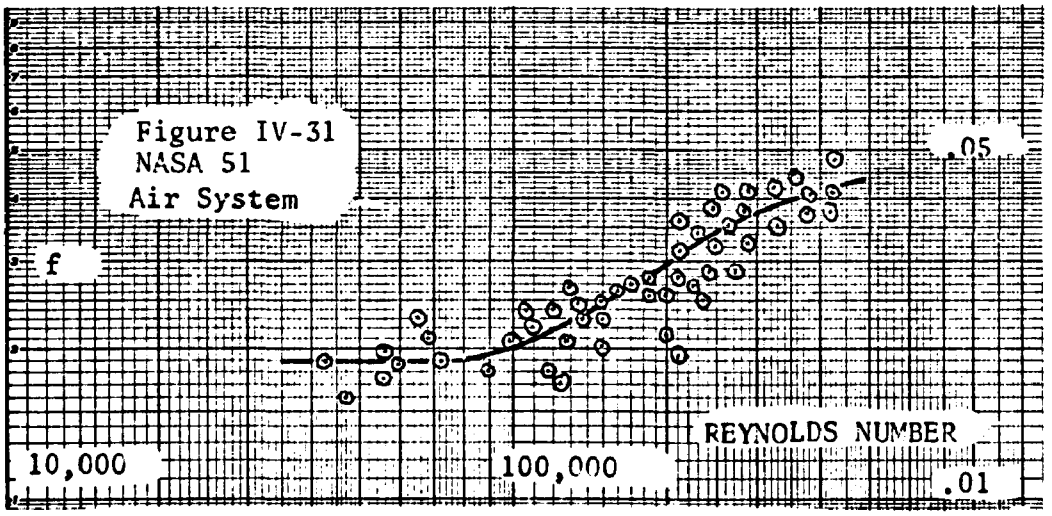
Figure IV-31
NASA 51
Air System
f
.05
REYNOLDS NUMBER
10,000
100,000
.01

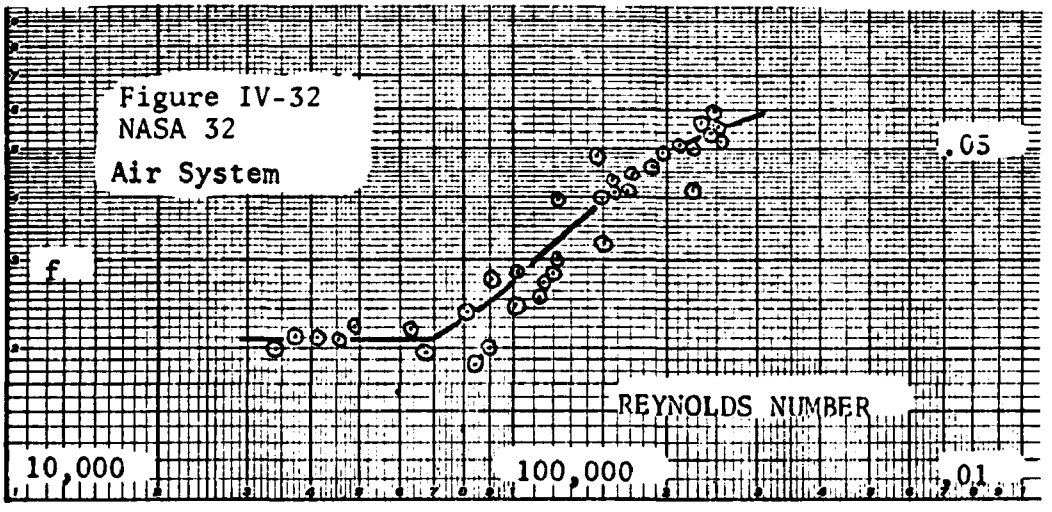
Figure IV-32
NASA 32
Air System
f
.05
REYNOLDS NUMBER
10,000
100,000
.01

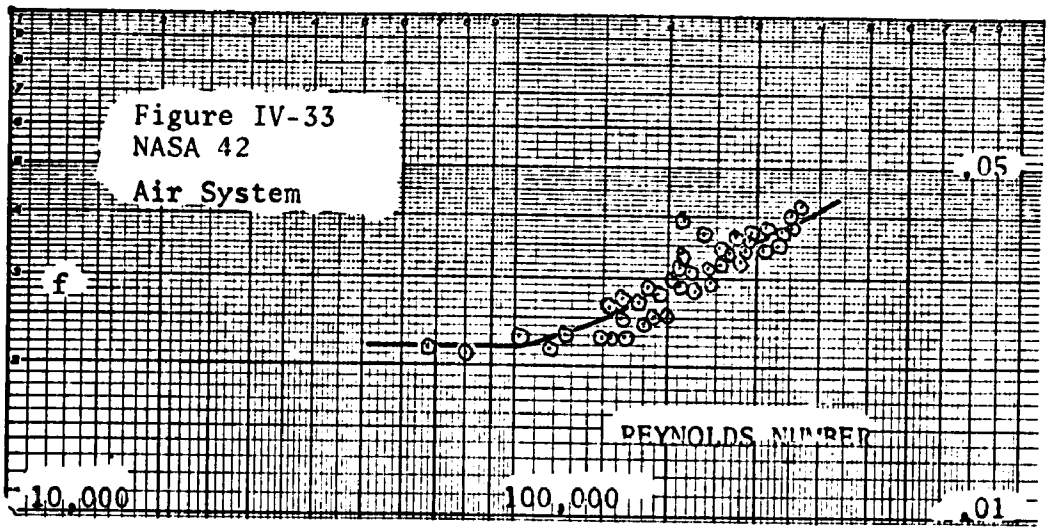
Figure IV-33
NASA 42
Air System
f
.05
.01
10,000
100,000
REYNOLDS NUMBER

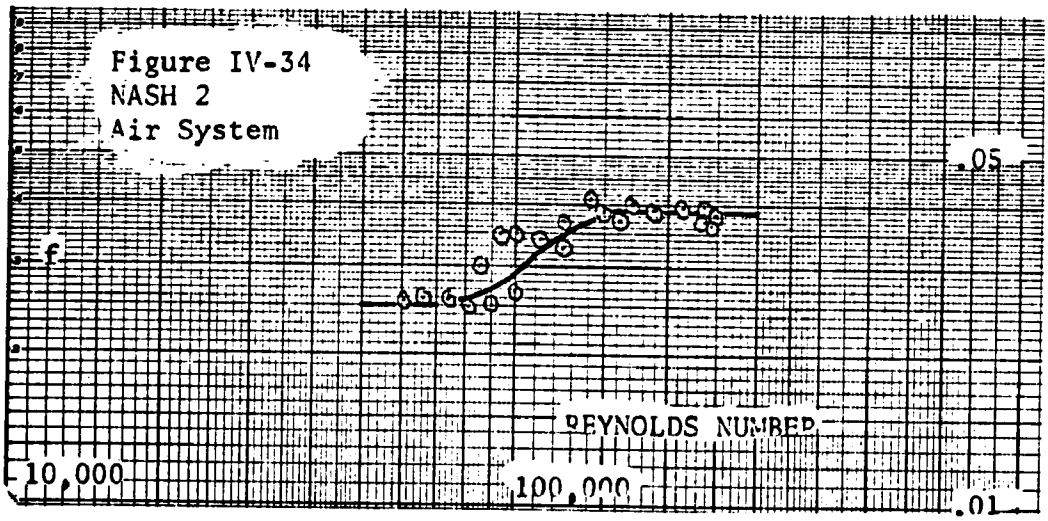
Figure IV-34
NASH 2
Air System
f
.05
.01
10,000
100,000
REYNOLDS NUMBER

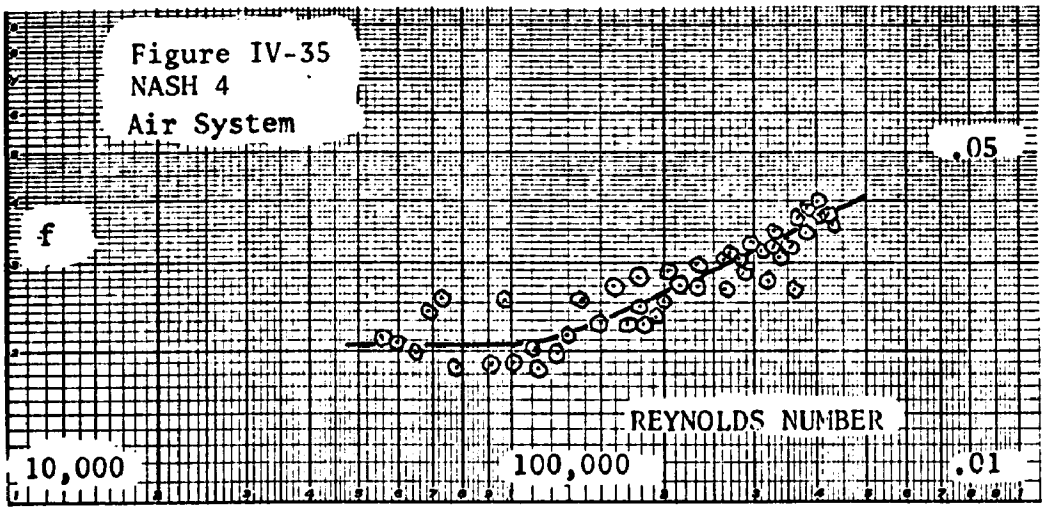
Figure IV-35
NASH 4
Air System
f
.05
REYNOLDS NUMBER
10,000
100,000
.01

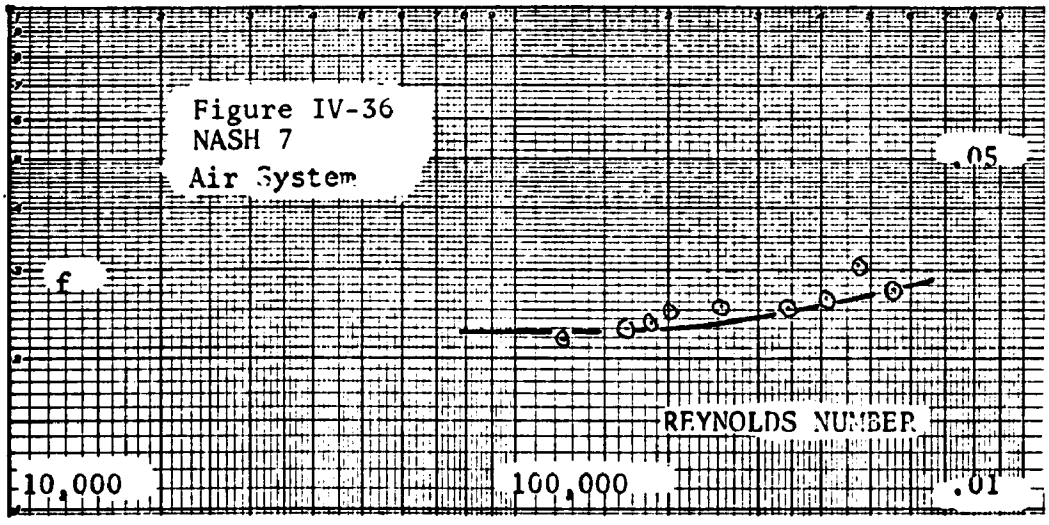
Figure IV-36
NASH 7
Air System
f
.05
REYNOLDS NUMBER
10,000
100,000
.01

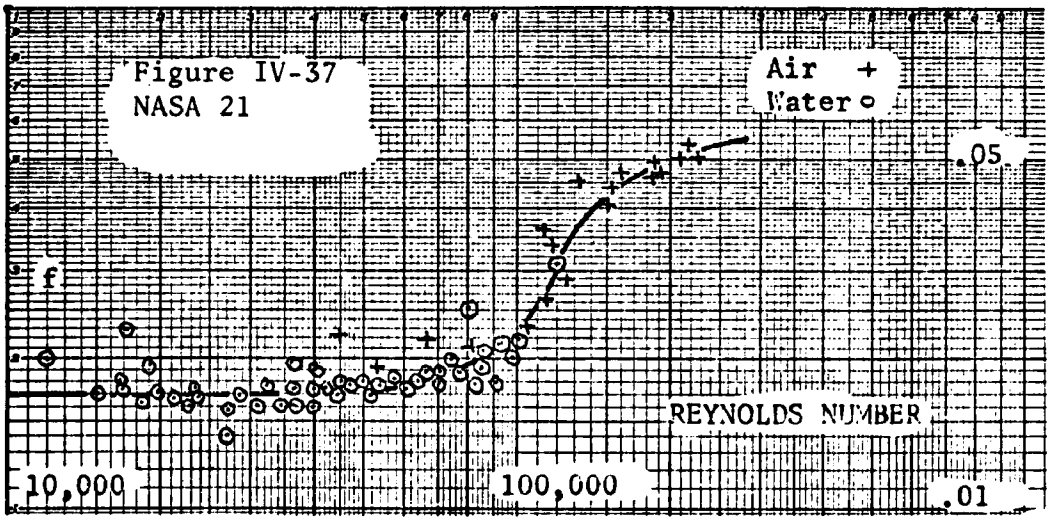
Figure IV-37
NASA 21
Air +
Water o
.05
f
REYNOLDS NUMBER
10,000
100,000
.01

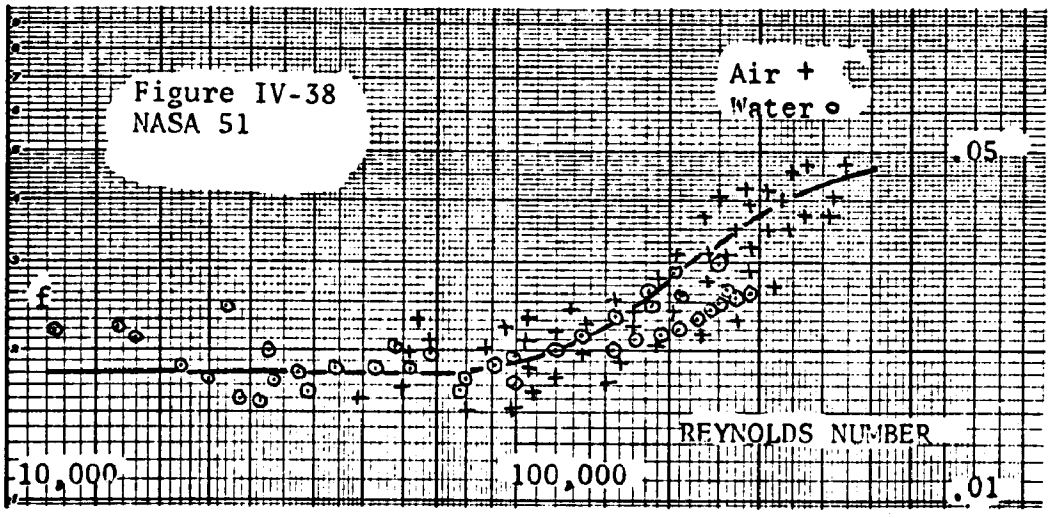
Figure IV-38
NASA 51
Air +
Water o
.05
f
REYNOLDS NUMBER
10,000
100,000
.01

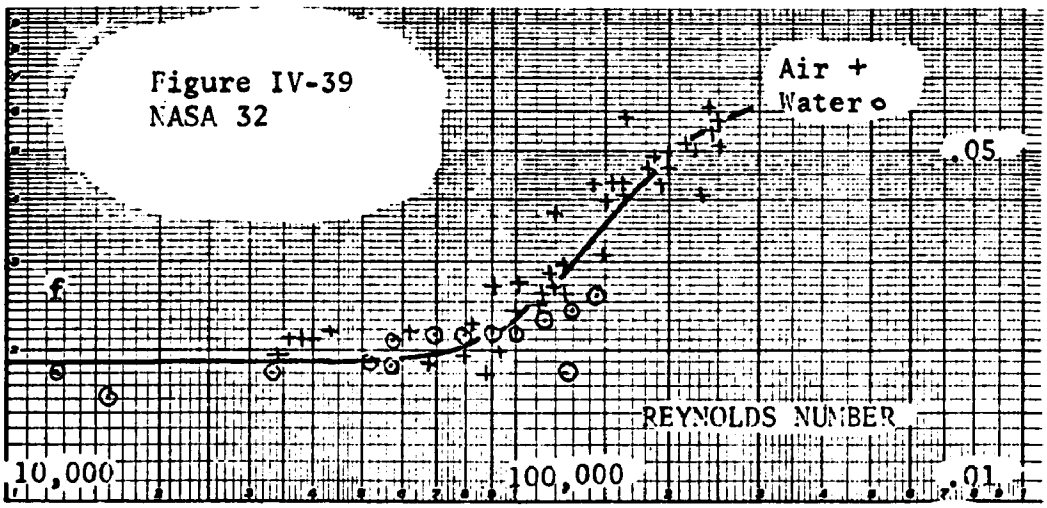
Figure IV-39
NASA 32
Air +
Water o
.05
f
REYNOLDS NUMBER
10,000
100,000
.01

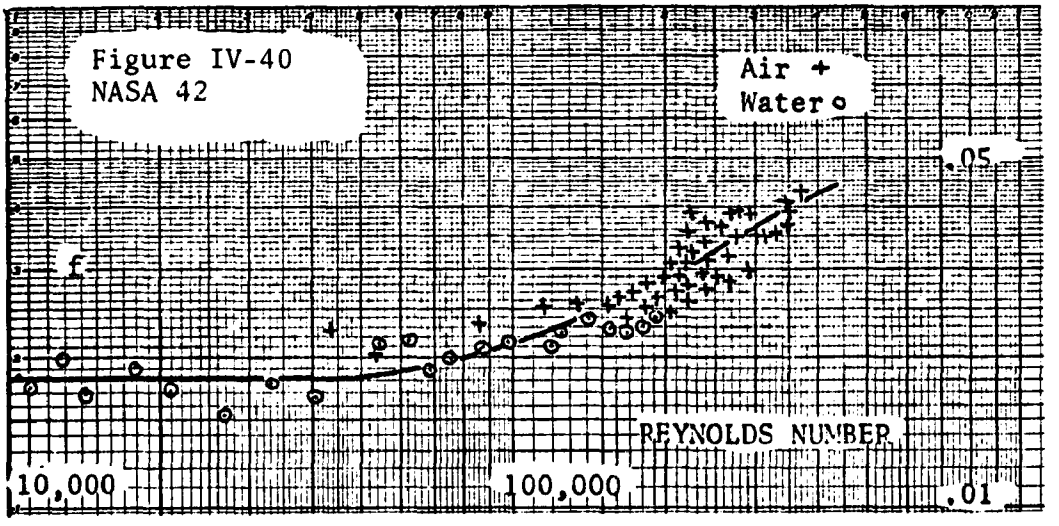
Figure IV-40
NASA 42
Air +
Water o
.05
f
REYNOLDS NUMBER
10,000
100,000
.01

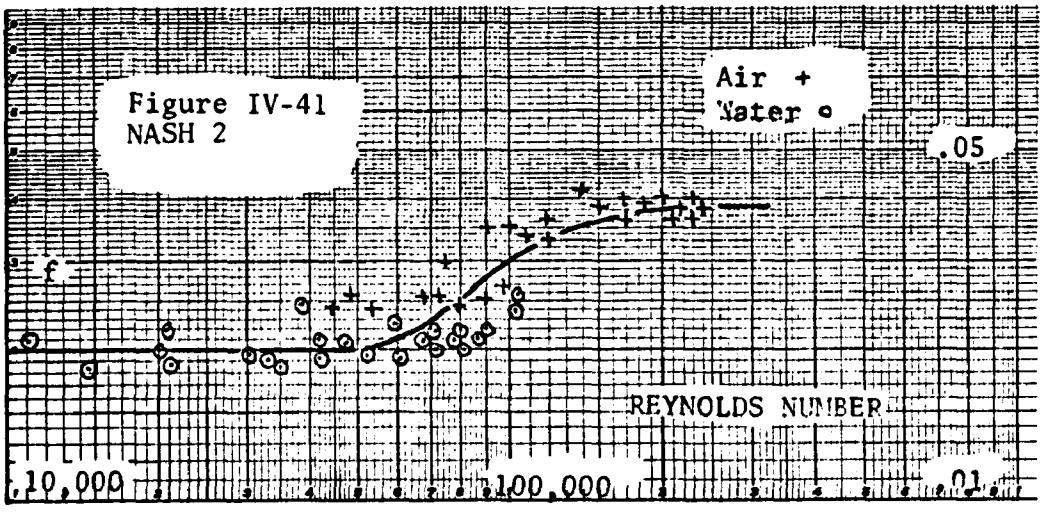
Figure IV-41
NASH 2
Air +
Water o
.05
f
REYNOLDS NUMBER
10,000
100,000
.01

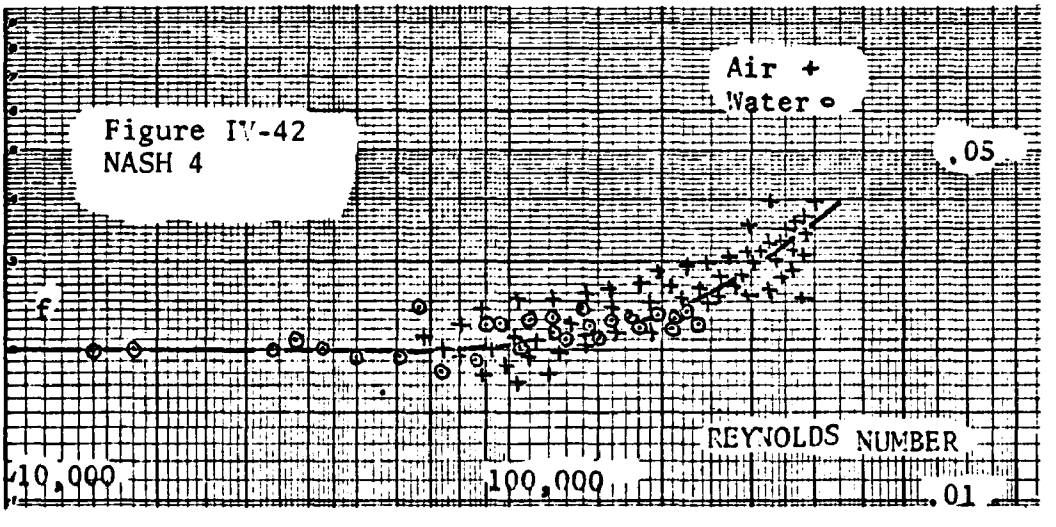
Figure IV-42
NASH 4
Air +
Water o
.05
f
REYNOLDS NUMBER
10,000
100,000
.01

hoses. This study found that two correlations are necessary to adequately describe the data obtained on all the flexible hoses. One correlation must be used to describe the data gathered on annular-type hoses and a different correlation used to describe the data obtained on helical-type hoses.

The graphical representation of the annular hose correlation is shown in Figure IV-43. The following variables apply to this figure:

$$Re^* = \frac{Re\sqrt{f}}{D/\lambda} \qquad \text{(IV-4)}$$

$$\psi(Re^*) = \frac{1}{\sqrt{f}} - 4 \log \left(\frac{D}{\lambda}\right) \qquad \text{(IV-5)}$$

This correlation can be divided into three parts. The first part corresponds to the initial region where the friction factor is independent of Reynolds number and a function of geometry above:

1. Region I $\quad 170 \leq Re^* \leq 1{,}400$

$$\psi\,(Re^*) = 4.35 \qquad \text{(IV-6)}$$

The second part of the correlation corresponds to the Reynolds number range where the friction factor is increasing:

2. Region II $\quad 1{,}400 < Re^* < 11{,}000$

$$\chi = \log Re^* - \log\,(1400) \qquad \text{(IV-7)}$$

$$\chi = \log Re^* - 3.146128$$

$$\phi = 4.35 - \psi\,(Re^*) \qquad \text{(IV-8)}$$

$$\S = \log \left\{ \frac{20\,\phi}{\log\,(100 - \phi)} \right\} \qquad \text{(IV-9)}$$

for $\chi \leq 0.54$

$$\S = \frac{\chi - 0.094}{0.090 + 0.539\,(\chi)} \qquad \text{(IV-10)}$$

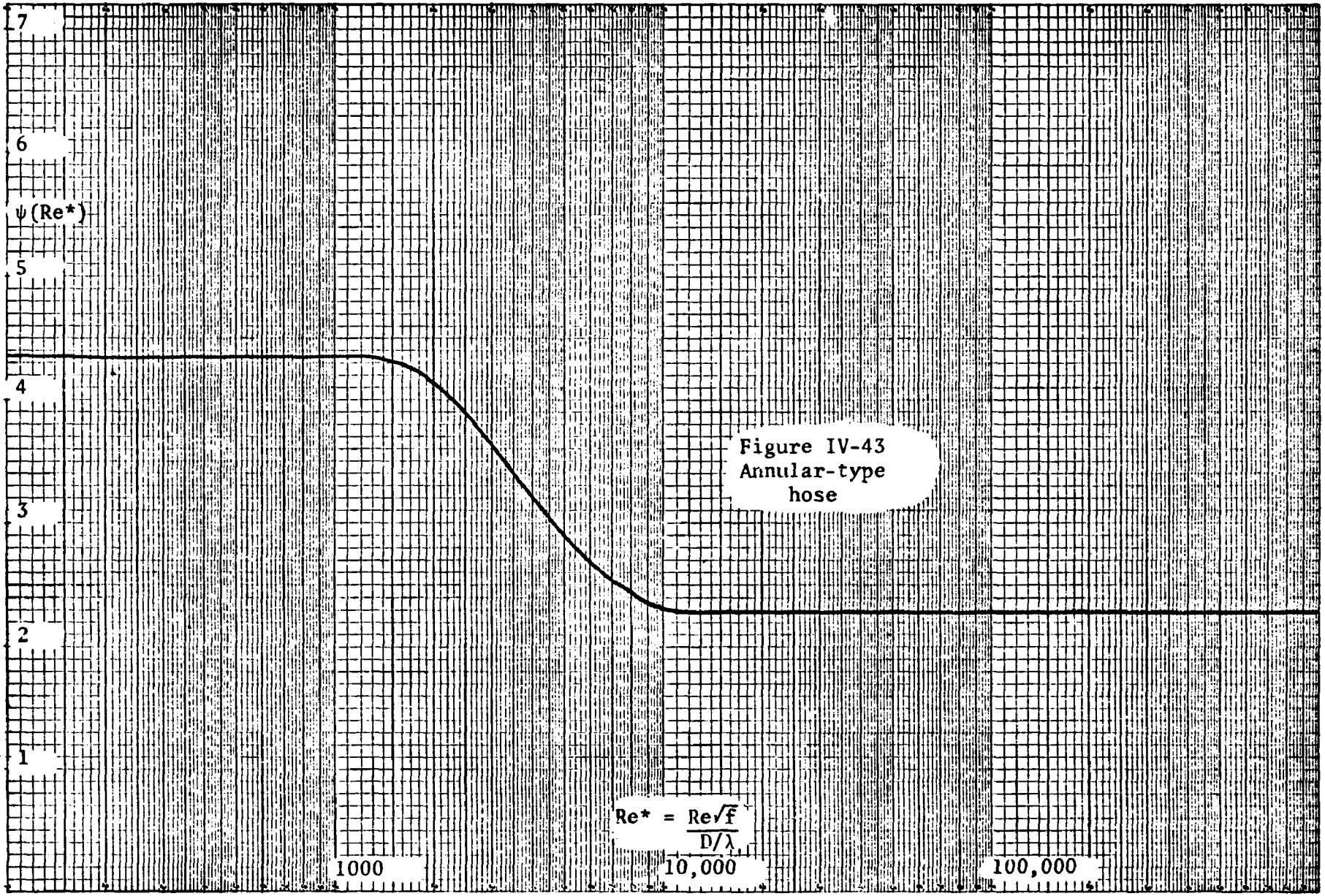

Figure IV-43
Annular-type
hose

for $\chi > 0.54$

$$\S = \frac{\chi - 0.094}{0.0395 + 0.633\ (\chi)} \qquad \text{(IV-11)}$$

The third part of the correlation corresponds to the high Reynolds number range where the friction factor is again constant:

3. Region III $\quad Re^* \geq 11{,}000$

$$\psi\ (Re^*) = 2.28 \qquad \text{(IV-12)}$$

The graphical correlation for the helical-type hose is shown in Figure IV-44. Again, the correlation can be divided into three parts:

1. Region I $\quad 180 \leq Re^* \leq 2{,}000$

$$\psi\ (Re^*) = 4.28 \qquad \text{(IV-13)}$$

2. Region II $\quad 2{,}000 < Re^* < 16{,}000$

for $\chi \leq 0.58$

$$\S = \frac{\chi - 0.116}{0.153 + 0.4375\ (\chi)} \qquad \text{(IV-14)}$$

for $\chi > 0.58$

$$\S = \frac{\chi - 0.116}{0.059 + 0.600\ (\chi)} \qquad \text{(IV-15)}$$

3. Region III $\quad Re^* \geq 16{,}000$

$$\psi(Re^*) = 2.28 \qquad \text{(IV-16)}$$

Equation (IV-9) is applicable for this figure but equations (IV-7) and (IV-8) are not. The corresponding equations for Figure IV-44 are:

$$\chi = \log\ (Re^*) - \log\ (2{,}000) \qquad \text{(IV-17)}$$

$$= \log\ (Re^*) - 3.30103$$

$$\phi = 4.28 - \psi(Re^*) \qquad \text{(IV-18)}$$

Alternate correlations have been developed for both types of hose when flow is described by Region I. Theoretical considerations suggest

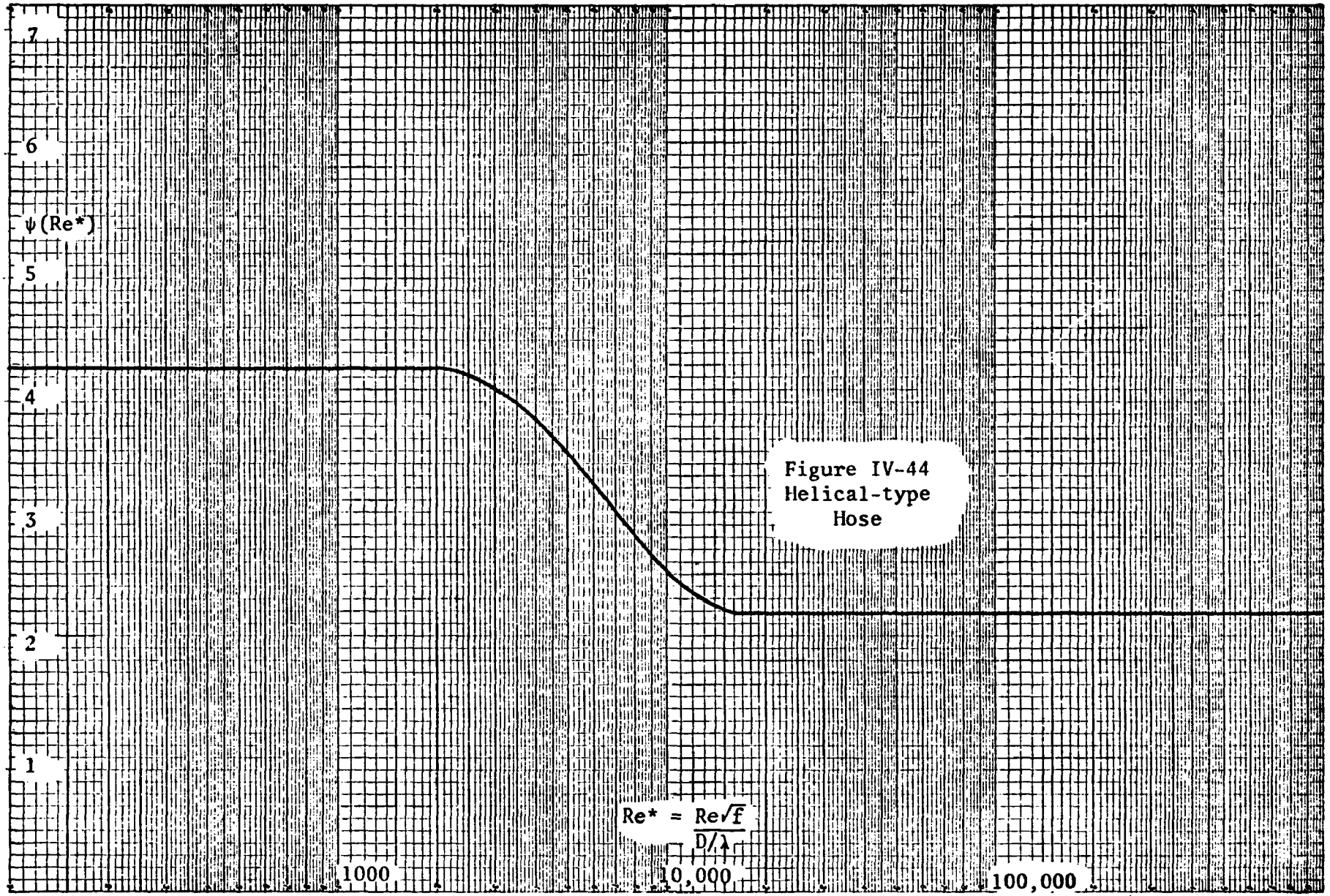

Figure IV-44
Helical-type
Hose

that in this region the friction factor might correlate better with λ/σ than with D/λ. This being the case, the following correlations have been developed:

1. Region I

   a. Annular-type hose

$$\frac{1}{\sqrt{f}} - 4 \log \frac{\lambda}{\sigma} = 6.34 \qquad \text{(IV-19)}$$

   b. Helical-type hose

$$\frac{1}{\sqrt{f}} - 4 \log \frac{\lambda}{\sigma} = 5.77 \qquad \text{(IV-20)}$$

To aid the designer of flexible metal hose systems Figure IV-43 and IV-44 have been put into more useful forms. Figure IV-45 shows the annular type hose correlation presented as a plot of friction factor versus Reynolds number with λ/D as a parameter. Figure IV-46 is a similar plot for the helical type hose.

Curved Hose Correlation:

Figures IV-47 through IV-49 show friction factor data taken at various degrees of curvature. The effect of increasing the friction factor by an increase in the curvature of the hose is readily apparent. However, note also that this effect tends to diminish as the Reynolds number becomes very large.

The following correlation has been shown to adequately describe the data for curved hoses obtained in this study:

$$\frac{f_B}{f} = 1.0 + 59.0 \left(\frac{D}{r_B}\right) (Re)^{-0.17} \qquad \text{(IV-21)}$$

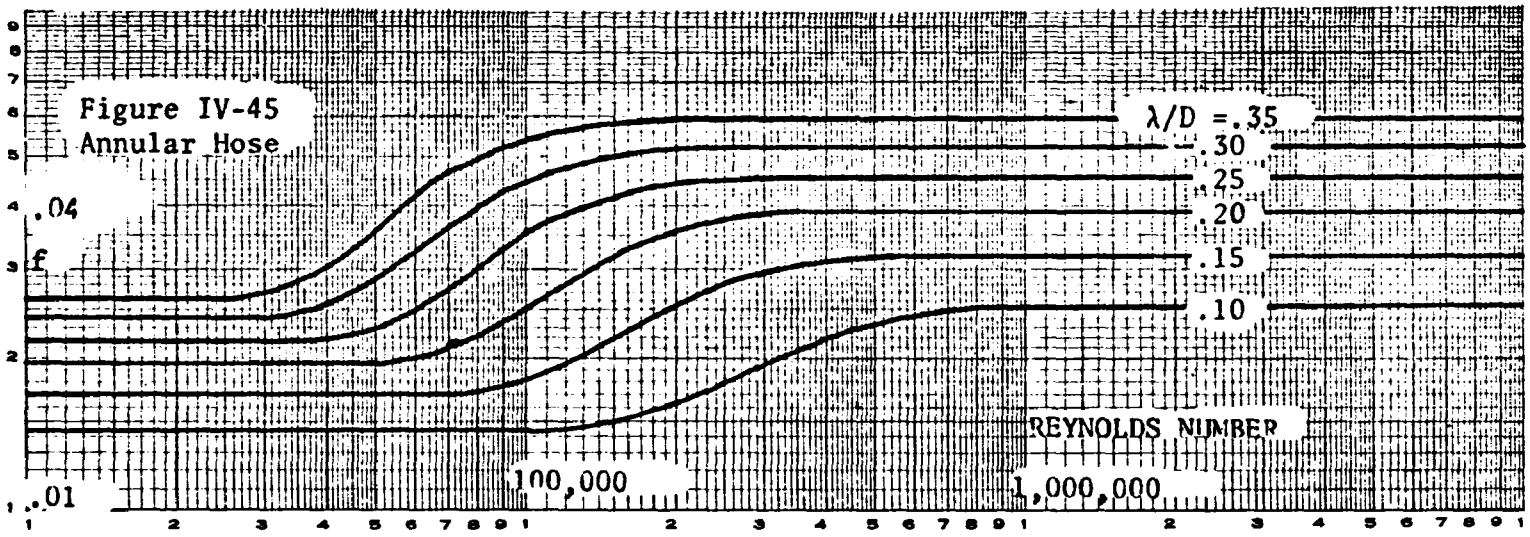
Figure IV-45
Annular Hose
.04
f
.01
λ/D =.35
.30
.25
.20
.15
.10
REYNOLDS NUMBER
100,000
1,000,000

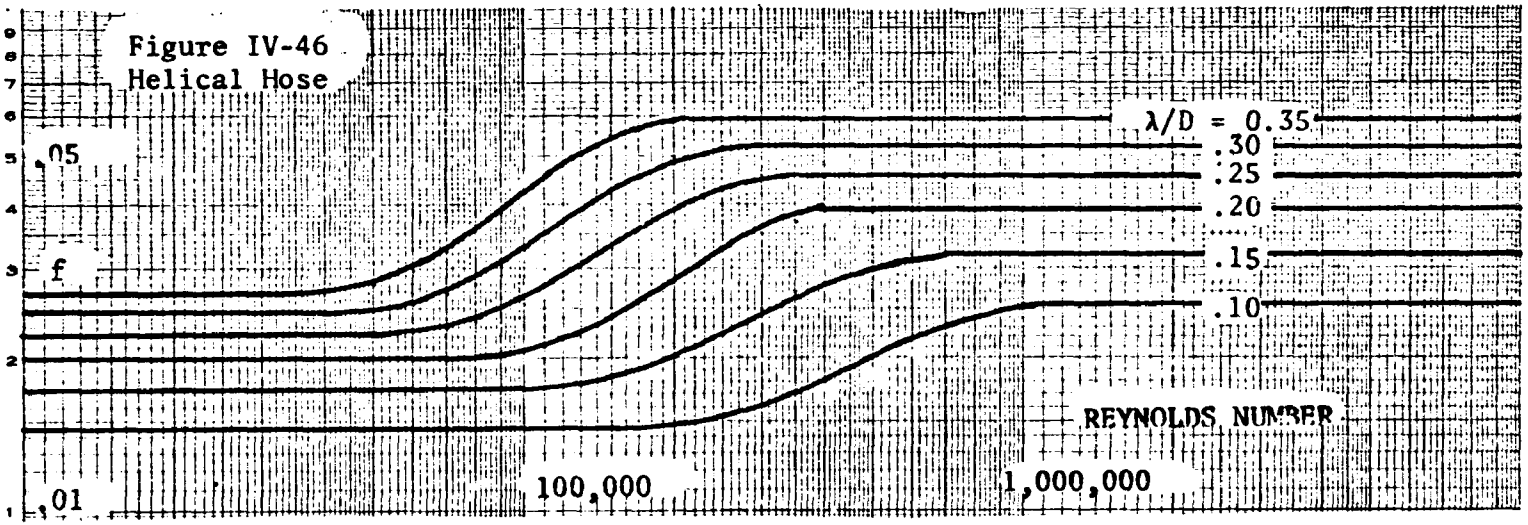
Figure IV-46
Helical Hose
.05
f
.01
λ/D = 0.35
.30
.25
.20
.15
.10
REYNOLDS NUMBER
100,000
1,000,000

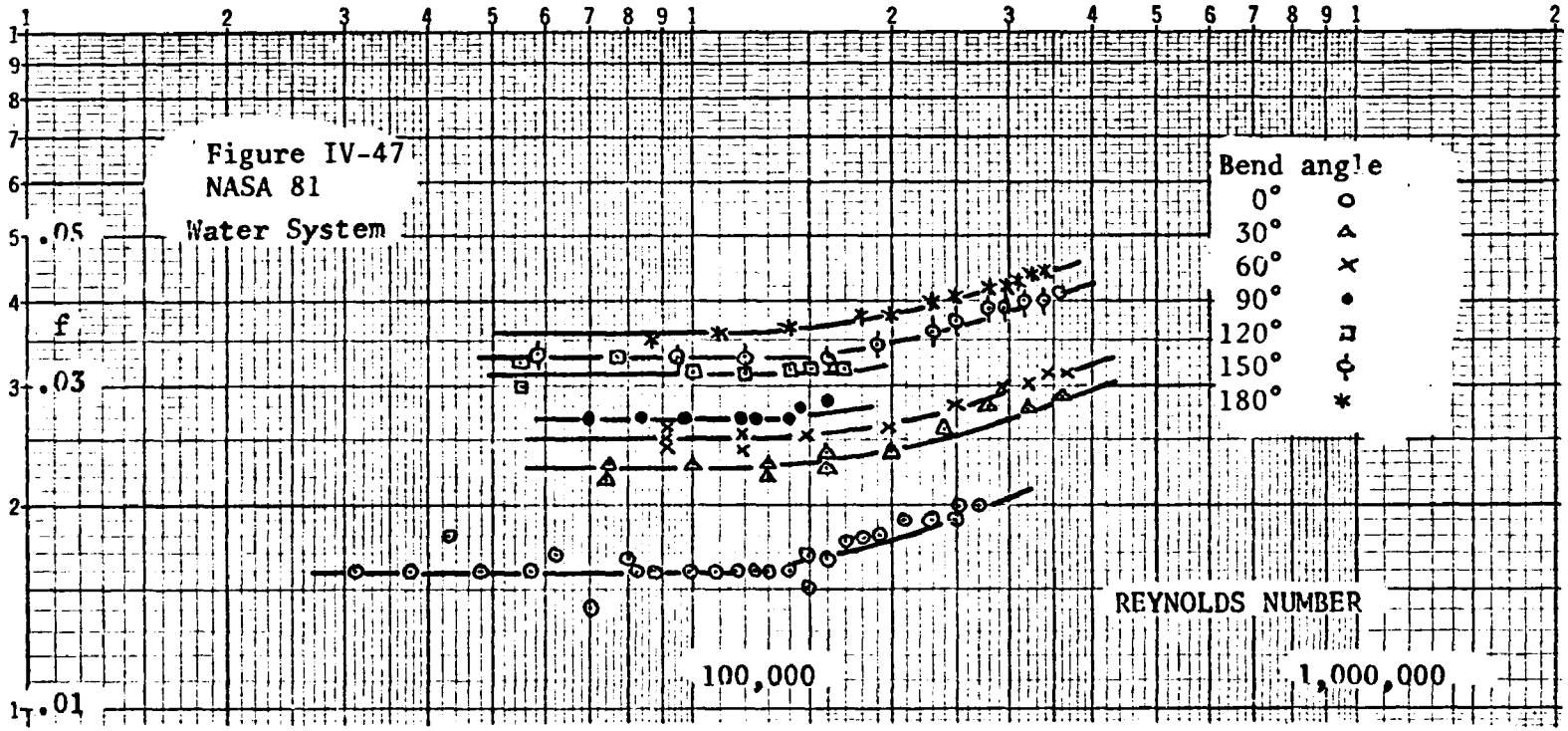
Figure IV-47
NASA 81
Water System
.05
f
.03
.01
Bend angle
0°
30°
60°
90°
120°
150°
180°
REYNOLDS NUMBER
100,000
1,000,000

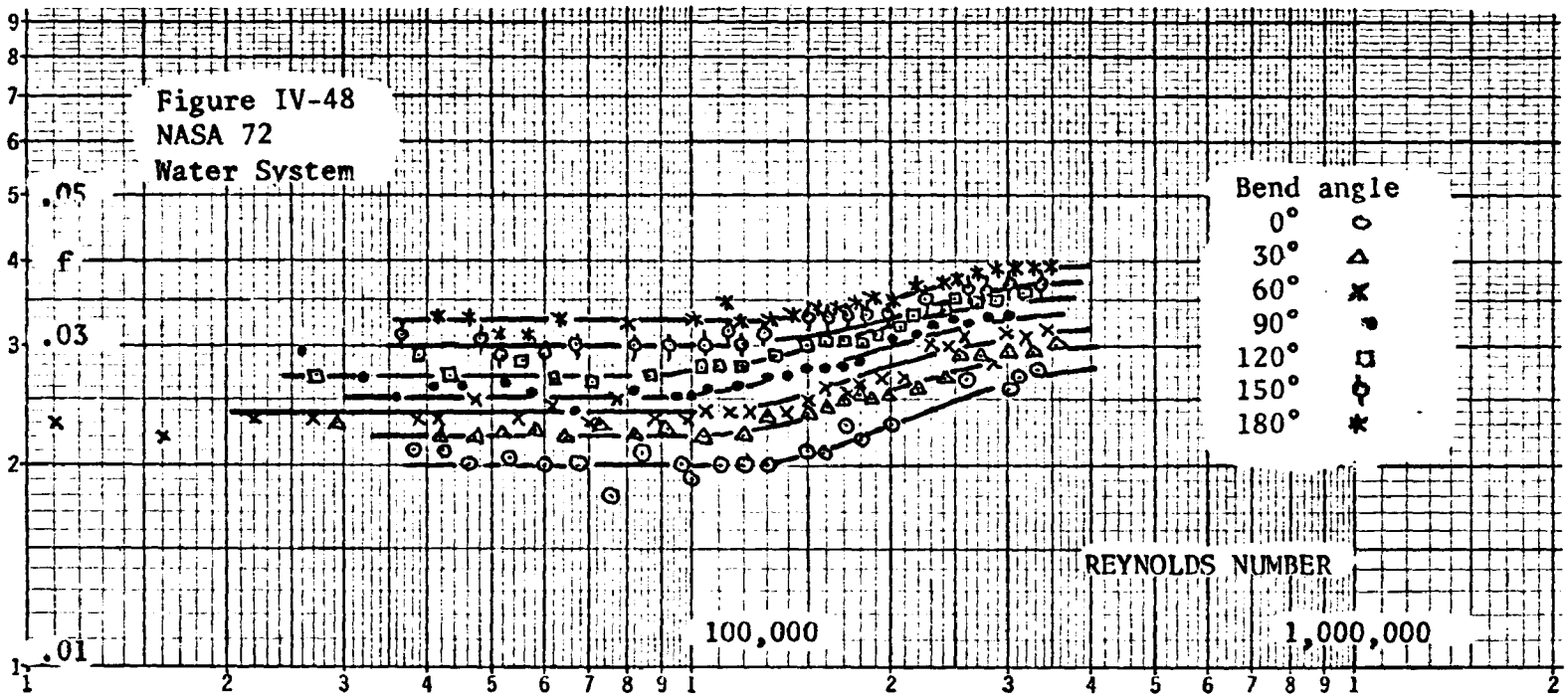
Figure IV-48
NASA 72
Water System
f
.05
.03
.01
Bend angle
0°
30°
60°
90°
120°
150°
180°
REYNOLDS NUMBER
100,000
1,000,000

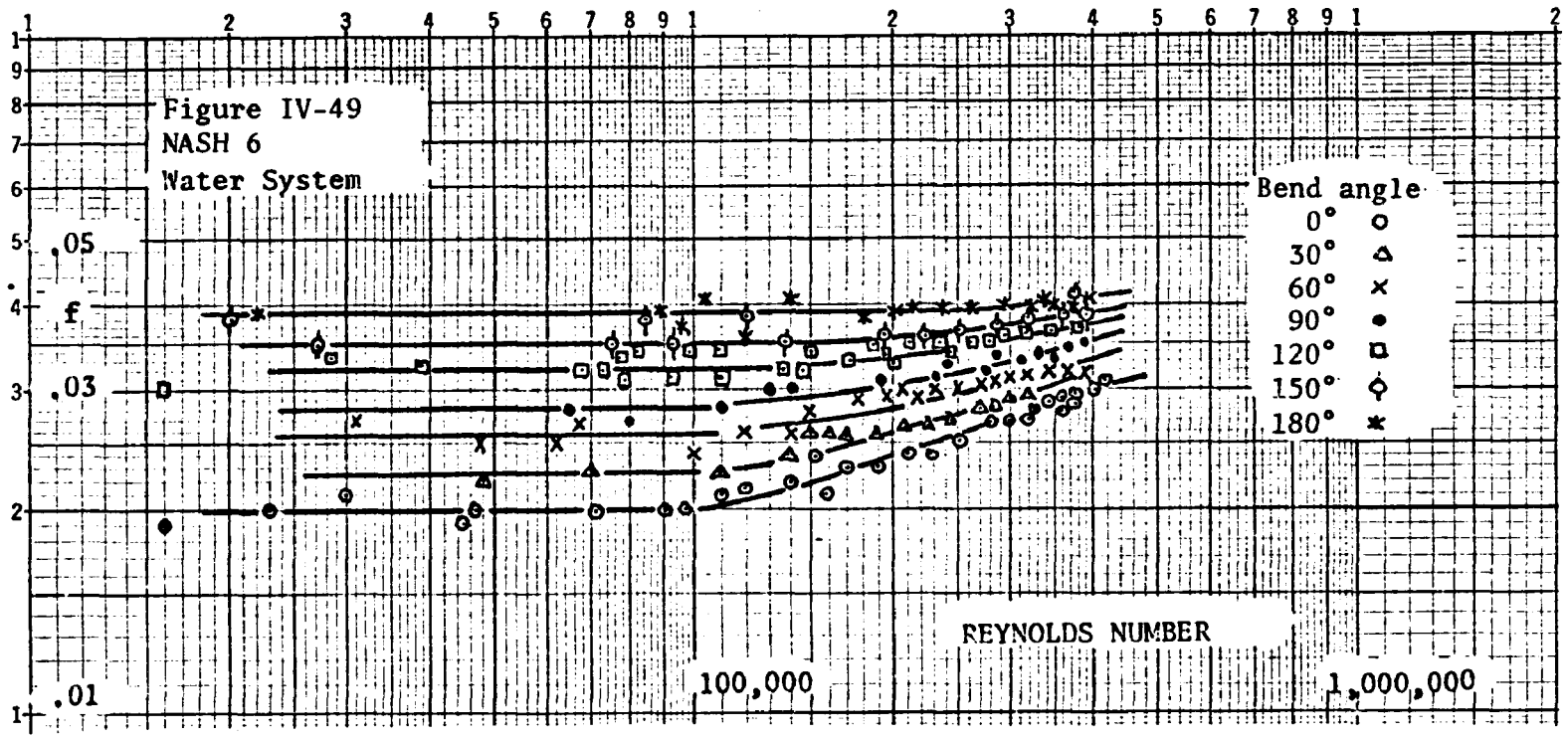
Figure IV-49
NASH 6
Water System
Bend angle
0°
30°
60°
90°
120°
150°
180°
.05
f
.03
.01
REYNOLDS NUMBER
100,000
1,000,000

Note that f_B is the friction factor for a curved section and f is the friction factor for a straight section of the same type of hose.

CHAPTER V

DISCUSSION OF RESULTS

This chapter attempts to interpret the results in the light of existing knowledge. First, a flow model is proposed in an attempt to give a rational explanation to the behavior observed for flow in flexible hoses. It is then shown how this model leads to certain conclusions as to which geometric parameters are important for the three flow regions discussed in Chapter IV. The correlations developed with these geometric parameters are then compared to previously published correlations for flow in flexible metal hoses.

Flow Model for Flexible Metal Hose:

Any proposed flow model must take into account the observed flow behavior. For flow in flexible metal hoses the flow behavior appears to be unique. However, as will be discussed later, there are other flow systems whose flow behavior is somewhat similar to that observed in flexible hose. Because of this similarity, some of the conclusions used to explain the behavior for these systems can be used to help explain the observed flow behavior in flexible hoses.

The flow behavior for flexible hose will be described using the relationship between friction factor, Reynolds number, and hose geometry. For the Reynolds number range used in this study there appears to be three distinct flow regions. At the low end of the turbulent regime the friction factor is independent of the Reynolds number and is a function

only of hose geometry. The lowest Reynolds number obtained in this study was about 10,000. However, the work of Allen (45) indicates that this region extends to Reynolds numbers much lower than this. Figure V-1 shows data obtained by Allen in the Reynolds number range 350 to 54,000. These data were taken on a flexible pipe of 0.5 inch minimum diameter, 0.813 inch maximum diameter and 0.104 inch pitch. Note that the critical Reynolds number for the transition from laminar to turbulent flow occurs at about 1700. Above a Reynolds number of 2100 the friction factor assumes a constant value of 0.020.

This indicates that, as soon as turbulent flow is established in the flexible hose a flow mechanism exists which is characterized by a friction factor which is independent of Reynolds number. Furthermore, experimental data indicates that this flow mechanism is present in the Reynolds number range from 2100 to about 60,000. Experiments further indicate that this upper limit of the Reynolds number is a function of hose geometry. It has not been established if the lower limit is similarly dependent on geometric factors.

At a Reynolds number of about 100,000 a change in flow mechanism obviously occurs in the flexible hose. This is indicated by a change in the behavior of the friction factor. Whereas initially the friction factor was independent of the Reynolds number, it now becomes a strong function of the Reynolds number increasing with an increase in the Reynolds number.

At very high Reynolds numbers, approximately 1,000,000 in some cases, the friction factor again enters a region in which it is independent of

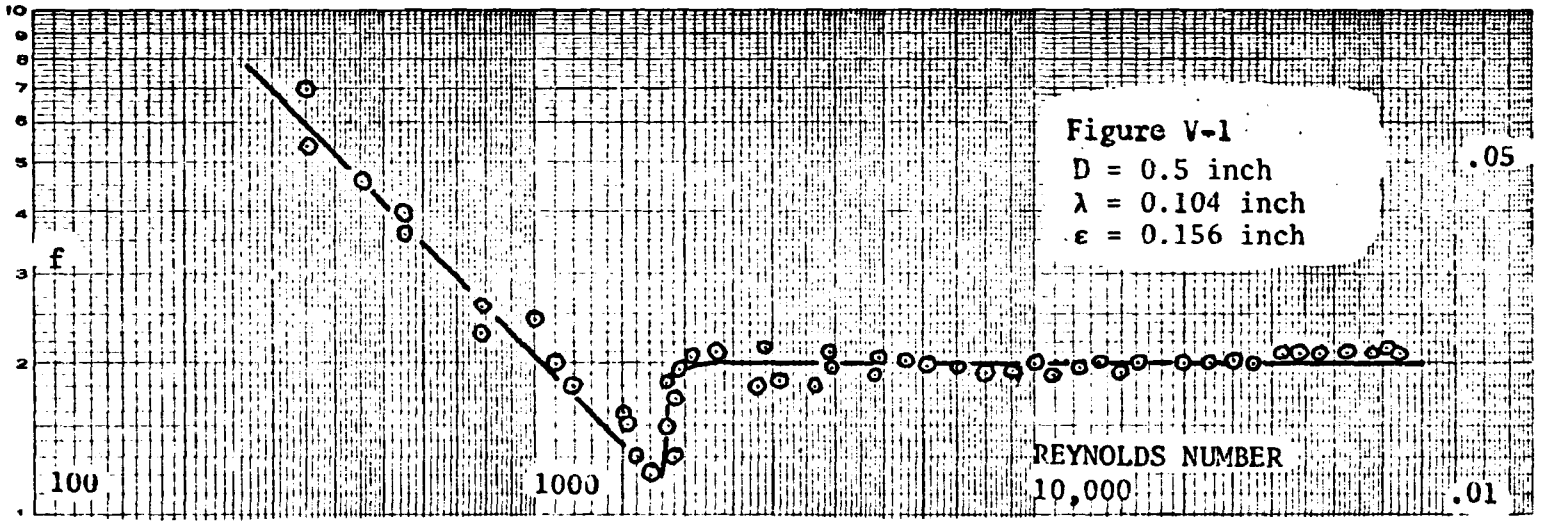
10
9
8
7
6
5
4
f
3
2
1
100
1000
10,000
REYNOLDS NUMBER
.05
.01
Figure V-1
D = 0.5 inch
λ = 0.104 inch
ε = 0.156 inch

the Reynolds number. This behavior is characteristic of all "rough" pipe. Nikuradse (26) observed this for sand-grain roughness elements and Daniels and Cleveland (51) found it for flow in flexible metal hoses.

The flow of liquids across a tube bank in a heat exchanger exhibits a behavior similar to that observed in flexible hose. Numerous investigations of the friction loss for flow across tube banks have been made. These data also are usually presented in the form of a plot of friction factor versus Reynolds number. However, because of the differences in geometry between the two flow systems, the friction factors and Reynolds numbers are not identical quantities. This presents no problem in interpreting the flow behavior of the two flow systems.

Figure V-2 is a plot of f_{KL} versus Re' showing data obtained by Kays, London, and Lo (55) for 4 different banks of tubes. The defining equations for f_{KL} and Re' are:

$$f_{KL} = \frac{2(-\Delta P)g_c\rho}{4G^2_{max}} \cdot \frac{d'}{L'} \qquad \text{(V-1)}$$

$$Re' = \frac{d'G_{max}}{\mu} \qquad \text{(V-2)}$$

The behavior shown by curve D is particularly interesting: its shape is distinctly different from the others and is similar to that observed for flow in flexible hoses. This curve represents data taken for tubes in an in-line arrangement.

Speculation as to what makes an in-line arrangement behave differently from a staggered arrangement may provide a clue to the flow mechanism occurring in a flexible hose in the region where the friction factor increases with an increase in Reynolds number.

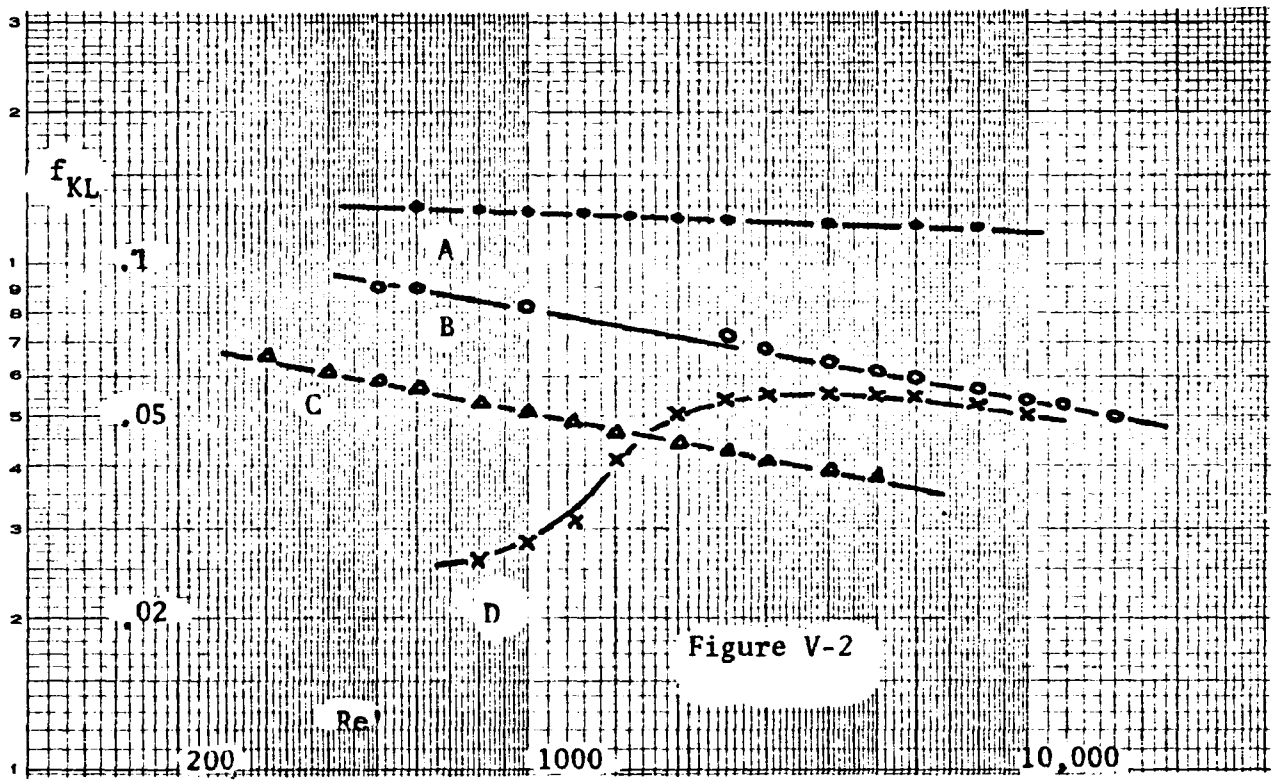

Figure V-2

Curve	Arrangement
A	Staggered
B	Staggered
C	Staggered
D	In-Line

Wallis (56) studied visually the flow of water perpendicular to tube banks by observing the motion of fine aluminum powder placed on the surface of the water. Wallis was able to obtain photographs of the flow patterns which occurred as the water flowed through the tube bank. Both the in-line arrangement and the staggered tube arrangement were studied. These arrangements are shown in Illustration V-1.

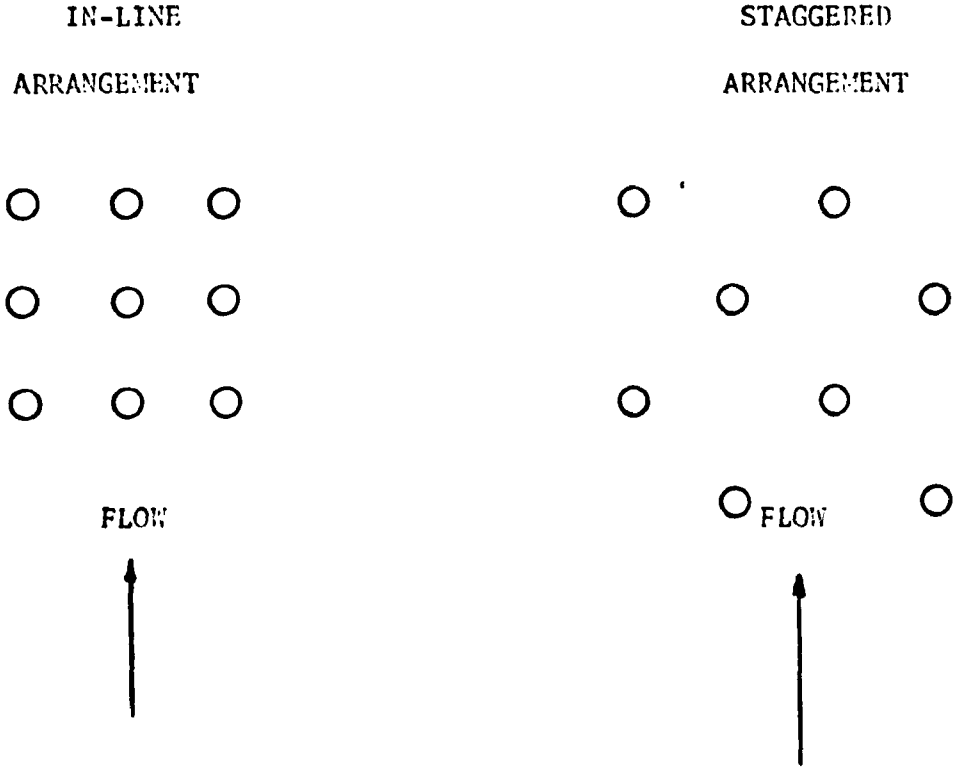

ILLUSTRATION V-1

The flow pattern for the in-line arrangement will be discussed first. At low flow rates the pattern around the tube is similar to that observed for flow around a single circular cylinder. The separation of the boundary layer and the turbulent wake behind each tube was quite evident. As the flow rate increased the turbulent wake increased in length until it encountered the next tube in the next transverse row, and only a very thin boundary layer formed on that tube. The spaces between the tubes in all transverse rows contained a turbulent wake, while in the unobstructed space between the longitudinal rows there was no evidence of excessive eddying or turbulence.

For the staggered tube arrangement in which the tubes are widely spaced, a turbulent wake also occurred behind each tube. However, since the next tube was two transverse rows away, this turbulent wake did not reach the next tube. It was found that a boundary layer was formed on the forward part of each tube in the bundle and subsequently separated. For closely spaced staggered arrangements the turbulent wake behind each tube was found to be considerably reduced. With these spacings the tubes are not in the turbulent wake of the tubes immediately upstream; this results in a reduced energy dissipation. The only place where there was a large turbulent wake was behind the last transverse row of tubes.

Since the flow behavior of the in-line tube arrangement was similar to that for flexible hose, it appears that similar mechanisms are at work. This mechanism can be described as a turbulent wake interfering

with boundary layer formation. Its characteristic behavior also seems to be an increasing friction factor with an increase in Reynolds number.

If the preceding discussion is taken as a basis, a model for the flow mechanisms occurring in flexible hose can now be proposed. The mechanical energy balance for an incompressible fluid in steady state flow through a pipe is:

$$\frac{\Delta \bar{v}^2}{2g_c} + \frac{g}{g_c}\Delta Z + \frac{\Delta P}{\rho} + H_f = 0 \qquad \text{(V-3)}$$

For a horizontal pipe of constant cross-sectional area the mechanical energy balance reduces to:

$$-\frac{\Delta P}{\rho} = H_f \qquad \text{(V-4)}$$

where H_f is the mechanical energy dissipated due to friction.

Frictional effects can be subdivided into two parts: (a) skin friction and (b) form friction. Using this concept equation (V-4) can then be written as:

$$-\frac{\Delta P}{\rho} = H_f = H_{f,s} + H_{f,d} \qquad \text{(V-5)}$$

where $H_{f,s}$ is the contribution of skin friction to the total friction and $H_{f,d}$ is the contribution of the form friction. In a given situation, both skin and form friction may be active in varying degrees. In general, when there is boundary layer separation and wake formation the total friction is largely form friction and skin friction is unimportant.

The following discussion deals with the proposed flow model for the low Reynolds number region in which the friction factor is independent of Reynolds number. There are two important regions in a flexible hose

where excessive friction, over and above that experienced in a smooth pipe, might be developed. One of these is in the valley between the convolutions. The flow model for this region assumes that a stable vortex (swirling eddy) is present in this valley and that this is the major contributor to skin friction. Another region of friction generation is at the crest of the convolution. The flow model assumes that on the front side of the convolution a boundary layer is built up and as it passes around the crest of the convolution boundary layer separation occurs and a wake is formed behind the convolution. However, an important assumption for this low Reynolds number range is that the wake has not developed to the extent that it interferes with boundary layer formation on the next convolution.

To evaluate the contributions of skin friction and form friction equation (V-5) can be written as:

$$\frac{-\Delta P}{\rho} = H_{f,s} + H_{f,d} = \frac{-\Delta P_s}{\rho} - \frac{\Delta P_d}{\rho} \qquad \text{(V-6)}$$

where $-\Delta P_s$ is the pressure drop due to skin friction and $-\Delta P_d$ is the pressure drop due to form friction. It now becomes necessary to evaluate the latter two terms in equation (V-6) in order to estimate the relative contributions of skin friction and form friction.

The defining equation for friction factors can be used as a basis for the estimation of the term $-\Delta P_d/\rho$.

$$F_k = A\ K\ f \qquad \text{(V-7)}$$

The assumption is now made that the convolutions behave as if they were doughnut-shaped with diameter equal to the flexible hose dimension σ. The characteristic velocity is taken to be a velocity near the crest of the convolutions and designated v_o. This velocity would be expected to

be less than the average velocity in the flexible hose. Using these assumptions equation (V-7) becomes:

$$F_{k,d} = \left(\frac{L}{\lambda}\right) \cdot C_D \cdot (\pi D\ \sigma) \cdot \frac{\rho v_o^2}{2g_c} \qquad \text{(V-8)}$$

Note that the term C_D has replaced f in equation (V-7). This is in keeping with the common convention of denoting drag coefficients by C_D and not f. The term (L/λ) has been introduced to take into account the number of convolutions per unit length. The kinetic force associated with form friction is the product of $-\Delta P_d$ and the cross-sectioned area of the flexible hose.

$$F_{k,d} = -\Delta P_d \cdot \left(\frac{\pi D^2}{4}\right) \qquad \text{(V-9)}$$

Combining this equation with equation (V-8) gives:

$$\frac{-\Delta P_d}{\rho} = 4 \left(\frac{L}{D}\right) \cdot \left[\frac{\sigma}{\lambda} \cdot C_D\right] \cdot \frac{v_o^2}{2g_c} \qquad \text{(V-10)}$$

To estimate the contribution of skin friction it is necessary to calculate the energy required to maintain the eddy motion in the valleys between the convolutions. These eddies can be regarded as essentially doughnut-shaped vortices of diameter equal to $(\lambda-\sigma)$, the clear spacing between the convolutions and of length equal to the flexible hose perimeter p. The velocity at the vortex perimeter is assumed equal to v_o. The angular velocity w is assumed constant at any radius.

The energy of flow per unit time through any concentric cylindrical shell (with differential thickness, dr) of the vortex is:

$$\dot{E} = \frac{dE}{dt} = \frac{dm}{dt} \frac{v_r^2}{2g_c} \qquad \text{(V-11)}$$

A material balance around this shell also gives:

$$\frac{dm}{dt} = \rho p v_r dr \qquad \text{(V-12)}$$

Combining these two equations results in

$$\dot{E} = \rho p \frac{v_r^3}{2g_c} dr \qquad \text{(V-13)}$$

Substituting the relationship $v_r = \omega_r$ into equation (V-13) and assuming that $\omega = \frac{v_o}{S/2}$, where $s = (\lambda - \sigma)$

$$\dot{E} = \rho p \left(\frac{1}{2g_c}\right) \frac{v_o^3}{(s/2)^3} r^3 dr \qquad \text{(V-14)}$$

To solve for the energy per unit time required to maintain vortex flow in the valleys between the convolutions, equation (V-14) is integrated with respect to r.

$$\text{Energy/time} = \int_o^{s/2} \rho p \frac{8}{2g_c} \frac{v_o^3}{s^3} \cdot r^3 dr$$

$$= \frac{\rho p s v_o^3}{16\, g_c} \qquad \text{(V-15)}$$

Since the quantity desired is $H_{f,s}$ equation (V-15) must be put on a per unit mass basis.

$$H_{f,s} = \left(\frac{L}{\lambda}\right) \cdot \left(\frac{\rho p s v_o^3}{16 g_c}\right) \cdot \left(\frac{1}{\rho \bar{v} \left(\frac{\pi}{4} D^2\right)}\right) \qquad \text{(V-16)}$$

This equation reduces to

$$H_{f,s} = \frac{1}{2} \cdot \frac{L}{D} \cdot \left(\frac{\lambda - \sigma}{\lambda}\right) \cdot \left(\frac{v_o}{\bar{v}}\right)^3 \cdot \frac{\bar{v}^2}{2g_c} \qquad \text{(V-17)}$$

Equation (V-10) can also be written in a form similar to equation (V-17)

$$H_{f,D} = 4 \cdot \frac{L}{D} \cdot \left(\frac{\sigma}{\lambda}\right) \cdot C_D \cdot \left(\frac{v_o}{\bar{v}}\right)^2 \cdot \frac{\bar{v}^2}{2g_c} \qquad \text{(V-18)}$$

Combining equations (II-8), (V-17), and (V-18) an expression for the friction factor can be obtained:

$$f = \left[\left(\frac{\sigma}{\lambda}\right) \cdot C_D + \frac{1}{8} \cdot \left(\frac{\lambda-\sigma}{\lambda}\right)\left(\frac{v_o}{\bar{v}}\right)\right]\left(\frac{v_o}{\bar{v}}\right)^2 \qquad \text{(V-19)}$$

This expression relates the friction factor to the quantities σ, λ, C_D and the velocity ratio $(v_o/\bar{v})$. For a given hose σ and λ are constant and equation (V-19) predicts that f would depend on the quantities C_D and $(v_o/\bar{v})$. The pertinent question now becomes, assuming that the flow model is correct, under what conditions would the quantities C_D and $(v_o/\bar{v})$ become independent of the Reynolds number and hence cause equation (V-19) to predict a constant friction factor.

The only thing which can be done at the present time to answer this question is to take systems for which data are available and assume that they are approximations to the real system. First, consider the effect of Reynolds number on C_D. The relationship between C_D and Re is well established for flow around a submerged cylinder. Assuming a typical case of the flow of water at 5 ft./sec. in a flexible hose having a σ value of 0.125 inch gives a Reynolds number $(\sigma\bar{v}/\nu)$ equal to about 6000. At this Reynolds number the value of C_D is about 1.0. However, the important point is that a Reynolds number with this order of magnitude defines a region where C_D is independent of Reynolds number, in fact C_D is about 1.0 for the Reynolds number range from 100 to 200,000. It appears reasonable to assume that for

flow at low Reynolds numbers C_D would be independent of Reynolds number for all of the hoses tested in this study.

Consideration now turns to the quantity $v_o/\bar{v}$. Assume that the velocity distribution in a flexible hose can be represented by an equation of the form:

$$\frac{v}{v^*} = 2.5 \ln\left(\frac{y}{\varepsilon}\right) + B \qquad \text{(V-20)}$$

where B is a constant whose magnitude depends on the roughness of the flexible hose. For the velocity v_o this equation becomes:

$$\frac{v_o}{v^*} = 2.5 \ln\left(\frac{y_o}{\varepsilon}\right) + B \qquad \text{(V-21)}$$

where y_o is some small distance measured from the crest of the convolution. From the definitions of the friction factor and v* the following relationship can be derived:

$$\frac{\bar{v}}{v^*} = \frac{1}{\sqrt{f/2}} \qquad \text{(V-22)}$$

Using equations (V-21) and V-22) to solve for $v_o/\bar{v}$:

$$\frac{v_o}{\bar{v}} = \sqrt{\frac{f}{2}} \left(2.5 \ln \frac{y_o}{\varepsilon} + B\right) \qquad \text{(V-23)}$$

This result indicates that for a given hose the ratio $v_o/\bar{v}$ depends on the value of the friction factor. However, since the friction factor remains constant for turbulent flow in the low Reynolds number region, equation (V-23) predicts that $v_o/\bar{v}$ will also be independent of Reynolds number.

These results indicate that in the low Reynolds number range equation (V-19) may be an acceptable model for the proposed flow mechanism. To get a rough idea of the order of magnitude of the friction factor predicted by equation (V-19) consider a case for flow through hose NASH 4. For this hose $\sigma/\lambda = 0.125/0.250 = 0.50$ and the value of C_D is assumed to be 1.0. At the present time, all that is known about the magnitude of $v_o/\bar{v}$ is that it is less than 1.0. For purposes of this calculation assume that it is of the order of 0.2. Using these figures the terms in equation (V-19) become:

$$\frac{\sigma}{\lambda} \cdot C_D \approx 0.50$$

$$\frac{1}{8} \cdot \left(\frac{\lambda-\sigma}{\lambda}\right) \cdot \left(\frac{v_o}{\bar{v}}\right) \approx 0.0125$$

$$\left(\frac{v_o}{\bar{v}}\right)^2 \approx 0.04$$

therefore, substitution in equation (V-19) gives:

$$f \approx (0.50 + 0.0125) \cdot (0.04) \approx 0.0205$$

The experimental values for the friction factors in the low Reynolds number range are all of the order of magnitude of 0.020. Note that equation (V-19) predicts that the contribution of skin friction to the overall friction factor is very small. For the assumed case just discussed skin friction contributed only a little more than 2% of the total friction. This is in general agreement with the statement that when boundary layer separation and wake formation is present the total friction is largely form friction and skin friction is unimportant.

Because of difficulties in measuring or estimating the various terms equation (V-19) does not appear to be acceptable as a design relationship. However, it does suggest that the friction factor for turbulent flow at low Reynolds numbers could be correlated with the geometric ratio σ/λ. This correlation has been developed for both annular and helical-type hoses.

1. Annular-type hose

$$\frac{1}{\sqrt{f}} - 4 \log \left(\frac{\lambda}{\sigma}\right) = 6.34 \qquad \text{(V-24)}$$

This relationship has been tested for values of $Re\sqrt{f}/(D/\lambda)$ from 170 to 1400.

2. Helical-type hose

$$\frac{1}{\sqrt{f}} - 4 \log \left(\frac{\lambda}{\sigma}\right) = 5.77 \qquad \text{(V-25)}$$

This expression has been tested in the range of $Re\sqrt{f}/(D/\lambda)$ from 180 to 2,000.

As the flow rate through the flexible hose increases the wake which has been generated behind the convolution begins to interfere with the boundary layer or the next convolution. The proposed flow model for flexible hose assumes that this is the point where the friction factor begins to increase with an increase in flow rate. This result follows from the assumption that the flow mechanism in flexible hose is similar to that observed for flow across tube banks.

As was mentioned in Chapter II, Morris (39) proposed a wake-interference flow mechanism in connection with his study of flow over rough pipe and channel surfaces. He states that for wake-interference

flow the relative roughness spacing D/λ will be an important correlating parameter. In general, rough pipe is correlated with the relative roughness parameter D/ε. However, Morris concluded that for wake-interference flow the height ε of the roughness element is relatively unimportant and the spacing λ is of major importance.

Figure V-3 shows a comparison between the correlation Morris obtained for flow in corrugated channels, Nikuradse's correlation for flow in pipes roughened by densely-packed uniform sand grains, and the correlation developed for annular hose from the results of this study. Nikuradse's correlation is usually interpreted in terms of the relative roughness parameter D/ε. However, it is evident that D/λ is numerically equal to D/ε for his pipes and hence either parameter can be used without affecting the numerical results. It should also be noted that Morris' correlation was derived from data obtained on pipes with diameters greater than 18 inches.

Experimental data for very high Reynolds numbers were not obtained in this study. This was due to capacity limitations in the pumps and compressors. In only a few cases did the experimental results demonstrate that the friction factor would approach a constant value at very high Reynolds numbers. However, Daniels and Cleveland (48) performed experiments at very high Reynolds numbers and their results clearly indicate that the friction factor does attain a constant value.

In the correlations for both annular and helical-type hoses the value of $\psi(Re^*)$ at very high Reynolds numbers is taken to be 2.28. Morris (39) concluded from his study that this limiting value is applicable to all types of roughness elements.

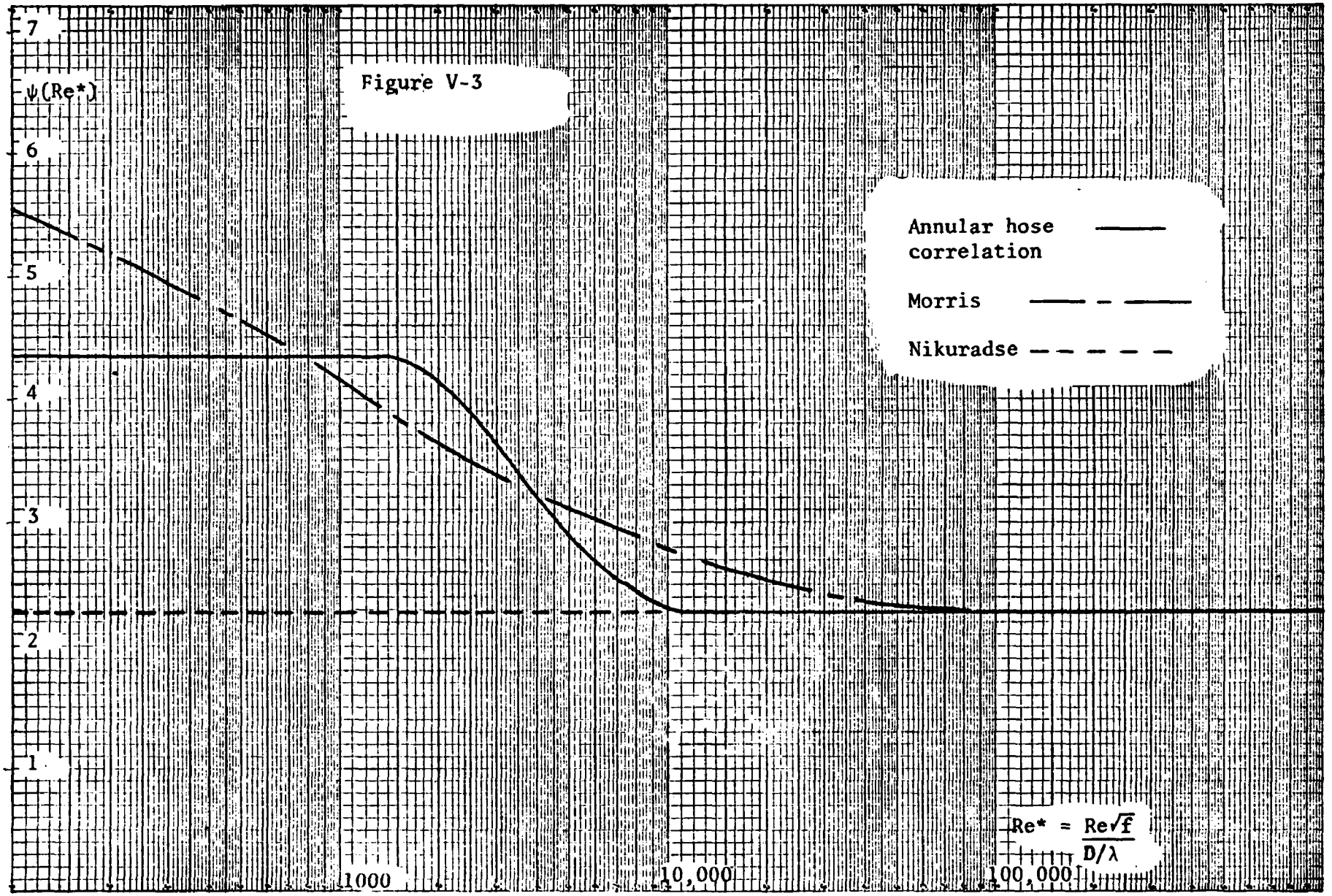
Figure V-3
ψ(Re*)
7
6
5
4
3
2
1
Annular hose correlation
Morris
Nikuradse
Re* = Re√f / D/λ
1000
10,000
100,000

Before the flow model proposed in this section can be accepted as fact further experimental work must be performed. Perhaps the most pressing need for the confirmation or rejection of this model is a good visual flow experiment. At the present time this has not been performed. The point to be emphasized is that available mathematical methods seem capable of solving fluid mechanics problems only when adequate knowledge of the flow models is provided beforehand, and more often than not this essential information has been provided by a skillful visual study.

The basic approach to further experimental work on flexible hoses should be modified. Experimental work should now be concerned with investigating fundamental quantities. For example, studies of the velocity profiles in the main stream of the hoses (i.e., the center core) and of flow patterns in the annular or helical segments created by the corrugations would contribute greatly to the understanding of the friction factor behavior. If the various mechanisms that consume mechanical energy as "friction" can be isolated and evaluated separately, the results would be of immeasurable value in predicting the friction factor or - at the very least - in guiding and interpreting empirical correlations.

Accuracy of Correlations:

Table V-1 gives an indication of the accuracy of various correlations for the data produced in this study. The appendix contains a listing of the computer program used to obtain the results given in this table. For each hose (straight sections only) the average error (%)[1]

[1] $\text{Error} = \dfrac{f_{calc} - f_{obs}}{f_{obs}}$

TABLE V-1

MODEL COMPARISONS FOR STRAIGHT HOSE

Hose	FNASA		FR		FR1		FN		FDF	
	(1)	(2)	(1)	(2)	(1)	(2)	(1)	(2)	(1)	(2)
NASA 11	9.4	30.1	7.2	29.4	-17.6	40.1	259.1	244.9	146.9	140.1
NASA 12	29.7	61.9	38.5	52.9	24.9	64.4	175.1	147.6	-1.2	49.5
NASA 21	7.5	35.8	1.1	27.4	-5.0	34.3	270.0	235.0	141.4	124.0
NASA 22	-23.6	39.4	-5.6	21.7	-33.2	48.6	165.2	146.0	56.8	52.7
NASA 31	0.8	35.0	-8.2	33.5	-18.7	33.4	189.3	166.8	87.8	80.4
NASA 32	32.5	52.0	34.7	35.3	33.8	47.6	336.9	163.3	152.8	70.8
NASA 41	1.4	25.9	-17.4	33.0	-12.3	29.9	180.5	161.0	84.8	77.7
NASA 42	-7.0	31.6	5.2	23.2	-20.6	38.0	168.5	144.1	41.0	40.4
NASA 51	11.5	24.0	-6.2	22.1	-15.2	30.0	182.2	163.0	68.5	62.7
NASA 52	10.7	20.9	38.7	53.8	-24.4	31.8	149.8	148.7	-18.0	26.3

(1) Average error (%)

(2) Average standard deviation (%)

Table V-1 (cont'd)

Hose	FNASA (1)	FNASA (2)	FR (1)	FR (2)	FR1 (1)	FR1 (2)	FN (1)	FN (2)	FDF (1)	FDF (2)
NASA 61	9.8	28.3	-16.5	33.2	-7.6	32.6	161.3	146.2	59.9	57.6
NASA 62	4.6	29.3	23.4	40.9	-16.4	38.4	129.1	120.1	-33.1	47.0
NASA 71	25.4	50.6	-5.7	54.5	-7.5	53.3	174.8	148.9	54.7	60.3
NASA 72	5.4	11.1	18.7	32.1	-14.2	17.0	168.0	174.3	10.3	13.8
NASA 81	45.1	49.6	13.8	26.0	2.6	9.0	250.9	259.6	102.9	108.0
NASA 82	13.7	17.8	22.9	30.4	-12.2	21.7	202.8	205.7	38.9	41.6
NASH 1	16.7	40.8	20.7	37.0	-13.6	51.1	240.9	185.6	33.9	42.4
NASH 2	-20.5	38.4	-3.6	25.7	-18.0	41.6	197.9	177.9	61.7	57.9
NASH 3	-15.6	29.0	-0.4	15.4	-27.6	38.3	176.7	165.5	49.7	48.6
NASH 4	- 3.8	26.8	3.3	19.2	- 9.1	28.6	194.3	173.8	56.0	52.2
NASH 5	- 4.5	19.3	3.7	23.1	-23.3	31.8	180.4	174.2	49.2	49.1
NASH 6	- 4.4	19.5	-7.8	20.7	-23.7	31.0	149.8	144.6	30.4	33.5
NASH 7	15.8	17.4	-3.3	10.7	-2.3	15.0	206.7	204.5	65.5	65.4
NASH 8	29.3	46.7	2.1	45.7	13.4	41.4	244.2	218.3	90.5	84.5

Table V-1 (cont'd)

Hose	FDC1		FMSU		FDC2		FHVH		FNK1	
	(1)	(2)	(1)	(2)	(1)	(2)	(1)	(2)	(1)	(2)
NASA 11	--	--	--	--	1.0	28.2	38.4	43.0	123.7	120.0
NASA 12	--	--	--	--	-16.7	52.5	56.0	57.4	61.3	62.2
NASA 21	9.0	19.8	25.0	50.6	11.0	31.1	41.4	50.7	121.1	107.7
NASA 22	-4.3	20.8	25.5	53.7	-11.7	28.9	88.8	30.7	58.2	54.4
NASA 31	4.8	26.7	8.1	39.1	0.2	31.7	6.5	40.0	68.1	65.8
NASA 32	35.9	29.9	23.3	30.0	37.8	41.8	75.8	52.8	153.8	71.8
NASA 41	-2.0	23.8	4.1	47.7	2.2	25.6	4.0	37.3	57.8	56.8
NASA 42	4.7	22.6	2.8	34.7	1.5	34.7	8.0	3.1	49.6	46.0
NASA 51	4.5	19.8	5.3	37.1	4.6	19.6	0.9	30.4	56.3	53.1
NASA 52	-4.8	20.6	9.0	51.7	-4.3	19.5	35.2	36.6	35.4	47.5
NASA 61	-3.6	28.3	16.2	51.0	0.5	26.8	-14.0	37.7	41.5	44.4
NASA 62	-12.4	32.1	-7.4	41.7	-12.5	32.3	22.3	31.6	20.3	31.1

Table V-1 (cont'd)

Hose	FDC1		FMSU		FDC2		FHVH		FNK1	
	(1)	(2)	(1)	(2)	(1)	(2)	(1)	(2)	(1)	(2)
NASA 71	0.9	52.1	16.1	64.8	7.7	51.5	-6.1	52.8	47.5	57.4
NASA 72	-3.1	15.0	3.5	42.7	2.1	13.6	16.9	19.2	43.2	46.7
NASA 81	19.2	28.5	21.0	56.4	32.7	41.4	19.7	21.6	89.4	95.4
NASA 82	6.1	11.8	4.5	29.5	16.6	20.6	23.1	27.0	62.6	66.0
NASH 1	--	--	--	--	-1.0	43.8	83.9	65.2	101.6	78.3
NASH 2	4.9	36.9	21.4	63.3	-3.2	24.6	30.4	36.6	78.1	72.1
NASH 3	13.0	32.1	6.8	39.7	0.05	14.9	20.2	27.7	64.0	61.4
NASH 4	16.8	26.0	21.2	51.4	12.1	20.5	21.6	31.1	66.9	61.2
NASH 5	14.6	35.5	10.9	52.3	9.6	23.2	17.1	24.0	60.3	59.6
NASH 6	0.07	20.1	8.8	41.4	4.0	18.9	-1.2	21.2	37.9	39.8
NASH 7	6.5	14.5	3.3	36.9	16.2	20.5	14.3	19.6	67.2	67.5
NASH 8	12.2	46.2	9.6	53.2	27.6	48.5	21.7	42.5	85.7	81.3

Table V-1. (cont'd)

Hose	FNK2		FCW		FM	
	(1)	(2)	(1)	(2)	(1)	(2)
NASA 11	88.8	86.9	111.4	108.2	-3.0	26.3
NASA 12	122.5	107.3	53.2	57.7	31.0	45.4
NASA 21	93.4	85.4	109.5	98.2	7.0	34.2
NASA 22	48.4	47.1	50.0	48.3	-10.6	26.8
NASA 31	47.1	51.9	59.6	59.8	-7.6	37.4
NASA 41	36.4	43.0	50.3	51.6	-17.5	35.7
NASA 42	49.6	46.0	42.5	41.6	-0.02	26.1
NASA 51	43.4	43.7	49.0	47.6	-0.7	26.6
NASA 61	27.3	36.2	35.2	40.4	-16.4	35.9
NASA 62	68.4	66.0	15.5	29.4	15.5	32.2

Table V-1 (cont'd)

Hose	FNK2		FCW		FM	
	(1)	(2)	(1)	(2)	(1)	(2)
NASA 71	39.1	54.1	41.0	54.8	-6.5	53.2
NASA 72	63.8	68.5	37.0	40.2	13.8	20.0
NASA 81	76.2	81.2	81.1	86.4	14.9	20.7
NASA 82	74.2	77.9	55.5	58.8	19.4	22.0
NASH 1	159.5	122.4	91.3	71.1	43.2	43.5
NASH 2	78.1	72.1	68.7	64.2	7.3	21.7
NASH 3	64.0	61.4	55.4	53.8	8.9	17.5
NASH 4	66.9	61.2	58.7	54.6	13.3	22.7
NASH 5	60.3	59.6	52.3	52.2	9.8	20.7
NASH 6	37.9	39.8	31.4	34.5	-2.3	18.5
NASH 7	62.8	63.2	59.6	60.1	8.2	11.0
NASH 8	77.3	74.7	77.6	74.9	12.9	45.1

and average standard deviation (%)[2] are given. The following is a list of the models compared in Table V-1:

FNASA - Equations (II-52) through (II-56)

FR - Equations (IV-3) through (IV-13)

FR1 - Equations (IV-16) and (IV-17)

FN - Equations (II-45)

FDF - Equation (II-45)

FDC1 - Equation (II-49)

FMSU - Equation (II-48)

FDC2 - Equation (II-50)

FHVH - Equation (II-51)

FNK1 - Equation (II-35)

FNK2 - This is the standard Nikuradse correlation corresponding to equation (II-35) except that (D/ε) is replaced by the relative roughness spacing (D/λ).

FCW - Equation (II-36)

FM - This is the Morris correlation for corrugated strip roughness as given in reference (39).

Table V-1 clearly indicates that Neill's correlation FN is unacceptable for flow in flexible hose. Also, it appears at first that correlation FR1 is not as accurate as correlation FR. However, it should be noted that correlation FR1 was tested only for data in the lower Reynolds number region where the friction factor is constant. Correlation FR, on the other

---

[2] Standard deviation = $\sqrt{\frac{\Sigma\,(f_{calc} - f_{obs})^2}{n - k - 1}}$

where: n = number of observed values
k = number of independent variables

hand, was tested over the entire range of Reynolds numbers. The conclusion to be made from the results presented in Table V-1 is that correlation FR1 can predict friction factors in the low Reynolds number range (10,000 to about 70,000) with an accuracy of about $\pm$ 30%. This lack of accuracy in the low range is to be expected since this is the region where the lowest pressure drops were measured. At low pressure drops any error in reading manometers or gages may be a significant per cent of the total readings and hence the accuracy and precision decreases.

Another important fact should be brought out about some of the correlations used in preparing Table V-1. Correlations FNASA, FN, FDF, FHVH, FNK1, FNK2, and FCW do not predict the correct behavior observed for flow in flexible hose. FNASA assumes that there is a straight line relationship between the logarithm of f and the logarithm of Re. The only instance where f would be independent of Re is where $\beta = 0$ in equation (II-52). This correlation was developed using pressure drop and Reynolds number data from the water system. As can be seen from Figures (IV-1) through (IV-9) a log-log plot of pressure drop versus Reynolds number appears to be a straight line. If more data at higher and lower flow rates would have been available the nonlinear nature of the curve would have been more apparent. However, with the data available all statistical tests indicated a straight line relationship. At very high flow rates the data does indicate a nonlinear relationship, for example, see Figure IV-26.

Correlations FN, FDF, FNK1, FNK2, and FHVH indicate that the friction factor is a function of hose geometry alone and independent of

Reynolds number. Surprisingly, correlations FR, FDC1, FMSU, FDC2, and FM all seem to do an adequate job of predicting friction factors for flow in flexible hose.

Data Obtained by other Workers:

Table V-2 gives the average error (%) and average standard deviation (%) for the various correlations using experimental data obtained by Daniels and Cleveland (51). Note that correlation FR predicts the friction factor with an accuracy of ± 24% for these data.

Figure V-4 shows data obtained by Daniels and Celveland for hose DCA4. These data clearly demonstrate that the friction factor assumes a constant value at high Reynolds numbers. The internal geometry of the five hoses tested by Daniels and Cleveland is given in Appendix A.

Curved Hose Correlation:

The curved hose correlation was developed from data covering a range of D/r_B from 0 to 0.079. This corresponds to a variation in the bend radius of from 3.18 ft. to a straight hose configuration (bend radius of infinity). The form of this correlation was given in Chapter IV:

$$\frac{f_B}{f} = 1.0 + 59.0 \left(\frac{D}{r_B}\right) (Re)^{-0.17} \qquad \text{(IV-18)}$$

Note the comparison between this expression and one given by White (22) for turbulent flow in a curved pipe:

$$\frac{f_B}{f} = 1.0 + 0.075 \left(\frac{D}{r_B}\right)^{1/2} Re^{1/4} \qquad \text{(II-32)}$$

For a value of D/r_B equal to 0.05 and a Reynolds number of 100,000, Equation (IV-18) predicts a value of f_B/f equal to 1.42 while Equation

TABLE V-2

CORRELATIONS TESTED AGAINST LITERATURE DATA FOR STRAIGHT HOSE

Hose	FR		FN		FDF		FDC1		FDC2	
	(1)	(2)	(1)	(2)	(1)	(2)	(1)	(2)	(1)	(2)
DCA1	7.4	17.4	115.7	107.0	-17.7	36.7	-5.7	15.5	18.6	25.5
DCA2	-14.5	34.8	94.0	71.7	13.2	36.4	9.2	14.1	-13.6	29.3
DCA3	17.4	24.0	152.0	137.0	26.9	30.6	20.3	25.1	19.0	25.5
DCA4	-5.8	15.3	104.1	98.8	19.8	23.2	5.9	12.1	13.4	15.5
DCA5	-23.9	29.6	81.3	82.0	35.4	37.1	-4.3	14.2	11.6	16.5

(1) **Average error (%)**

(2) Average standard deviation (%)

Table V-2 (cont'd)

Hose	FHVII		FNK1		FNK2		FCW		FM	
	(1)	(2)	(1)	(2)	(1)	(2)	(1)	(2)	(1)	(2)
DCA1	7.5	27.4	18.5	29.9	46.6	47.2	13.0	28.5	0.3	16.8
DCA2	-21.0	50.2	14.1	36.6	7.8	37.8	8.1	37.8	-20.3	45.5
DCA3	2.5	25.8	39.0	38.6	42.3	41.0	32.5	34.2	8.0	20.4
DCA4	-26.5	35.0	12.7	19.6	4.5	17.9	7.4	18.1	-13.5	21.0
DCA5	-47.2	51.3	-0.2	13.4	-20.1	26.2	-4.9	14.9	-32.6	37.6

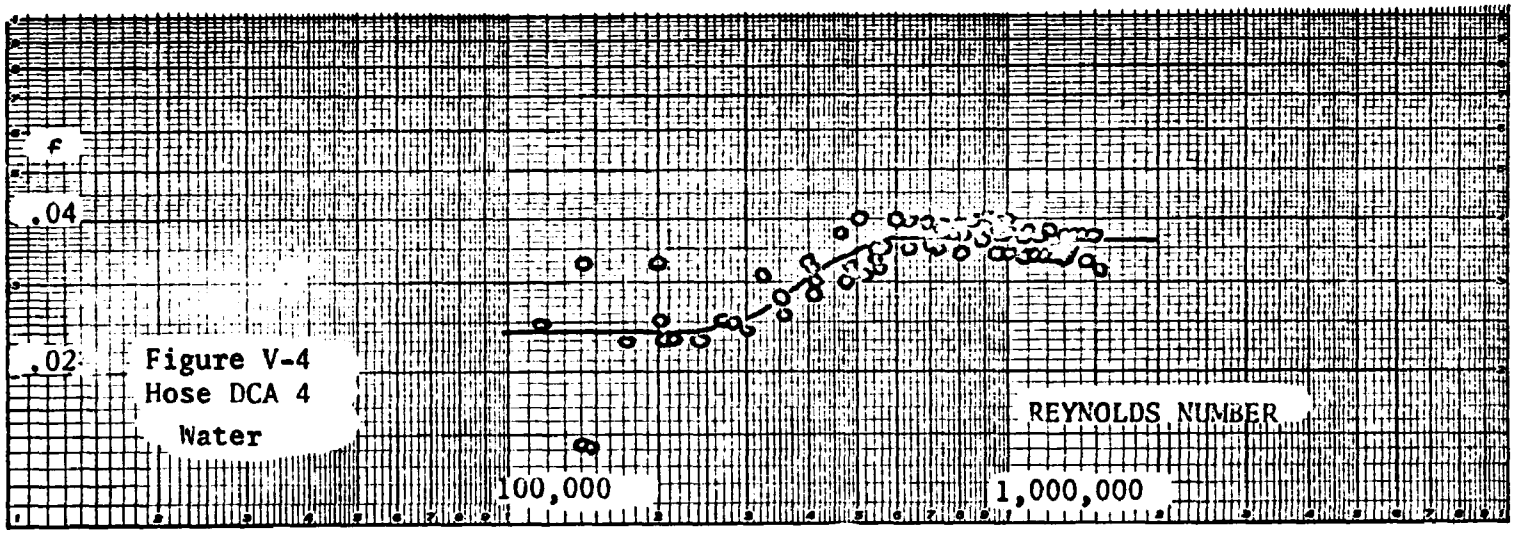

Figure V-4
Hose DCA 4
Water

(II-32) predicts a value of 1.30. This implies that curvature has a greater effect on energy dissipation due to friction for flexible hose than for common pipe. However, note that this effect decreases as the Reynolds number is increased for flexible hose while in standard pipe the effect becomes greater for an increase in Reynolds number.

Table V-3 gives an indication of the accuracy with which equation (IV-21) predicts values of the friction factor for curved sections of flexible hose. The results reported in this table are (1) the average error (%) and (2) the average standard deviation (%).

TABLE V-3

MODEL COMPARISON FOR CURVED HOSE

Hose	30°		60°		90°		120°		150°		180°	
	(1)	(2)	(1)	(2)	(1)	(2)	(1)	(2)	(1)	(2)	(1)	(2)
NASA 11	12.9	28.2	-13.6	20.9	-14.5	21.5	-12.0	23.9	-15.2	30.2	2.1	24.9
NASA 12	34.4	70.8	37.1	68.8	33.4	59.0	34.5	54.6	34.1	54.5	36.7	56.3
NASA 21	6.1	9.8	6.6	11.0	4.4	8.8	0.4	11.8	2.3	13.9	-0.9	13.9
NASA 22	13.2	25.3	-4.0	24.2	2.5	35.5	7.6	14.5	2.4	17.4	-0.3	20.8
NASA 31	-6.6	16.0	-7.6	14.0	-11.9	18.7	-21.9	27.7	-26.9	36.0	-24.4	29.8
NASA 32	2.4	12.0	0.3	14.5	11.6	33.2	-8.8	23.8	-10.2	27.4	-14.5	28.2
NASA 41	-8.6	12.7	-11.2	15.5	-18.1	22.5	-24.5	30.6	-19.9	27.2	-28.2	33.1
NASA 42	3.2	21.5	1.3	18.5	-5.7	16.9	-6.1	24.3	-6.6	16.4	-7.0	22.8
NASA 51	-9.3	17.8	-13.7	19.4	-15.8	24.0	-21.4	81.2	-16.7	23.9	-23.4	30.4
NASA 52	45.4	69.7	51.0	76.5	52.2	74.2	50.1	72.1	49.0	71.1	53.2	75.7
NASA 61	-6.8	14.3	-10.9	23.0	-8.9	14.4	-13.6	18.4	-11.8	21.0	-13.8	24.4
NASA 62	16.0	29.3	13.8	27.2	14.0	25.3	11.2	28.9	7.2	23.6	8.7	23.7

(1) Average error (%)

(2) Average standard deviation (%)

Table V-3 (cont'd)

Nose	30°		60°		90°		120°		150°		180°	
	(1)	(2)	(1)	(2)	(1)	(2)	(1)	(2)	(1)	(2)	(1)	(2)
NASA 71	9.5	16.3	-0.7	7.6	-7.8	11.7	-8.7	13.4	-6.7	16.9	-12.4	18.1
NASA 72	1.3	44.9	7.6	28.3	2.1	36.3	-2.5	30.0	6.2	25.4	4.1	24.8
NASA 81	-11.1	17.7	-8.7	16.0	-17.0	22.3	-24.5	33.9	-14.5	20.9	-19.8	39.3
NASH 1	15.1	21.9	16.8	24.5	16.6	23.9	19.3	27.8	22.8	31.3	16.7	27.5
NASH 2	1.2	15.6	1.5	11.3	1.2	12.7	0.5	17.2	5.1	13.9	-0.5	11.0
NASH 3	3.1	14.7	5.3	14.2	2.7	17.9	1.6	14.2	3.5	11.1	0.7	12.6
NASH 4	4.3	16.9	6.3	16.0	-0.9	22.0	-3.6	20.5	-3.9	18.1	-3.9	36.4
NASH 5	4.7	32.4	11.0	25.6	9.6	23.1	5.0	23.2	2.9	19.2	0.4	22.5
NASH 6	-7.9	34.8	-10.5	24.3	-12.0	17.9	-20.3	38.5	-22.3	55.4	-14.5	20.2
NASH 7	-7.2	15.2	-7.2	12.7	-10.2	15.0	-19.4	27.7	-14.8	17.9	-22.7	37.8
NASH 8	-1.3	7.8	-6.2	12.5	-11.8	15.1	-18.9	22.3	-13.0	18.0	-21.6	40.6

CHAPTER VI

CONCLUSIONS and RECOMMENDATIONS

Conclusions:

1. Energy consumption due to friction is 4 to 5 times greater for flow in flexible metal hose than for flow in a smooth tube of the same size and at the same Reynolds number.

2. The empirical correlation presented in this dissertation predicts values of the Fanning friction factor for flow in flexible metal hose with an accuracy of $\pm$ 20%.

3. For turbulent flow in the low Reynolds number regime the friction factor is independent of Reynolds number. However, as the Reynolds number increases above this regime the friction factor begins to increase with further increase in the Reynolds number. This indicates that a change in flow mechanism has occurred. At very high Reynolds numbers the friction factor again becomes independent of the Reynolds number.

4. A flow model has been proposed which attempts to explain the behavior of the friction factor for flow in flexible metal hose. Results obtained from studies of flow across tube banks in heat exchangers form the basis for the model.

5. For turbulent flow in straight hose the friction factor is a function of Reynolds number and the dimensionless geometric parameter D/λ.

For annular hose the correlation is:

$$170 \leq Re^* \leq 1{,}400$$

$$\frac{1}{\sqrt{f}} - 4 \log\left(\frac{D}{\lambda}\right) = 4.35 \qquad \text{(VI-1)}$$

$$1{,}400 < Re^* < 11{,}000$$

$$\frac{1}{\sqrt{f}} - 4 \log\left(\frac{D}{\lambda}\right) = \psi(Re^*) \qquad \text{(VI-2)}$$

where $\psi(Re^*)$ is a function of Re^* and is given in Figure (IV-43). Note that $Re^* = Re\sqrt{f}/(D/\lambda)$

$$Re^* \geq 11{,}000$$

$$\frac{1}{\sqrt{f}} - 4 \log\left(\frac{D}{\lambda}\right) = 2.28 \qquad \text{(VI-3)}$$

For helical hose the correlation is:

$$180 \leq Re^* \leq 2{,}000$$

$$\frac{1}{\sqrt{f}} - 4 \log\left(\frac{D}{\lambda}\right) = 4.28 \qquad \text{(VI-4)}$$

$$2{,}000 < Re^* < 16{,}000$$

$$\frac{1}{\sqrt{f}} - 4 \log\left(\frac{D}{\lambda}\right) = \psi(Re^*) \qquad \text{(VI-5)}$$

where $\psi(Re^*)$ is a function of Re^* and is given in Figure (IV-44).

$$Re^* \geq 16{,}000$$

$$\frac{1}{\sqrt{f}} - 4 \log \frac{D}{\lambda} = 2.28 \qquad \text{(VI-6)}$$

These correlations are also presented in the form of plots of friction factor versus Reynolds number with λ/D as a parameter. Figure (IV-45) is the plot for annular hose and Figure (IV-46) the plot for helical hose.

6. The correlation for turbulent flow in a curved hose is applicable to both annular and helical hoses. The ratio of the friction factor for a curved hose to that for a straight hose is:

$$\frac{f_B}{f} = 1.0 + 59.0 \left(\frac{D}{r_B}\right) (Re)^{-0.17} \qquad \text{(VI-7)}$$

where D is the inside minimum diameter and r_B the bend radius.

Recommendations:

1. A better understanding should be obtained of the flow mechanisms and phenomena which are responsible for the differences in the behavior of friction factors in flexible metal hose and those in smooth rigid pipe. The behavior found in the present study was noted in some of the literature references which were cited in Chapter II. A qualitative explanation of this behavior has been proposed but further study is needed to verify the flow model.

2. To accomplish this objective the basic approach should be modified to investigate the fundamental quantities which the work just concluded has pointed out as being most needed. For example,

studies of the velocity profiles in the main stream of the tubes and of the flow patterns in the annular or helical segments created by the corrugations would contribute greatly to the understanding of the friction factor behavior.

A skillful visual study would be a powerful tool in obtaining adequate knowledge of the flow model in flexible metal hose. The importance of this technique has been shown by the studies conducted on flow across tube banks of heat exchangers.

3. Existing empirical correlations should be expanded and improved. Work in this area might take the form of developing a correlation for two-phase flow in flexible hoses. Another problem area which might be investigated concerns the flow of cryogenic fluids through flexible hose. This would be particularly important to workers in the Missiles and Aerospace Vehicles Sciences.

LITERATURE CITED

(1) Stanton, T. E. and J. R. Pannell. Phil. Trans. Roy. Soc. A., 214, (1914), p. 199.

(2) Senecal, V. E. and R. R. Rothfus. "Transition Flow of Fluids in Smooth Tubes", Chem. Engr. Progr., 49, (1953), p. 533.

(3) Dean, W. R. Phil. Mag. (7) 4, (1927), p. 208.

(4) Adler, M. "Stromung in gekrummten Rohren", ZAMM, 14, (1934).

(5) Prandtl, L. "Fuhrer durch die Stromungslehre", 3rd ed., Braunschweig, (1949), p. 159.

(6) McAdams, W. H. Heat Transmission, 3rd ed., McGraw-Hill Book Co., Inc., (1954), p. 151.

(7) Blasius, H. "Das Ahnlichkeitsgesetz Bei Reibungsvargangen in Flussigkeiten, Forschungsheft, 131, Berlin, (1913).

(8) Nikuradse, J. "GesetzmaBigkeit der turbulenten Stromung in glatten Rohren", Forschungsheft, 356, (1932).

(9) von Karman, T. "Mechanische Ahnlichkeit und Turbulenz", Nach. Ges. Wiss. Gottingen, Math. Phys. Klasse, 58, (1930).

(10) Prandtl, L. "Uber die ausgebidete Turbulenz", ZAMM, 5, (1925), p. 136.

(11) Frossel, W. "Stromung in glatten, geraden Rohren mit Uber-und Unterschollgeschwindigkeit", Forschungsheft a.d. Geb. d. Ing-Wesens, 7, (1936), p. 75.

(12) Keenan, J. and E. Neumann. "Measurements of Friction in a Pipe for Subsonic and Supersonic Flow of Air", J. Applied Mechanics, 13, (1946), p. A-91.

(13) Drew, T. E., E. C. Koo, and W. H. McAdams. "The Friction Factor for Clean Round Pipes", Trans. AICh.E., 28, (1932), p. 56.

(14) Perry, J. H. Chemical Engineers' Handbook, 3rd ed., McGraw Hill Book Co., Inc., New York, 1950.

(15) Walker, W. H., W. K. Lewis, W. H. McAdams, and E. P. Gilliland. Principles of Chemical Engineering, 3rd ed., McGraw Hill Book Co., Inc., New York, 1937.

(16) Stanton, T. E., D. Marshall, and C. N. Bryant. "On the Conditions of the Boundary of a Fluid in Turbulent Motion", Proc. Roy. Soc. (London), 97-A, (1920), p. 413.

(17) Reichardt, H. NACA TM 1047, 1943.

(18) Deissler, R. G. NACA TN, 2138, 1950.

(19) Rothfus, R. P. and C. C. Monrad. "Correlation of Turbulent Velocities for Tubes and Parallel Plates", Ind. Eng. Chem. 47, (1955), p. 1144.

(20) Bird, R. B., W. E. Stewart, and E. N. Lightfoot. Transport Phenomena, John Wiley & Sons. Inc., New York, 1960, pp. 161-165.

(21) Knudsen, J. G. and D. L. Katz. Fluid Dynamics and Heat Transfer, McGraw Hill Book Co., Inc., New York, 1958, pp 158-162.

(22) White, C. M. "Fluid friction and its relation to heat transfer", Trans. Inst. Chem. Engr., 10, (1932), p. 66.

(23) Ito, H. "Friction factors in turbulent flow in curved pipes", Trans. ASME, DS1 (Jour. Basic Eng'g.), (1959), p. 123.

(24) Hawthorne, W. R. "Secondary circulation in fluid flow", Proc. Roy. Soc. (London) A206, (1951), p. 374.

(25) Detra, R. W. "The secondary flow in curved pipes", Reports of the Aero. Inst. of the E.T.H. Zurich, 20, (1953).

(26) Nikuradse, J. "Stromungsgesetze in rauhen Rohren", Forschungsheft, (1933), p. 361.

(27) Colebrook, C. F. "Turbulent flow in pipes with particular reference to the transition region between the smooth and rough pipe laws. Journ. Institution Civil Engrs., 1939.

(28) Nedderman, R. M. and C. J. Shearer. "Correlations for the friction factor and velocity profile in the transition region for flow in sand-roughened pipes", Chemical Engineering Science, 19, (1964), pp. 423-428.

(29) Dukler, A. E. "An Analytical Expression for Friction Factor", A.I.Ch.E. Journal, (1961), p. 708.

(30) Tyul'panov, R. S. "The laws of flow in very rough tubes", International Chemical Engineering, 5:1, (1965), pp. 77-78.

(31) Schlicting, H. Boundary Layer Theory, 4th ed., McGraw Hill Book Co., Inc., New York, 1960.

(32) Schlicting, H. "Experimentelle Untersuchungen zum Rauhig keits-problem", Ing.-Arch. 7, (1936) pp. 1-34.

(33) Mobius, H. "Experimentelle Untersuchungen des Widerstandes und der Rauhigkeiten bei turbulenter Stromung", Phys. Z., 41, (1940), pp. 202-225.

(34) Knudsen, J. G. and D. L. Katz. Fluid Dynamics and Heat Transfer, McGraw Hill Book Co., Inc., New York, 1958, p. 193.

(35) Konobeev, V. I. and N. M. Zhavoronkov. "Hydraulic resistances in tubes with wavy roughness", International Chemical Engineering, 2:3, (1962), pp. 431-437.

(36) Nunner, W. "Heat transfer and pressure drop in rough pipes", VDI, Forschungsheft, (1958) p. 455.

(37) Koch, R. "Pressure drop and heat transfer for flow through empty, baffled, and packed tubes", VDI, Forschungsheft, (1958), p. 469.

(38) Wieghardt, K. "Erhohung Des Turbulenten Reibungswiderstandes Durch Oberflachenstorungen", Forschungshefte Fur Schiffstechnik, 1, (1953), pp. 65-81.

(39) Morris, H. M. "A New Concept of Flow in Rough Conduits", A thesis submitted to the University of Minnesota (Minneapolis, Minn.), in partial fulfillment of the requirements for the degree of Doctor of Philosophy, 1950.

(40) Gibson, A. H. "Flow of water in a corrugated pipe", Phil. Mag., 50:6, (1925), pp. 199-204.

(41) Neill, C. R. "Hydraulic roughness of corrugated pipe", Proc. Amer. Soc. Civ. Engrs., 85:HY9, (1959), pp. 35-67.

(42) Straub, L. G. and H. M. Morris. "Hydraulic tests on corrugated metal culvert pipes", Tech. Pap. 5, Ser. B., Hydraulics Laboratory, St. Anthony Fallas, 1950.

(43) Streeter, V. L. "Frictional resistance in artificially roughened pipe", Proc. Amer. Soc. Civil Engr., 61, (1935), p. 163.

(44) Finniecome, J. R. "Friction coefficient for circular pipes at turbulent flow", Emmott, Manchester, 1954.

(45) Allen, J. "Flow of incompressible fluids through corrugated pipes", The Institute of Civil Engineers, 28, (1964), pp. 31-38.

(46) Daniels, C. M. "Pressure Losses in Flexible Metal Tubing", Product Engineering, 27:4, (1956), pp. 223-227.

(47) Daniels, C. M. and R. E. Fenton. "Determining Pressure Drop in Flexible Metal Hose", Machine Design, (1960), pp. 195-198.

(48) Daniels, C. M. and J. R. Cleveland. "Determining Pressure Drop in Flexible Metal Hose", Machine Design, (1965), pp. 187-188.

(49) Pepersack, F. J. "Pressure losses in flexible metal hose utilized in propulsion fluid systems of XSM-68B and SM-68B. Technical Memorandum, Baltimore, Martin-Baltimore, September, 1960, pp. 25-40.

(50) Bouchillon, C. W. and A. G. Holmes. ""A Study of Pressure Losses in Tubing and Fittings", Mississippi State University Interim Report, 1965 (prepared under Contract NAS8-11297).

(51) Private communication.

(52) Hawthorne, R. C. and H. C. von Helms. "Flow in Corrugated Hose", Product Engineering, (1963), pp. 98-100.

(53) Riley, K. L. et al. "Flow Losses in Flexible Hose", Southeastern Symposium on Missiles and Aerospace Vehicles Sciences, American Astronautical Society, Vol. I, Huntsville, Alabama, Dec., 1966, pp. 50-1-50-13.

(54) Whitehurst, C. A. and B. S. Pressburg. "Flow Losses in Flexible Hose", Louisiana State University, 1966 (prepared under Contract NAS 9-4630).

(55) Kays, W. M., A. L. London, and P. K. Lo. "Heat Transfer and Friction Characteristics for Gas Flow Normal to Tube Banks - Use of a Transient-Test Technique", Trans. ASME, 76:387 (1954).

(56) Wallis, R. P. "Photographic Study of Fluid Flow Between Bands of Tubes", Engineering, 148, (1934), p. 423.

(57) Hoeck, E. "Druckverluste in Druckleitungen grossen Kraftwerke", Dissertation, A. G. Gebr. Lehman, Zurich, 1943.

(58) Knudsen, J. G. and D. L. Katz. Fluid Dynamics and Heat Transfer, McGraw Hill Book Co., Inc., New York, 1958, p. 173.

APPENDIX A

Flexible Metal Hose Dimensions

FLEXIBLE METAL HOSE
NOMENCLATURE

All flexible metal hoses used in this study are denoted by the letters NAS. A fourth letter is added to indicate whether the hose is annular or helical, e.g., NASA means an annular hose and NASH, a helical hose. The number following these four letters is used with Table A-1 to define the internal geometry of the flexible hose, e.g., NASA 62 stands for an annular hose with D = 2.044", λ = 0.375", ϵ = 0.219", and σ = 0.203".

The flexible hoses used by Daniels and Cleveland are denoted by DCA. Table A-2 can be used to find the internal geometry.

APPENDIX A

TABLE A-1

Flexible Metal Hose Dimensions

Annular:	D (inches)	λ (inches)	ε (inches)	σ (inches)
NASA 11	0.551	0.125	0.156	0.0781
NASA 12	0.555	0.1875	0.125	0.109
NASA 21	0.771	0.156	0.1875	0.0937
NASA 22	0.774	0.172	0.1875	0.09375
NASA 31	1.0102	0.181	0.219	0.1094
NASA 32	1.012	0.203	0.219	0.109
NASA 41	1.266	0.1875	0.234	0.125
NASA 42	1.255	0.219	0.219	0.109
NASA 51	1.483	0.219	0.250	0.125
NASA 52	1.500	0.344	0.219	0.172
NASA 61	2.046	0.250	0.297	0.172
NASA 62	2.044	0.375	0.219	0.203
NASA 71	2.565	0.3125	0.344	0.1875
NASA 72	2.535	0.406	0.328	0.2188
NASA 81	2.990	0.375	0.422	0.1875
NASA 82	3.003	0.453	0.406	0.203
Helical:				
NASH 1	0.535	0.172	0.125	0.0781
NASH 2	0.768	0.1875	0.1875	0.09375
NASH 3	1.061	0.250	0.250	0.1094
NASH 4	1.299	0.250	0.250	0.125
NASH 5	1.560	0.3125	0.3125	0.133
NASH 6	2.081	0.344	0.344	0.156
NASH 7	2.573	0.375	0.391	0.172
NASH 8	3.111	0.406	0.4375	0.1875

TABLE A-2

Dimensions of Flexible Hose
Reported by Daniels and Cleveland

Hose	D (inches)	λ (inches)	ε (inches)
DCA1	0.55	0.120	0.088
DCA2	0.75	0.158	0.171
DCA3	1.015	0.174	0.168
DCA4	1.480	0.218	0.245
DCA5	2.000	0.226	0.324

APPENDIX B

An Equation for Sigmoid Curves

APPENDIX B

Many sigmoid curves, both normal and skewed, can be fitted satisfactorily by the equation

$$\S = \frac{x - x_1}{a + bx} \qquad \text{(B-1)}$$

where

$$\S = \log \left[\frac{20y}{\log (100 - y)} \right] \qquad \text{(B-2)}$$

and x_1 corresponds to $y = 0.1$, and a and b are the intercept and slope, respectively, of the straight line that results when $\frac{x - x_1}{\S}$ is plotted against x.

Equation (B-1) holds if, when $\frac{x - x_1}{\S}$ is plotted against x, a single straight line results for the entire practical range of x. In some instances improved fitting can be attained by dividing the range of x and by working with two intersecting straight lines.

Davis (1) gives a detailed calculation procedure to be used with this technique.

Illustration B1:

Figure IV-44 indicates that the curve representing the relationship between ψ(Re*) and Re* for helical-type hose has a sigmoid shape in the range of Re* from 2000 to 16,000. The data in this range are given below:

Re*	ψ(Re*)
2000	4.28
2250	4.25
2500	4.20
3000	4.10
3400	4.00
3800	3.90
4500	3.75
4800	3.60
5600	3.40
6000	3.30
6900	3.10
8000	2.90
8600	2.80
9300	2.70
10000	2.61
12000	2.45
13000	2.40
14000	2.35
15000	2.30
16000	2.28

The following mathematical transformations are made:

$$x = \log Re^* - \log (2000)$$

$$x = \log Re^* - 3.301 \qquad \text{(B-3)}$$

$$y = 4.28 - \psi(Re^*) \qquad \text{(B-4)}$$

A plot of y versus x is then constructed and a value of x_1 (corresponding to $y = 0.1$) is obtained. Figure B-1 shows this plot. For the helical - type hose data $x_1 = 0.116$.

Figure B-2 is a plot of $\frac{x - 0.116}{\S}$ versus x for these data. Note that the plot clearly indicates that two intersecting straight lines are required to accurately describe the data.

Upon determination of the slopes and intercepts for these lines the following results are obtained:

for $x \leq 0.58$

$$\S = \frac{x - 0.116}{0.153 + 0.4375\ (x)} \qquad \text{(B-5)}$$

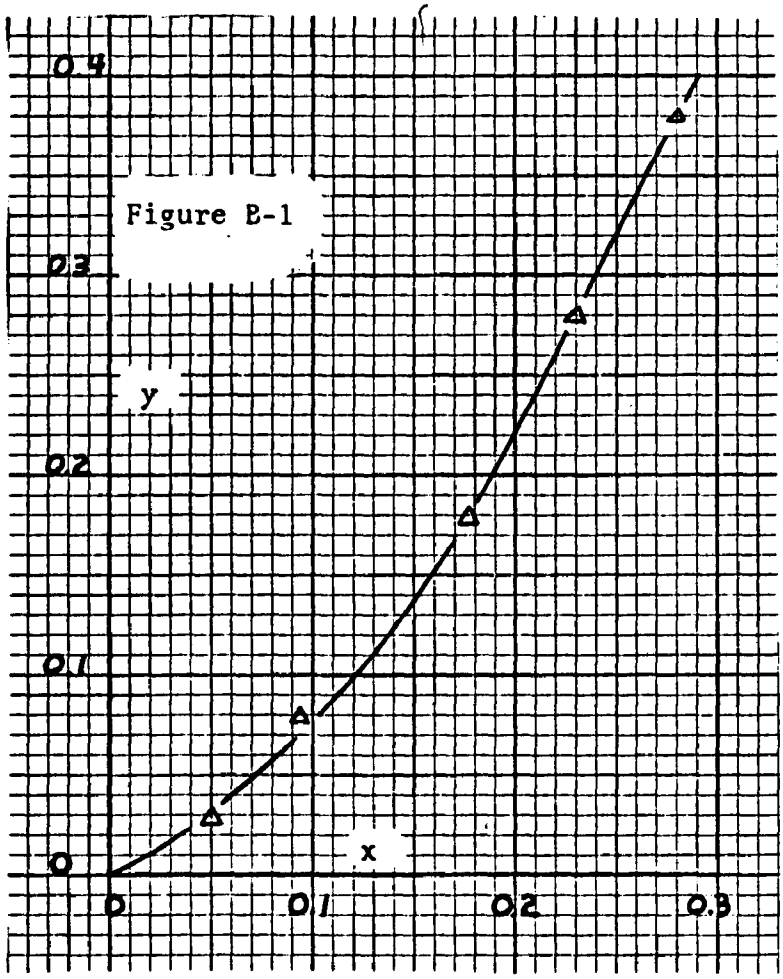

Figure B-1

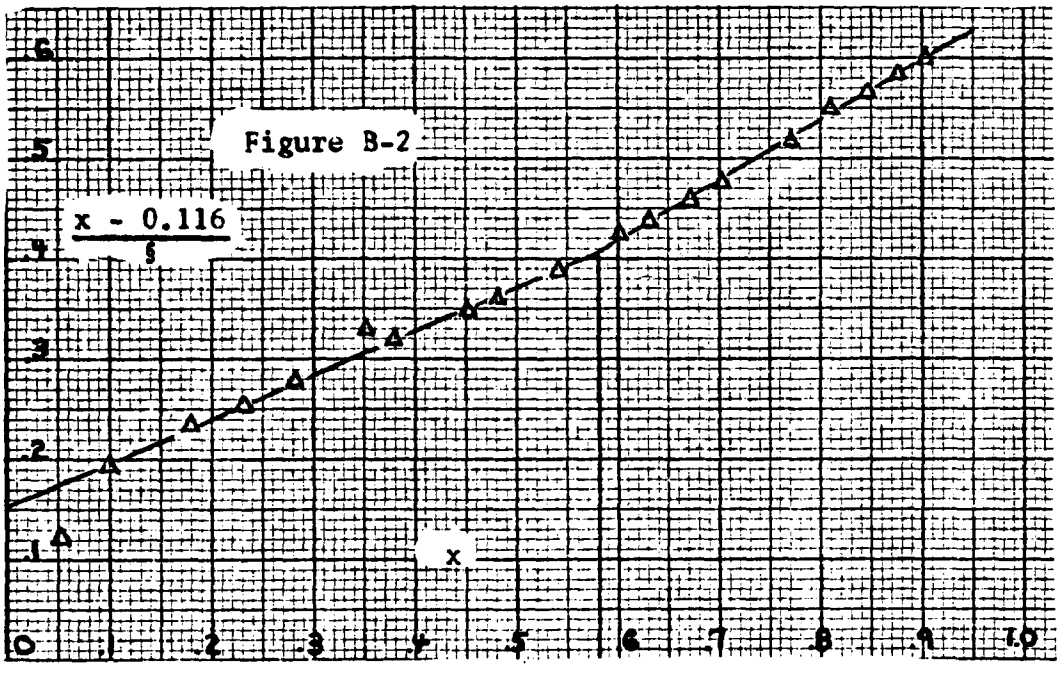

Figure B-2

for $x > 0.58$

$$\S = \frac{x - 0.116}{0.059 + 0.600\ (x)} \qquad \text{(B-6)}$$

These are the equations reported in Chapter IV.

Literature Cited

(1) Davis, D. S. Nomography and Empirical Equations, 2nd ed., Reinhold Publishing Co., New York, (1962) pp 79-89.

APPENDIX C

Computer Program for Model Comparison

```
C THIS PROGRAM IS WRITTEN IN FORTRAN IV FOR AN IBM 7040 COMPUTER.
C THE PROGRAM CALCULATES PREDICTED FRICTION FACTORS FROM VARIOUS
C MODELS AND COMPARES THEM TO OBSERVED FRICTION FACTORS. THE
C OUTPUT FROM THE PROGRAM IS ERROR(PER CENT) AND STANDARD DEVIATION
C (PER CENT).
C
C K L RILEY 1303-4C060 MODEL COMPARISON FOR FLEX-HOSE
C DIMENSION VARIABLES
      DIMENSION RE(200),FA(200),FP(200),R(7),FAA(200)
      DIMENSION DIAM(3,8),PITCH(3,8),DEPTH(3,8),AXIAL (3,8)
C READ INTERNAL GEOMETRIC PARAMETERS
      DO1I=1,3
      DO1K=1,8
      READ2,DIAM(I,K),PITCH(I,K),DEPTH(I,K),AXIAL (I,K)
 2    FORMAT(4F10.0)
 1    CONTINUE
C READ BEND RADII
      READ51,(R(I),I=1,7)
 51   FORMAT(7F10.0)
C READ HEADER CARD
C N=NUMBER OF DATA POINTS
C NN=INDICATES TYPE OF HOSE, IF 1 OR 2 ANNULAR-TYPE, IF 3 HELICAL
C D=INSIDE DIAMETER, INCHES
C LANG=BEND ANGLE, DEGREES
 78   READ43,N,NN,D,LANG
 43   FORMAT(I10,10X,I10,F10.0,I10)
C READ OBSERVED DATA POINTS
C RE(I)=REYNOLDS NUMBER
C FA(I)=OBSERVED FRICTION FACTOR
      READ50,(RE(I),FA(I),I=1,N)
 50   FORMAT(2F20.0)
      PRINT64,NN,D,N,LANG
 64   FORMAT(I10,F10.3,2I10)
C SET SUBSCRIPTS FOR GEOMETRIC VARIABLES
```

```
      IF(D.GT.0.500)NG=1
      IF(D.GT.0.750)NG=2
      IF(D.GT.1.000)NG=3
      IF(D.GT.1.250)NG=4
      IF(D.GT.1.480)NG=5
      IF(D.GT.2.000)NG=6
      IF(D.GT.2.500)NG=7
      IF(D.GT.2.900)NG=8
      IF(LANG.EQ.0)NA = 7
      IF(LANG.EQ.30)NA=1
      IF(LANG.EQ.60)NA=2
      IF(LANG.EQ.90)NA=3
      IF(LANG.EQ.120)NA=4
      IF(LANG.EQ.150)NA=5
      IF(LANG.EQ.180)NA=6
C CALCULATE PREDICTED FRICTION FACTOR, FP(I)
      DO 300 I = 1,N
      FP(I) = FNASA(NN,RE(I),DIAM(NN,NG),DEPTH(NN,NG),PITCH(NN,NG),
     *AXIAL (NN,NG),R(NA),LANG)
 300  CONTINUE
C CALCULATE ERROR AND STANDARD DEVIATION
      PCER = ERROR(N,FA,FP)
      PCSER = DEVR(N,FA,FP,LANG)
      PRINT 32,PCER,PCSER
 32   FORMAT(/10X,5HFNASA,2X,E20.8,E20.8)
C CALCULATE PREDICTED FRICTION FACTOR, FP(I)
      DO500I=1,N
      FP(I)=FR(NN,RE(I),DIAM(NN,NG),PITCH(NN,NG),LANG,R(NA))
 500  CONTINUE
C CALCULATE ERROR AND STANDARD DEVIATION
      PCER=ERROR(N,FA,FP)
      PCSER=DEVR(N,FA,FP,LANG)
      PRINT52,PCER,PCSER
 52   FORMAT(/10X,2HFR,5X,E20.8,E20.8)
```

```
      IF(LANG)416,416,78
  416 J=0
C CALCULATE PREDICTED FRICTION FACTOR, FP(I)
      DO 440 I=1,N
      RRS=DIAM(NN,NG)/PITCH(NN,NG)
      RSS=PITCH(NN,NG)/AXIAL(NN,NG)
      RES=(RE(I)*FA(I)/RRS)
      IF(NN-2)411,411,412
  411 IF(RES-1400.0)413,413,440
  413 J=J+1
      FAA(J)=FA(I)
      FRES=6.34
      GO TO 415
  412 IF(RES-2000.0)414,414,440
  414 J=J+1
      FAA(J)=FA(I)
      FRES=5.77
  415 FP(J)=1.0/((FRES+4.0*ALOG10(RSS))**2)
  440 CONTINUE
C CALCULATE ERROR AND STANDARD DEVIATION
      PCER=ERROR(J,FAA,FP)
      PCSER=DE3(J,FAA,FP)
      PRINT42,PCER,PCSER
   42 FORMAT(/10X,3HFR1,4X,E20.8,E20.8)
C CALCULATE PREDICTED FRICTION FACTOR, FP(I)
  417 DO600I=1,N
      FP(I)=FN(DEPTH(NN,NG),DIAM(NN,NG))
  600 CONTINUE
C CALCULATE ERROR AND STANDARD DEVIATION
      PCER=ERROR(N,FA,FP)
      PCSER=DE3(N,FA,FP)
      PRINT53,PCER,PCSER
   53 FORMAT(/10X,2HFN,5X,E20.8,E20.8)
C CALCULATE PREDICTED FRICTION FACTOR, FP(I)
```

```
      DO700I=1,N
      FP(I)=FDF(PITCH(NN,NG),DIAM(NN,NG),DEPTH(NN,NG))
 700  CONTINUE
C CALCULATE ERROR AND STANDARD DEVIATION
      PCER=ERRCR(N,FA,FP)
      PCSER=DE4(N,FA,FP)
      PRINT54,PCER,PCSER
 54   FORMAT(/1CX,3HFDF,4X,E20.8,E20.8)
C CALCULATE PREDICTED FRICTION FACTOR, FP(I)
      DO800I=1,N
      FP(I)=FDC1(RE(I),DIAM(NN,NG),DEPTH(NN,NG))
 800  CONTINUE
C CALCULATE ERRCR AND STANDARD DEVIATION
      PCER=ERROR(N,FA,FP)
      PCSER=DEV(N,FA,FP)
      PRINT55,PCER,PCSER
 55   FORMAT(/1CX,4HFDC1,3X,E20.8,E20.8)
C CALCULATE PREDICTED FRICTION FACTOR, FP(I)
      DC900I=1,N
      FP(I)=FMSU(RE(I),DIAM(NN,NG),DEPTH(NN,NG),PITCH(NN,NG),AXIAL(NN,NG
     *))
 900  CONTINUE
C CALCULATE ERROR AND STANDARD DEVIATION
      PCER=ERROR(N,FA,FP)
      PCSER=DE7(N,FA,FP)
      PRINT56,PCER,PCSER
 56   FORMAT(/1OX,4HFMSU,3X,E20.8,E20.8)
C CALCULATE PREDICTED FRICTION FACTOR, FP(I)
      DO100CI=1,N
      FP(I)=FDC2(RE(I),DEPTH(NN,NG),DIAM(NN,NG))
 1000 CONTINUE
C CALCULATE ERROR AND STANDARD DEVIATION
      PCER=ERROR(N,FA,FP)
      PCSER=DEV(N,FA,FP)
```

```
      PRINT57,PCER,PCSER
 57   FORMAT(/10X,4HFDC2,3X,E20.8,E20.8)
C CALCULATE PREDICTED FRICTION FACTOR, FP(I)
      DO1200I=1,N
      FP(I)=FHVH(DIAM(NN,NG),PITCH(NN,NG))
 1200 CONTINUE
C CALCULATE ERROR AND STANDARD DEVIATION
      PCER=ERROR(N,FA,FP)
      PCSER=DE3(N,FA,FP)
      PRINT59,PCER,PCSER
 59   FORMAT(/10X,4HFHVH,3X,E20.8,E20.8)
C CALCULATE PREDICTED FRICTION FACTOR, FP(I)
      DO1300I=1,N
      FP(I)=FNK1(RE(I),DIAM(NN,NG),DEPTH(NN,NG))
 1300 CONTINUE
C CALCULATE ERROR AND STANDARD DEVIATION
      PCER=ERROR(N,FA,FP)
      PCSER=DEV(N,FA,FP)
      PRINT60,PCER,PCSER
 60   FORMAT(/10X,4HFNK1,3X,E20.8,E20.8)
C CALCULATE PREDICTED FRICTION FACTOR, FP(I)
      DO1400I=1,N
      FP(I)=FNK2(RE(I),DIAM(NN,NG),PITCH(NN,NG))
 1400 CONTINUE
C CALCULATE ERROR AND STANDARD DEVIATION
      PCER=ERROR(N,FA,FP)
      PCSER=DEV(N,FA,FP)
      PRINT61,PCER,PCSER
 61   FORMAT(/10X,4HFNK2,3X,E20.8,E20.8)
C CALCULATE PREDICTED FRICTION FACTOR, FP(I)
      DO1500I=1,N
      FP(I)=FCW(RE(I),DIAM(NN,NG),DEPTH(NN,NG))
 1500 CONTINUE
C CALCULATE ERROR AND STANDARD DEVIATION
```

```
      PCER=ERROR(N,FA,FP)
      PCSER=DEV(N,FA,FP)
      PRINT62,PCER,PCSER
 62   FORMAT(/10X,3HFCW,4X,E20.8,E20.8)
C CALCULATE PREDICTED FRICTION FACTOR, FP(I)
      DO1600I=1,N
      FP(I)=FM(RE(I),DIAM(NN,NG),PITCH(NN,NG))
 1600 CONTINUE
C CALCULATE ERROR AND STANDARD DEVIATION
      PCER=ERROR(N,FA,FP)
      PCSER=DEV(N,FA,FP)
      PRINT63,PCER,PCSER
 63   FORMAT(/10X,2HFM,5X,E20.8,E20.8)
      PRINT1450
 1450 FORMAT(1H1)
      GOTO78
      END
```

```
C THIS SUBPROGRAM IS WRITTEN IN FORTRAN IV FOR AN IBM 7040 COMPUTER.
C THIS SUBPROGRAM IS USED BY THE MAIN PROGRAM TO CALCULATE PREDICTED
C FRICTION FACTORS FROM MODEL FNASA.
C
      FUNCTION FNASA(NN,REN,DI,EPS,PH,S,RB,LANG)
      GEOM1 = (S*EPS)/(PH**2)
      B1 = 2.9866834E-01*GEOM1-3.1293821E-02
      GEOM2 = (PH-S)/EPS
      IF(NN.EQ.3)GO TO 720
      BO = 1.5882587E-02*GEOM2-2.1482511E-03
      GO TO 703
  720 BO=2.9156283E-02*GEOM2-8.8616099E-03
  703 FFM = BO*(REN**B1)
      IF(LANG)701,701,702
  701 FNASA = FFM
      RETURN
  702 GEOM3 = DI/(12.0*RB)
      RFF = 1.0+7.897679*(GEOM3**.8956039)
      FNASA = RFF*FFM
      RETURN
      END
```

```
C THIS SUBPROGRAM IS WRITTEN IN FORTRAN IV FOR AN IBM 7040 COMPUTER.
C THIS SUBPROGRAM IS USED BY THE MAIN PROGRAM TO CALCULATE PREDICTED
C FRICTION FACTORS FROM MODEL FR.
C
      FUNCTION FR(NN,REN,DI,PH,LANG,BR)
      DIMENSION YA(100),YH(100),F(100)
      RRS=DI/PH
      F(1)=0.020
      DO200J=1,100
      JJ=J+1
      RES=(REN*(F(J)**0.5))/RRS
      IF(NN-2)7,7,8
 7    IF(RES-1400.0)4,5,5
 4    FRES = 4.35
      GO TO 141
 5    IF(RES-11000.0)6,9,9
 6    XA = ALOG10(RES)-3.146128
      IF(XA-.54)11,12,12
 11   S = (XA-0.094)/(0.090+0.539*XA)
      YA(1) = 0.5
      GO TO 142
 12   YA(1) = 1.6
      S = (XA-0.094)/(0.0395+0.633*XA)
 142  DO 300 L = 1,100
      LL = L + 1
      YA(LL)=((10.0**S)/20.0)*(ALOG10(100.0-YA(L)))
      IF(ABS(YA(LL)-YA(L))-0.0001)13,13,300
 13   FRES = 4.35 - YA(LL)
      GO TO 141
 300  CONTINUE
 9    FRES = 2.28
      GO TO 141
 8    IF(RES-2000.0)14,15,15
 14   FRES = 4.28
```

```
      GO TO 141
15    IF(RES-16000.0)16,17,17
16    XH = ALOG10(RES)-3.30103
      IF(XH-.58)18,18,19
18    S = (XH-0.116)/(0.153+0.4375*XH)
      YH(1) = 0.5
      GO TO 143
19    YH(1) = 1.6
      S = (XH-0.116)/(0.059+0.600*XH)
143   DO 400 M = 1,100
      MM = M + 1
      YH(MM)=((10.0**S)/20.0)*(ALOG10(100.0-YH(M)))
      IF(ABS(YH(MM)-YH(M))-0.0005)21,21,400
21    FRES = 4.28-YH(MM)
      GO TO 141
400   CONTINUE
17    FRES = 2.28
141   F(JJ) = 1.0/((FRES+4.0*ALOG10(RRS))**2)
      IF(ABS(F(JJ)-F(J))-0.0015)22,22,200
200   CONTINUE
22    IF(LANG)23,23,24
24    CONTINUE
      RFF=1.0+59.0*((DI/12.0)/BR)*(REN**(-0.17))
      FFB=RFF*F(JJ)
      FR=FFB
      RETURN
23    CONTINUE
      FR=F(JJ)
      RETURN
      END
```

```
C THIS SUBPROGRAM IS WRITTEN IN FORTRAN IV FOR AN IBM 7040 COMPUTER.
C THIS SUBPROGRAM IS USED BY THE MAIN PROGRAM TO CALCULATE PREDICTED
C FRICTION FACTORS FROM MODEL FN.
C
      FUNCTION FN(EPS,DI)
      FN=0.16*(EPS/DI)**0.5
      RETURN
      END


C THIS SUBPROGRAM IS WRITTEN IN FORTRAN IV FOR AN IBM 7040 COMPUTER.
C THIS SUBPROGRAM IS USED BY THE MAIN PROGRAM TO CALCULATE PREDICTED
C FRICTION FACTORS FROM MODEL FDF.
C
      FUNCTION FDF(PH,DI,EPS)
      FDF=0.1*(1.0/PH)*DI*((EPS/DI)**1.6)
      RETURN
      END


C THIS SUBPROGRAM IS WRITTEN IN FORTRAN IV FOR AN IBM 7040 COMPUTER.
C THIS SUBPROGRAM IS USED BY THE MAIN PROGRAM TO CALCULATE PREDICTED
C FRICTION FACTORS FROM MODEL FDC1.
C
      FUNCTION FDC1(REN,DI,EPS)
      X = (.384E 07)/(REN**1.224)
      Y=2.0/((2.713**X)+1.0/(2.713**X))
      A=0.01975/(DI**0.2)
      B=(0.595*Y)/((6.0*ALOG10(DI/EPS)-1.5)**3)
      FDC1=A+B
      RETURN
      END
```

```
C THIS SUBPROGRAM IS WRITTEN IN FORTRAN IV FOR AN IBM 7040 COMPUTER.
C THIS SUBPROGRAM IS USED BY THE MAIN PROGRAM TO CALCULATE PREDICTED
C FRICTION FACTORS FROM MODEL FMSU.
C
      FUNCTION FMSU(REN,DI,EPS,PH,S)
      DIMENSION F(100)
      RA=S/2.0
      B1=(200.00*RA*EPS)/(DI**2)
      C=17.0*(RA*EPS/(PH*DI))-0.3
      B2=0.868/B1
      D1=3.63E13*((RA*EPS)/(DI**2))**(-3.71)
      H=0.1415*(1000.0*((RA*EPS)/(DI**2)))**3.5
      A=(C**B2)/(1.0+(D1/(REN**4)))
      F(1)=0.020
      DO101J=1,100
      JJ=J+1
      F(JJ)=1.0/((3.48-B1*ALOG(A+H/(REN*SQRT(F(J)))))**2)
      IF(ABS(F(JJ)-F(J))-0.0001)102,102,101
 101  CONTINUE
 102  FMSU=F(JJ)
      RETURN
      END
```

```
C THIS SUBPROGRAM IS WRITTEN IN FORTRAN IV FOR AN IBM 7040 COMPUTER.
C THIS SUBPROGRAM IS USED BY THE MAIN PROGRAM TO CALCULATE PREDICTED
C FRICTION FACTORS FROM MODEL FDC2.
C
      FUNCTION FDC2(REN,EPS,DI)
      DIMENSION F(100)
      RR=EPS/(DI+2.0*EPS)
      F(1)=0.020
      DO201J=1,100
      JJ=J+1
      ES=REN*SQRT(F(J)/2.0)*RR
      IF(ES-1000.0)202,202,203
  202 AES=11.0
      GOTO241
  203 IF(ES-10000.0)205,206,206
  205 AES=-3.0*ALOG10(ES)+20.0
      GOTO241
  206 AES=8.0
  241 F(JJ)=2.0/((AES-3.75-2.0*ALOG(2.0*RR))**2)
      IF(ABS(F(JJ)-F(J))-0.0001)204,204,201
  201 CONTINUE
  204 FDC2=F(JJ)
      RETURN
      END
```

```
C THIS SUBPROGRAM IS WRITTEN IN FORTRAN IV FOR AN IBM 7040 COMPUTER.
C THIS SUBPROGRAM IS USED BY THE MAIN PROGRAM TO CALCULATE PREDICTED
C FRICTION FACTORS FROM MODEL FNK1.
C
      FUNCTION FNK1(REN,DI,EPS)
      DIMENSION F(100),YY(100)
      RRR=EPS/DI
      F(1)=0.020
      DO301J=1,100
      JJ=J+1
      RES=REN*SQRT(F(J))*(RRR)
      RESL=ALOG10(RES)
      IF(RESL-0.65)302,302,303
  302 FRES=4.0*RESL-0.40
      GOTO341
  303 IF(RESL-1.20)304,304,305
  304 FRES=2.20+0.75*(1.0-EXP(-5.34*(RESL-0.65)))
      GOTO341
  305 IF(RESL-2.10)306,307,307
  306 XX=RESL-1.20
      IF(XX-0.47)308,308,309
  308 S=(XX-0.20)/(0.14+0.49*XX)
      YY(1)=0.25
      GOTO342
  309 S=(XX-0.2)/(-0.06+0.93*XX)
      YY(1)=0.68
  342 DO350L=1,100
      LL=L+1
      YY(LL)=((10.0**S)/20.0)*(ALOG10(100.0-YY(L)))
      IF(ABS(YY(LL)-YY(L))-0.0001)310,310,350
  310 FRES=2.95-YY(LL)
      GOTO341
  350 CONTINUE
  307 FRES=2.15
```

```
  341  F(JJ)=1.0/((FRES+4.0*ALOG10(1.0/RRR))**2)
       IF(ABS(F(JJ)-F(J))-0.0001)361,361,301
  301  CONTINUE
  361  FNK1=F(JJ)
       RETURN
       END



C THIS SUBPROGRAM IS WRITTEN IN FORTRAN IV FOR AN IBM 7040 COMPUTER.
C THIS SUBPROGRAM IS USED BY THE MAIN PROGRAM TO CALCULATE PREDICTED
C FRICTION FACTORS FROM MODEL FHVH.
C
       FUNCTION FHVH(DI,PH)
       RRS=DI/PH
       FHVH=0.25*RRS*((1.0-(1.0/(1.0+0.438/RRS))**2)**2)
       RETURN
       END
```

```
C THIS SUBPROGRAM IS WRITTEN IN FORTRAN IV FOR AN IBM 7040 COMPUTER.
C THIS SUBPROGRAM IS USED BY THE MAIN PROGRAM TO CALCULATE PREDICTED
C FRICTION FACTORS FROM MODEL FNK2.
C
      FUNCTION FNK2(REN,DI,PH)
      DIMENSION F(100),YY(100)
      RRS=DI/PH
      F(1)=0.020
      DO401J=1,100
      JJ=J+1
      RES=REN*SQRT(F(J))*(1.0/RRS)
      RESL=ALOG10(RES)
      IF(RESL-0.65)402,402,403
  402 FRES=4.0*RESL-0.40
      GOTO441
  403 IF(RESL-1.20)404,404,405
  404 FRES=2.20+0.75*(1.0-EXP(-5.34*(RESL-0.65)))
      GOTO441
  405 IF(RESL-2.10)406,407,407
  406 XX=RESL-1.20
      IF(XX-0.47)408,408,409
  408 S=(XX-0.20)/(0.14+0.49*XX)
      YY(1)=0.25
      GOTO442
  409 S=(XX-0.2)/(-0.06+0.93*XX)
      YY(1)=0.68
  442 DO450L=1,100
      LL=L+1
      YY(LL)=((10.0**S)/20.0)*(ALOG10(100.0-YY(L)))
      IF(ABS(YY(LL)-YY(L))-0.0001)410,410,450
  410 FRES=2.95-YY(LL)
      GOTO441
  450 CONTINUE
  407 FRES=2.15
```

```
 441  F(JJ)=1.0/((FRES+4.0*ALOG10(RRS))**2)
      IF(ABS(F(JJ)-F(J))-0.C001)461,461,401
 401  CONTINUE
 461  FNK2=F(JJ)
      RETURN
      END
```

```
C THIS SUBPROGRAM IS WRITTEN IN FORTRAN IV FOR AN IBM 7040 COMPUTER.
C THIS SUBPROGRAM IS USED BY THE MAIN PROGRAM TO CALCULATE PREDICTED
C FRICTION FACTORS FROM MODEL FCW.
C
      FUNCTION FCW(REN,DI,EPS)
      DIMENSION F(100)
      RR=DI/EPS
      F(1)=C.020
      DC601J=1,100
      JJ=J+1
      RES=REN*SQRT(F(J))/RR
      FRES=2.28-4.0*ALOG10(1.0+4.67/RES)
      F(JJ)=1.0/((FRES+4.0*ALOG10(RR))**2)
      IF(ABS(F(JJ)-F(J))-0.C001)602,602,601
 601  CONTINUE
 602  FCW=F(JJ)
      RETURN
      END
```

```
C THIS SUBPROGRAM IS WRITTEN IN FORTRAN IV FOR AN IBM 7040 COMPUTER.
C THIS SUBPROGRAM IS USED BY THE MAIN PROGRAM TO CALCULATE PREDICTED
C FRICTION FACTORS FROM MODEL FM.
C
      FUNCTION FM(REN,DI,PH)
      DIMENSION F(100),YY(100)
      RRS=DI/PH
      F(1) =.020
      DO501J=1,100
      JJ=J+1
      RES=REN*SQRT(F(J))/RRS
      RESL=ALOG10(RES)
      IF(RES-52.5)502,503,503
  502 FRES=5.68
      GOTO541
  503 IF(RES-75000.0)504,505,505
  504 XX=RESL-1.720159
      IF(XX-0.90)506,506,507
  506 S=(XX-0.25)/(0.16+0.566*XX)
      YY(1)=0.30
      GOTO542
  507 IF(XX-2.24)508,508,509
  508 S=(XX-0.25)/(0.208+0.513*XX)
      YY(1)=0.13
      GOTO542
  509 IF(XX-3.15)510,510,505
  510 S=(XX-0.25)/(0.058+0.580*XX)
      YY(1)=0.25
  542 DO550L=1,100
      LL=L+1
      YY(LL)=((10.0**S)/20.0)*(ALOG10(100.0-YY(L)))
      IF(ABS(YY(LL)-YY(L))-0.0001)513,513,550
  513 FRES=5.68-YY(LL)
      GOTO541
```

```
  550  CONTINUE
  505  FRES=2.30
  541  F(JJ)=1.0/((FRES+4.0*ALOG10(RRS))**2)
       IF(ABS(F(JJ)-F(J))-0.0001)522,522,501
  501  CONTINUE
  522  FM=F(JJ)
       RETURN
       END



C THIS SUBPROGRAM IS USED BY THE MAIN PROGRAM TO CALCULATE THE PER
C CENT ERROR OF THE PREDICTED FRICTION FACTORS FROM THE OBSERVED
C FRICTION FACTORS.
C
       FUNCTION ERROR(N,FA,FP)
       DIMENSION FA(200),FP(200)
       SUMER=0.0
       SUMFF=0.0
       DO1800L=1,N
       SUMER=SUMER+(FP(L)-FA(L))/FA(L)
  1800 CONTINUE
       AN=N
       AVEER=SUMER/AN
       ERROR=AVEER*100.0
       RETURN
       END
```

```
C THIS SUBPROGRAM IS USED BY THE MAIN PROGRAM TO CALCULATE THE PER
C CENT STANDARD DEVIATION OF THE PREDICTED FRICTION FACTORS FROM
C THE OBSERVED FRICTION FACTORS.
C
      FUNCTION DEV(N,FA,FP)
      DIMENSION FA(200),FP(200)
      SUMSF=0.0
      SUMFF=0.0
      DO190CL=1,N
      SUMSF=SUMSF+(FP(L)-FA(L))**2
      SUMFF=SUMFF+FA(L)
 1900 CONTINUE
      AN=N
      AVEFF=SUMFF/AN
      SSDEV=SUMSF/(AN-5.0)
      DEV=(SQRT(SSDEV)/AVEFF)*100.0
      RETURN
      END


C THIS SUBPROGRAM IS USED BY THE MAIN PROGRAM TO CALCULATE THE PER
C CENT STANDARD DEVIATION OF THE PREDICTED FRICTION FACTORS FROM
C THE OBSERVED FRICTION FACTORS.
C
      FUNCTION DEVR(N,FA,FP,LANG)
      DIMENSION FA(200),FP(200)
      SUMSF=0.0
      SUMFF=0.0
      DO190CL=1,N
      SUMSF=SUMSF+(FP(L)-FA(L))**2
      SUMFF=SUMFF+FA(L)
 1900 CONTINUE
      AN=N
      AVEFF=SUMFF/AN
```

```
      IF(LANG)1901,1901,1902
 1901 SSDEV=SUMSF/(AN-5.0)
      GOTO1903
 1902 SSDEV=SUMSF/(AN-6.0)
 1903 DEVR=(SQRT(SSDEV)/AVEFF)*100.0
      RETURN
      END


C THIS SUBPROGRAM IS USED BY THE MAIN PROGRAM TO CALCULATE THE PER
C CENT STANDARD DEVIATION OF THE PREDICTED FRICTION FACTORS FROM
C THE OBSERVED FRICTION FACTORS.
C
      FUNCTION DEVN(N,FA,FP,LANG)
      DIMENSION FA(200),FP(200)
      SUMSF=0.0
      SUMFF=0.0
      DO1900L=1,N
      SUMSF=SUMSF+(FP(L)-FA(L))**2
      SUMFF=SUMFF+FA(L)
 1900 CONTINUE
      AN=N
      AVEFF=SUMFF/AN
      IF(LANG)1901,1901,1902
 1901 SSDEV=SUMSF/(AN-7.0)
      GOTO1903
 1902 SSDEV=SUMSF/(AN-8.0)
 1903 DEVN=(SQRT(SSDEV)/AVEFF)*100.0
      RETURN
      END
```

```
C THIS SUBPROGRAM IS USED BY THE MAIN PROGRAM TO CALCULATE THE PER
C CENT STANDARD DEVIATION OF THE PREDICTED FRICTION FACTORS FROM
C THE OBSERVED FRICTION FACTORS.
C
      FUNCTION DE3(N,FA,FP)
      DIMENSION FA(200),FP(200)
      SUMSF=0.0
      SUMFF=0.0
      DO190L=1,N
      SUMSF=SUMSF+(FP(L)-FA(L))**2
      SUMFF=SUMFF+FA(L)
 1900 CONTINUE
      AN=N
      AVEFF=SUMFF/AN
      SSDEV=SUMSF/(AN-3.0)
      DE3=(SQRT(SSDEV)/AVEFF)*100.0
      RETURN
      END


C THIS SUBPROGRAM IS USED BY THE MAIN PROGRAM TO CALCULATE THE PER
C CENT STANDARD DEVIATION OF THE PREDICTED FRICTION FACTORS FROM
C THE OBSERVED FRICTION FACTORS.
C
      FUNCTION DE4(N,FA,FP)
      DIMENSION FA(200),FP(200)
      SUMSF=0.0
      SUMFF=0.0
      DO190L=1,N
      SUMSF=SUMSF+(FP(L)-FA(L))**2
      SUMFF=SUMFF+FA(L)
 1900 CONTINUE
      AN=N
      AVEFF=SUMFF/AN
```

```
      SSDEV=SUMSF/(AN-4.0)
      DE4=(SQRT(SSDEV)/AVEFF)*100.0
      RETURN
      END


C THIS SUBPROGRAM IS USED BY THE MAIN PROGRAM TO CALCULATE THE PER
C CENT STANDARD DEVIATION OF THE PREDICTED FRICTION FACTORS FROM
C THE OBSERVED FRICTION FACTORS.
C
      FUNCTION DE7(N,FA,FP)
      DIMENSION FA(200),FP(200)
      SUMSF=0.0
      SUMFF=0.0
      DO190L=1,N
      SUMSF=SUMSF+(FP(L)-FA(L))**2
      SUMFF=SUMFF+FA(L)
 1900 CONTINUE
      AN=N
      AVEFF=SUMFF/AN
      SSDEV=SUMSF/(AN-7.0)
      DE7=(SQRT(SSDEV)/AVEFF)*100.0
      RETURN
      END
```

VITA

The author was born in New Orleans, Louisiana, on February 25, 1941. He attended St. Matthias Elementary School and was graduated from De La Salle High School, New Orleans, in May, 1959.

His undergraduate work was at Louisiana State University where he was a member of Phi Eta Sigma, Tau Beta Pi, Phi Kappa Phi, and Phi Lambda Upsilon honorary societies. He received the Bachelor of Science degree in Chemical Engineering from that institution in June, 1963. In September, 1963, he entered the LSU Graduate School and proceeded with work on the Master of Science degree in Chemical Engineering, which he received in June, 1965. He is now a candidate for the degree of Doctor of Philosophy in the Department of Chemical Engineering.

EXAMINATION AND THESIS REPORT

Candidate: Kenneth Lloyd Riley

Major Field: Chemical Engineering

Title of Thesis: Flow Losses in Flexible Hose

Approved:

Major Professor and Chairman

Dean of the Graduate School

EXAMINING COMMITTEE:

Date of Examination:

May 8, 1967